ISSN-2222-5013

SCIENTIFIC WORKS

AZERBAIJAN UNIVERSITY OF
ARCHITECTURE AND CONSTRUCTION

SW AZUAC
https://swjournal.az
No.1 / 2026

EDITORIAL TEAM

The Journal **Elmi Əsərlər/Scientific Works of Azerbaijan University of Architecture and Construction** (SW AzUAC) is an open-access, peer-reviewed scientific journal. It publishes original and state-of-the-art review papers, as well as brief reports on topics in architecture, construction engineering, applied mathematics, and information sciences. The journal aims to provide a platform for researchers to share their theoretical, experimental, and practical research. It focuses on recent developments and provides insights into future advancements. Registered by the Ministry of Press and Information of the Republic of Azerbaijan under certificate 313 (April 2, 1996). SW AzUAC was founded by the Azerbaijan University of Architecture and Construction.

CONTENT

https://doi.org/10.58225/sw.2026.1-5-14

GRID SQUARE DIAGRAM ANALYSIS OF THE PHYSICAL PARAMETERS OF AUTOCLAVED POROUS AGGREGATE

Mukhamedbaev Abdugafur Abduvalievich*
Tashkent University of Architecture and Civil-Engineering, Uzbekistan
mabdugofira@gmail.com

Abstract. This paper presents a comparative analysis of the physical parameters of autoclaved porous aggregate using a grid square diagram. The study showed that the granulometric composition significantly influences the bulk density, fill volume (height), and water absorption of the material. An increase in the proportion of fine fractions (2.5–5 mm) results in higher bulk density and lower fill volume (height) due to denser packing of the grains. As the content of fine particles increases, water absorption also rises because of the larger specific surface area and porosity. Coarse fractions (20–40 mm) contribute to reduced bulk density and water absorption but increase the fill volume (height) at a fixed mass. During the research, clear dependencies were established between the fractional composition of porous aggregate and its main physical and technical characteristics. The results make it possible to optimize the composition of porous aggregate to improve the technical characteristics of lightweight concrete.
Keywords: aerated concrete crumb, aggregate, autoclave, bulk density, fill volume (height), water absorption

Cite this article as: M. A. Abduvalievich, "GRID SQUARE DIAGRAM ANALYSIS OF THE PHYSICAL PARAMETERS OF AUTOCLAVED POROUS AGGREGATE", SW AzUAC, vol. 1, 2026, https://doi.org/10.58225/sw.2026.1-5-14
Article history: Received: 16 December 2025 / Revised: 20 January 2026 / Accepted: 04 February 2026

1. Introduction. Lightweight concrete with porous aggregates is a special type of concrete in which lightweight materials with a porous structure are used instead of heavy aggregates. As a result, the density of such concrete is lower than that of conventional concrete. Materials such as expanded clay, agloporite, expanded vermiculite, perlite, slag pumice, and foam glass are used as aggregates. These materials have different physical and mechanical properties compared to heavy aggregates. The amount and type of aggregate influence important concrete properties, such as density, strength, thermal conductivity, workability, water absorption, and shrinkage. To obtain concrete with high strength and a dense structure while reducing cement consumption, a mixture of aggregates of different grain sizes is used, which promotes denser particle packing and reduces porosity. Multifractional aggregates are often used to ensure better contact between particles. Important characteristics of aggregates include their bulk density and water absorption capacity—these parameters determine the physical properties of the aggregates [1–5].

In recent years, considerable attention has been given in Uzbekistan to the production of autoclaved cellular concrete. Autoclaved aerated concrete is characterized by a uniformly distributed porous structure throughout the entire volume of the material. During the production process, defective products are generated; these are either stored in open areas or crushed using a crusher. The resulting crushed aerated-concrete granulate is used in construction as a loose thermal insulation material [6–9].

Aerated-concrete granulate is considered a promising alternative to traditional porous aggregates such as expanded clay. The scientific and technical literature presents various approaches to using aerated-concrete granulate in the production of building materials [10–14].

When designing mixes for lightweight concrete, two, three, or sometimes more fractions of coarse and fine aggregates are typically used. The ratio between these fractions affects grain packing

density, intergranular void content, bulk density, water absorption, and other properties of the porous aggregate. Optimizing these parameters has a significant impact on the technological characteristics of concrete mixes, as well as on the structural and thermal-insulation properties of the finished concrete products.

The grid square diagram is a graphical method of data representation in which information is visualized as a grid of squares, each reflecting a specific parameter or characteristic [15–18]. In construction materials science, such a diagram can be useful for comparing the properties of various building materials (for example, strength, thermal conductivity, water absorption, cost, etc.). The color or intensity of each square (a heat map) represents the level of the corresponding parameter [19–22].

Comparative analysis of the influence of fractional composition on certain characteristics of building materials using a grid square diagram is of interest, as the granulometric composition affects packing density, water permeability, bulk density, and other properties.

2. Purpose and objectives of the study. The aim of the present work is to develop and apply a grid square diagram for studying certain physical characteristics of autoclaved porous aggregate.

3. Raw materials and research methods. The selected fractions were 2.5–5 mm, 5–10 mm, 10–20 mm, and 20–40 mm. In the mixtures, the content of the fractions varied from 0 to 50% by mass. Additionally, all fractions were examined individually at a content of 100%. Autoclaved aerated-concrete granulate from the *"Arton" (SP LLS "EAST MINING INVEST")* plant was used to determine the characteristics. The granulate was first separated into fractions using a sieve and then dried to constant mass in a laboratory drying oven at a temperature of 100 ± 5 °C. Figure 1 shows photographs of the fractions under study.

Fig. 1. Fractions of autoclaved porous aggregate

Bulk density, fill height (or volume), and water absorption were selected as the parameters to be determined. The average grain diameters of the mixtures were also calculated. In this case, the varying parameter was the fractional composition of the aggregate.

The bulk density in an uncompacted state and the water absorption were determined using standard methods. To determine the fill height (volume), a 1000-ml graduated glass vessel with 20-ml divisions was used.

The formula for calculating the average diameter is as follows:

$$d_{avg} = \frac{\sum(d_i \cdot \Delta P_i)}{100}$$

where: d_i — the average diameter of the particles retained on the *i*-th sieve (in mm);
ΔP_i — the percentage of the aggregate mass retained on the *i*-th sieve (in %).

Typically, d_i is taken as the arithmetic mean of the sizes of two neighboring sieves.
In our case, this is expressed as follows:

$$d_{avg} = \frac{d_1 \cdot m_1 + d_2 \cdot m_2 + d_3 \cdot m_3 + d_4 \cdot m_4}{m_1 + m_2 + m_3 + m_4}$$

4. Research results and discussion. The obtained results allow us to draw important conclusions. The table presents the results for individual fractions at 100% mass content.

Table 1. Physical characteristics of autoclaved porous aggregate

№	Fraction content (mm), %				Average grain diameter (d_{avg}), mm	Bulk density, g/cm³	Fill height (volume), ml (for 150 g)	Water absorption, % (24 hours)
	2,5-5	**5-10**	**10-20**	**20-40**				
1	100	0	0	0	3,75	0,3625	463,33	138,80
2	0	100	0	0	7,50	0,3213	500,00	114,77
3	0	0	100	0	15,0	0,3104	523,33	99,21
4	0	0	0	100	30,0	0,2775	573,33	86,93

An inverse relationship is observed between the average grain diameter and the bulk density of the material: as the grain size increases, the bulk density decreases from 0.3625 to 0.2775 g/cm³. This is due to the increase in intergranular space as particle size grows, which leads to a reduction in the density of the bulk layer.

At a constant aggregate mass, the fill height (volume) increases with increasing average grain size, which is associated with the decrease in bulk density. This effect reflects the increase in porosity and the volumetric space between larger grains.

Water absorption also shows a decreasing trend with increasing fraction size: from 138.80% for the 2.5–5 mm fraction to 86.93% for the 20–40 mm fraction. This is due to the reduction in the specific surface area of the grains and the decrease in the volume of capillary pores capable of retaining moisture. Fine-grained fractions have a larger specific surface area and, consequently, higher water absorption capacity.

Figure 2 shows photographs illustrating the packing density of different fractions of autoclaved porous aggregate. It can be seen that as the grain size decreases, a denser packing of the material is achieved, with smaller intergranular voids.

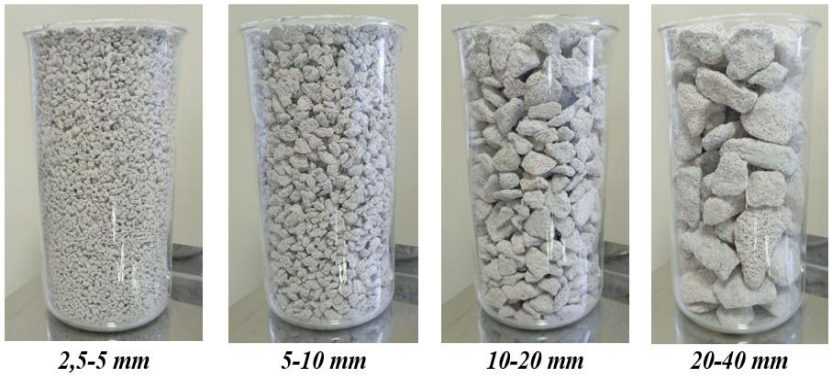

Fig. 2. Packing density of different fractions of autoclaved porous aggregate

Analysis of mixtures with different fraction ratios. Analysis of mixtures with different fraction ratios showed that at low fine-particle content, there is a shortage of grains needed to fill the intergranular voids created by coarse fractions. This leads to increased porosity and reduced packing density of the mixture.

In the case of high fine-fraction content, a visual *"floating"* effect of the coarse particles in the material mass is observed. Despite minimal intergranular voids, an excess of fine grains disrupts the stability of the framework formed by the coarse fractions, reducing their mutual cohesion and the ability to form a stable structure.

Further analysis focused on studying these characteristics in mixtures with different fraction proportions. At a constant content of coarse fractions, increasing the share of the finest fraction (2.5–5 mm) leads to an increase in bulk density. This is explained by the improved filling of intergranular space with fine particles, which reduces the overall porosity of the mixture.

Increasing the content of the 5–10 mm and 10–20 mm fractions also contribute to higher bulk density, though to a lesser extent. These fractions help form a more compact structure due to the optimal size ratio and efficient filling of voids between coarse grains (*Fig. 3*).

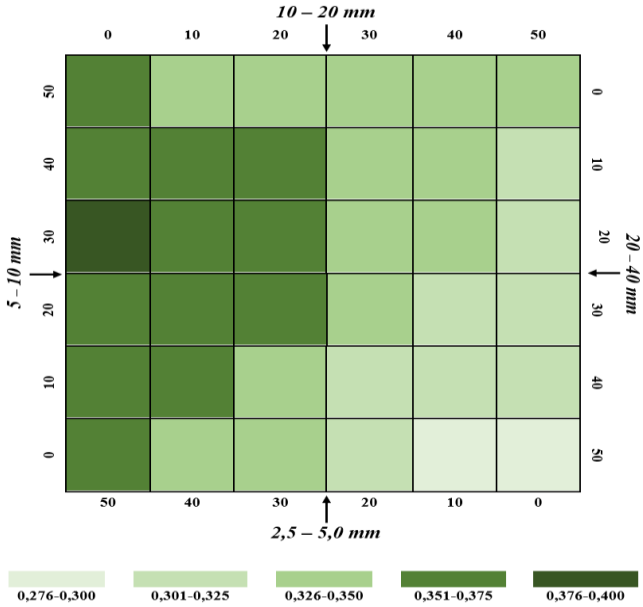

Fig. 3. Grid square diagram of bulk density of porous aggregate mixtures (g/cm³)

Effect of fractional composition on density and fill volume. Reducing the proportion of coarse fractions leads to an increase in packing density. Large grains form a looser structure with larger pores, so mixtures with a higher content of coarse fractions have lower bulk density. High bulk density is achieved with an increased proportion of fine and medium grains, which promotes denser particle packing and reduces the total void volume.

As the fine-fraction content increases, the fill height decreases. This is explained by the denser packing of fine grains, which reduces the fill volume at a constant mass. Increasing the proportion of coarse-grained fractions (10–20 mm and 20–40 mm) results in a higher fill height, which is associated with an increase in volume and porosity of the packing. At a constant mixture mass, larger grains form a more voluminous but less dense layer. Thus, the fill height is inversely proportional to bulk density: as the mixture density increases, the volume, and hence the fill height, decreases (*Fig. 4*).

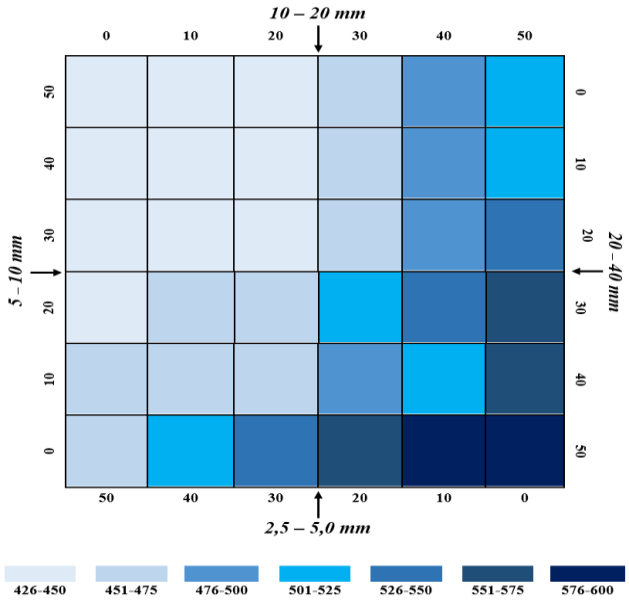

Fig. 4. Grid square diagram of fill volume (height) of porous aggregate mixtures (ml)

Structural features of the aggregate and its behavior during water saturation. It should be noted that the grains of the porous aggregate differed in terms of their internal structure. The mixture contained both coarse-porous and fine-porous grains. However, the majority of the particles had a medium-porous macrostructure, evenly distributed throughout the grain volume. These structural features were clearly visible both in the dry state and after water absorption, indicating the stability and reproducibility of the material's porous structure.

During the immersion of the aggregate in water, dust particles located on the grain surfaces and within the pores of their surface layer are washed out. This causes the water to become cloudy, visually appearing as a beige tint in the water. As these particles settle to the bottom of the vessel, the water gradually becomes clearer and more transparent, confirming the mechanical nature of the contamination and the limited volume of easily removable particles.

After testing, the water-saturated grains retained their shape and porous structure, indicating sufficient strength and resistance of the material to water saturation. Upon careful visual inspection, it was found that the grains differed in color: the sample contained dark and light gray, dark and light beige, as well as mustard-colored grains (*Fig. 5*).

The variety of color shades and pore sizes in the grains of the porous aggregate may indicate that the material is a crushed product of industrial origin. Most likely, the aggregates were obtained by crushing rejected autoclaved aerated concrete blocks, which differed in composition and average density. This explains both the heterogeneity of the macrostructure and the color variability of the grains.

When the aggregate mixtures were immersed in water, it was observed that the fine fractions (2.5–5.0 mm and 5.0–10.0 mm) quickly settled to the bottom of the vessel, while the coarse fractions exhibited positive buoyancy—some rose upward, and individual grains even floated to the water surface. This behavior indicates a lower average density of the coarse fractions, likely due to their more developed porous structure and, consequently, lower bulk density compared to the fine grains.

Fig. 5. Photographs taken during the study of water absorption characteristics of autoclaved porous aggregate

In mixtures with an increased content of fine fractions (2.5–5.0 mm and 5.0–10.0 mm), it was noted that individual coarse grains became mechanically trapped between fine particles. As a result, they remained at the bottom and could not move upward or float to the surface, despite their potential positive buoyancy. This demonstrates the significant influence of dense packing of fine grains on the mobility and redistribution of coarse particles in the aqueous medium.

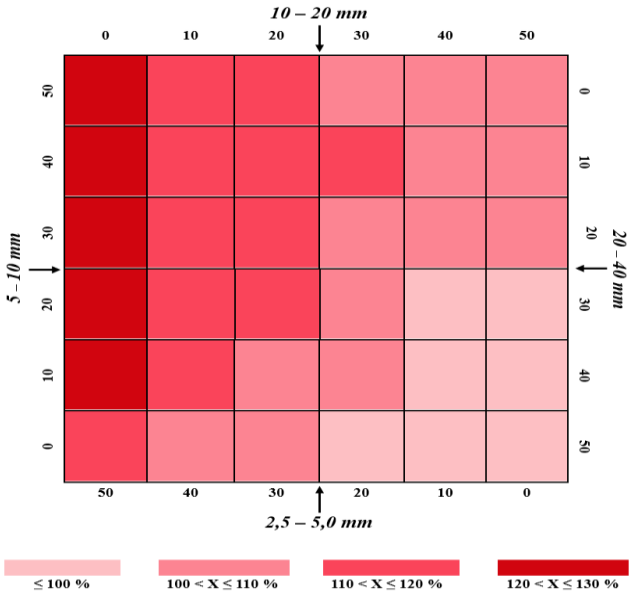

Fig. 6. Grid square diagram of water absorption of porous aggregate mixtures (%)

As the content of the finest fraction (2.5–5.0 mm) increases, a significant rise in water absorption is observed (*Fig. 6*). This is explained by the increased specific surface area of the fine particles, as well as the higher porosity and capillarity of the fine-grained components. An increase in the proportion of medium-sized grains is accompanied by a moderate increase in water absorption.

A decrease in the content of coarse fractions leads to higher water absorption, since coarse grains have a smaller specific surface area and form a less dense packing. Fine grains, having a larger specific surface area, contribute to the adsorption of a greater amount of water. The denser packing of the mixture with a higher content of fine grains enhances capillary effects, further increasing the water absorption of the material.

Relationship between average grain diameter, bulk density, and water absorption. Next, the average grain diameter of the porous aggregate mixtures was calculated. An increase in the content of the 2.5–5.0 mm fraction reduces the average diameter of the mixture, whereas an increase in the 20–40 mm fraction, on the contrary, leads to its growth (*Fig. 7*). Changes in the average diameter occur smoothly, indicating a correct gradation of the composition.

A clear relationship was established between the content of fine and coarse fractions and the average diameter. At the same time, some mixtures, despite differences in fractional composition, exhibited the same average diameter. This indicates that mixtures with different structures can achieve the same average diameter when the mass balance is appropriately adjusted.

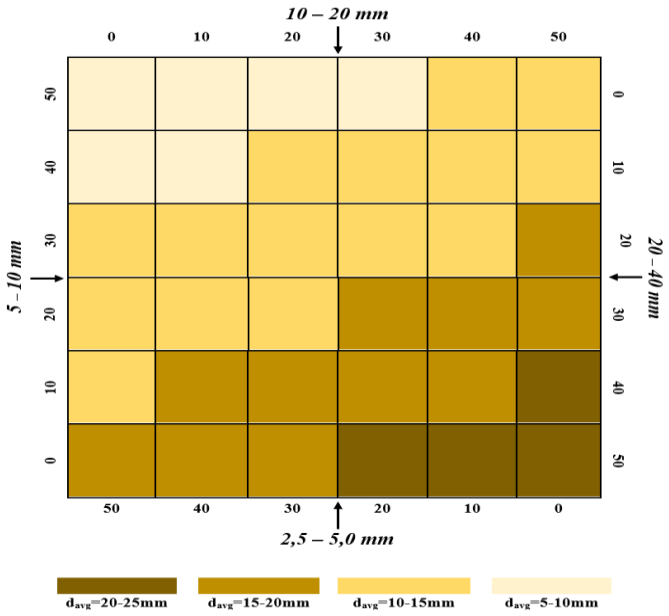

Fig.7. Grid square diagram of the average grain diameter (d_{avg}) of porous aggregate mixtures

The analysis showed that the smaller the average grain diameter, the higher the bulk density. This is because fine particles can pack more efficiently, creating fewer voids, which increases the mass of material per unit volume. Thus, bulk density depends not only on the average diameter but also on the quality gradation of the mixture—that is, on the compatibility of fractions in terms of dense packing. Maximum bulk density is achieved not by using a single fine fraction, but by an optimally selected combination of different fractions. The increase in bulk density is particularly noticeable when the 2.5–5.0 mm fraction is introduced.

Interestingly, different mixtures can exhibit the same bulk density despite differences in average diameter. This confirms that the distribution of fractions is at least as important as the average grain size itself.

An inverse relationship is observed between the average diameter and water absorption: the finer the grain (smaller d_{avg}), the higher the water absorption. This is because fine fractions have a larger specific surface area, well-developed microporosity, and capillary structure, which promote moisture retention. In contrast, coarse fractions have a smaller surface area and form a less dense packing with larger pores, reducing the overall water absorption capacity.

A direct relationship was also established between water absorption and bulk density. Denser packing of grains (higher bulk density) promotes an increase in the number of capillaries that retain moisture. Mixtures containing a higher proportion of fine fractions (especially 2.5–5.0 mm) exhibit the maximum water absorption values. To reduce water absorption, it is recommended to increase the proportion of coarse fractions (20–40 mm) and decrease the content of the finest fraction (2.5–5.0 mm).

Analysis of the results revealed the possibility of developing a model to predict the fill height:

$$h = f(\text{fraction composition}) \text{ or } h = f(d_{avg})$$

where: h – fill height, d_{avg} – average grain diameter.

The study also established clear relationships between the fractional composition of the porous aggregate and its main physical and technical characteristics. In particular, the following correlations were identified:

- *Fractional composition – bulk density:* an increase in the proportion of fine fractions (2.5–5.0 mm) promotes higher bulk density of the mixture;
- *Fractional composition – fill volume (height):* predominance of coarse fractions (10–20 mm and mainly 20–40 mm) leads to an increase in the mixture volume (height) in a graduated vessel due to less dense packing;
- *Fractional composition – water absorption:* an increase in the content of fine fractions is accompanied by higher water absorption of the mixture due to the larger specific surface area and developed porosity of fine grains;
- *Fractional composition – average grain diameter:* the higher the proportion of coarse fractions, the larger the average grain diameter, and conversely, an increase in the fine fraction (2.5–5.0 mm) reduces d_{avg}.

5. Conclusion. The granulometric composition has a significant impact on the physical properties of granular material. As the average grain diameter increases, bulk density and water absorption decrease, while the fill height at a constant mass increase. The fill height at a constant mass of the granular mixture is an indicator of its packing density and porosity. An increase in the proportion of fine fractions contributes to denser packing, a reduction in fill height, and an increase in bulk density. Conversely, an increase in grain size leads to a decrease in the bulk density and water absorption of the porous aggregate, as well as an increase in the fill height at a fixed mass.

Author Contributions. M.A.M. (Mukhamedbaev Abdugafur Mukhamedbaev) conceived and designed the study, developed the research methodology, performed the experimental investigation and data analysis, interpreted the results, prepared the figures and tables, wrote the original draft of the manuscript, revised the manuscript, and approved the final version for publication.

Funding. The author received no specific financial support from any funding agency, commercial organization, or not-for-profit institution for the research, authorship, and/or publication of this article.

Data Availability. The data supporting the findings of this study are available from the corresponding author upon reasonable request.

Declarations

Conflict of Interest. The author declares that there are no competing interests or conflicts of interest related to this work.

Ethical Approval. This article does not involve studies with human participants or animals. Therefore, ethical approval was not required.

Informed Consent. Not applicable.

References

[1] Buzhevich GA, editor. Technology and Properties of New Types of Lightweight Concretes on Porous Aggregates [in Russian]. Moscow: Stroyizdat; 1971. 207 p.

[2] Ivanov IA. Technology of Lightweight Concretes on Artificial Porous Aggregates [in Russian]. Moscow: Stroyizdat; 1974. 287 p.

[3] Kamilov KhKh, Turakhanov SI. Physical and mechanical properties of artificial lightweight aggregates produced in Uzbekistan. Central Asian Journal of Mathematical Theory and Computer Sciences. 2022;3(12):338–341.
[4] Inozemtsev AS, Korolev EV. High-Strength Lightweight Concretes [in Russian]. Saint Petersburg: SPbGASU; 2022. 192 p.
[5] Makridin NI, Maksimova IN. Artificial Porous Aggregates and Lightweight Concretes [in Russian]. Penza: PGUAS; 2013. 324 p.
[6] Aeroc. Aerated Concrete Crumb. Technical Specifications. Available from: https://aeroc.nt-rt.ru/images/manuals/2.pdf
[7] Baikal Aerated Concrete. Instructions for Using Aerated Concrete Crumb as Bulk Insulation. https://bgazobeton.ru/upload/iblock/c25/instrukciya_po_primeneniyu_kroshki_gazobetona_v_kachestve_nasypnogo_uteplitelya.pdf
[8] Arton. Aerated Concrete Crumb (Bulk Insulation). Available from: https://arton.uz/categories/gazobetonnaya-kroshka
[9] TU 2661-003-82651425-2019. Crushed Cellular Aerated Concrete Crumb [in Russian]. Saratov; 2019. 4 p.
[10] Leontev SV, Kharitonov VA. Development of structural-heat-insulating lightweight concrete composition using production of aerated concrete waste as a porous aggregate. Journal of Physics: Conference Series. 2021;2124:012009. https://doi.org/10.1088/1742-6596/2124/1/012009
[11] Belov IA, Bogdanova NP, Vlasenko ZN, Fedosov NN, Klinchuk ES, Verbitskaya TL. Use of Autoclaved Aerated Concrete Waste [in Russian]. Sovremennye Materialy. 2008. Available from: https://ais.by/story/1528
[12] Leontev SV, Smirnova TV. Evaluation of the possibility of using crushed autoclaved aerated concrete as aggregate in lightweight concretes [in Russian]. Modern Technologies in Construction. Theory and Practice. 2019;2:360–365.
[13] Fedorov VI, Abdimezhitov MK, Dyakonov AA, Popov AL, Mestnikov AE. Lightweight concretes from autoclaved foam concrete waste [in Russian]. Modern High Technologies. 2016;(11):61–65.
[14] Udodov SA. Plaster and Masonry Compositions of Reduced Density for Cellular Concrete [in Russian]. Rostov-on-Don; 2006. https://new-disser.ru/_avtoreferats/01003043620.pdf
[15] Hoque MA, Shrestha A, Sapkota SC, et al. Prediction of autogenous shrinkage in ultra-high-performance concrete (UHPC) using hybridized machine learning. Asian Journal of Civil Engineering. 2025;26:649–665. https://doi.org/10.1007/s42107-024-01212-8
[16] Sapkota SC, Panagiotakopoulou C, Dahal D, et al. Optimizing high-strength concrete compressive strength with explainable machine learning. Multiscale Modeling, Experiment and Design. 2025;8:160. https://doi.org/10.1007/s41939-025-00737-y
[17] Sun C, Wang K, Liu Q, Wang P, Pan F. Machine-learning-based comprehensive properties prediction and mixture design optimization of ultra-high-performance concrete. Sustainability. 2023;15:15338. https://doi.org/10.3390/su152115338
[18] Targino D, Sousa I, Freitas I, Dantas A, Babadopulos L. Exploratory data analysis of mix designs for prediction models and compressive strength estimation of self-compacting concrete. In: Congreso Latino-Americano de Patología de Construcción; 2021. https://doi.org/10.4322/conpat2021.706
[19] Alsaadawi MM, Elshaarawy MK, Hamed AK. Concrete compressive strength classification using hybrid machine learning models and interactive GUI. Innovative Infrastructure Solutions. 2025;10:198. https://doi.org/10.1007/s41062-025-01983-2
[20] Elhishi S, Elashry AM, El-Metwally S. Unboxing machine learning models for concrete strength prediction using XAI. Scientific Reports. 2023;13:19892. https://doi.org/10.1038/s41598-023-47169-7

[21] Ziolkowski P, Niedostatkiewicz M, Kang SB. Model-based adaptive machine learning approach in concrete mix design. Materials. 2021;14:1661. https://doi.org/10.3390/ma14071661
[22] Rathakrishnan V, Beddu S, Ahmed AN, et al. Predicting compressive strength of high-performance concrete with high-volume slag replacement using boosting machine learning algorithms. Scientific Reports. 2022;12:9539. https://doi.org/10.1038/s41598-022-13614-6

https://doi.org/10.58225/sw.2026.1-15-24

EFFECT OF GAMMA IRRADIATION AND THERMAL ANNEALING ON THE STRUCTURAL AND DEFECT PROPERTIES OF ZrB_2 CERAMICS

Samadov Samir[1*], Nguyen Minh Trung[1,2], Popov Evgeni[1,3], Sidorin Anatoliy[1]
[1]Joint Institute for Nuclear Research, Dubna, 141980, Russia*
[2]Institute of Physics, Vietnam Academy of Science and Technology, Hanoi, 10000, Vietnam
[3]Institute of Catalysis, Bulgarian Academy of Sciences, Sofia, 1113, Bulgaria
samirsamedov@jinr.ru

Abstract. This work examines the influence of gamma irradiation and subsequent thermal annealing on the structural and defect-related properties of zirconium diboride (ZrB_2) nanocrystals. The samples were irradiated with absorbed doses of 1500 and 3000 kGy and analyzed by X-ray diffraction, Fourier-transform infrared spectroscopy, positron annihilation lifetime spectroscopy, and Doppler broadening spectroscopy. The results showed that ZrB_2 preserved its hexagonal structure without the formation of secondary phases, confirming its high radiation stability. At the same time, small shifts in diffraction peaks, slight lattice expansion, and changes in FTIR bands indicated local structural distortions and surface oxidation processes. Positron annihilation measurements revealed irradiation-induced modification of vacancy-type defects and redistribution of positron trapping centers. Electron momentum analysis also confirmed changes in the local electronic structure after irradiation. Overall, ZrB_2 demonstrates high resistance to gamma irradiation, while exhibiting limited but detectable structural and defect evolution.
Keywords: ZrB_2 ceramics; gamma irradiation; X-ray diffraction; PAS; vacancy-type defects

Cite this article as: *S. Samadov, N. M. Trung, E. Popov, and A. Sidorin, "EFFECT OF GAMMA IRRADIATION AND THERMAL ANNEALING ON THE STRUCTURAL AND DEFECT PROPERTIES OF ZrB_2 CERAMICS", SW AzUAC, vol. 1, 2026, doi:10.58225/sw.2026.1-15-24*
Article history: *Received: 14 January 2026 / Revised: 20 February 2026 / Accepted: 04 March 2026*

1. Introduction. Zirconium diboride (ZrB_2) is one of the most promising ultra-high-temperature ceramic materials due to its high melting point, excellent thermal and electrical conductivity, high hardness, as well as strong resistance to chemical attack and corrosive environments. Owing to this combination of properties, ZrB_2 has attracted considerable interest for applications in aerospace technology, nuclear engineering, protective coatings, high-temperature electrodes, and other fields where structural stability is required under severe external conditions [1-3]. In particular, its resistance to thermal effects and irradiation makes ZrB_2 a promising material for components operating under extreme service conditions.

In recent years, interest in the behavior of ZrB_2 under the influence of external factors such as temperature, pressure, and various types of radiation has increased significantly. Previous studies have shown that irradiation with heavy ions, neutrons, and electrons can induce measurable changes in the lattice parameters, defect structure, degree of amorphization, and local atomic arrangement in zirconium diboride [4-6]. However, the hexagonal crystal structure of ZrB_2 is largely preserved in most cases, indicating a high structural stability of the material. Previous studies based on X-ray diffraction have also shown that irradiation can induce lattice expansion, local disorder, and limited amorphization [7-8]. While these results confirm that ZrB_2 is a structurally stable material, they also indicate that its response is strongly dependent on the irradiation conditions and subsequent thermal history.

However, the effect of high-dose gamma irradiation on the structural and defect evolution in ZrB_2 remains insufficiently understood, particularly when crystallographic and defect-sensitive

techniques are applied in a combined manner. Conventional structural methods such as X-ray diffraction provide important information on phase composition, lattice deformation, and long-range order, while FTIR spectroscopy is useful for identifying changes in surface bonding, oxidation-related groups, and local chemical environments induced by irradiation [9, 10]. However, these techniques alone are not sufficient to fully reveal the evolution of vacancy-type defects and the redistribution of local electron density in irradiated ceramics. In this context, positron annihilation techniques are of particular importance, as positron lifetime and Doppler broadening parameters exhibit high sensitivity to vacancies, vacancy clusters, open-volume defects, and changes in the electronic environment [11]. Previous PAS-based studies on ZrB_2 have shown that gamma irradiation can significantly alter the size and distribution of vacancy-related defects.

Therefore, a comprehensive approach combining XRD, FTIR, positron annihilation lifetime spectroscopy, Doppler broadening spectroscopy, and electron momentum distribution analysis is essential for a more complete interpretation of irradiation-induced changes in ZrB_2. Such an approach enables the correlation between long-range structural stability and local bond rearrangement, defect formation, and modifications in the electronic structure. In the present study, ZrB_2 powder samples were subjected to gamma irradiation at absorbed doses of 1500 and 3000 kGy. The primary objective of this work is to clarify the effects of gamma irradiation on the crystal structure, surface chemical state, vacancy-type defects, and electron momentum characteristics of ZrB_2.

2. Materials and Methods. The zirconium diboride (ZrB_2) material employed in this study possesses a hexagonal crystal structure, a particle size below 3 μm, and a purity level of 99%. Gamma irradiation of the samples was conducted using a ^{60}Co source in the Gamma MRX-25 facility at the Institute of Radiation Problems, Ministry of Science and Education of Azerbaijan. The irradiation was performed at room temperature with two different absorbed doses, namely 1500 kGy and 3000 kGy. During the process, the source activity was 4160 Ci, and the dose rate was maintained at 6.05 Gy/s.

The crystal structure, phase composition, texture, and grain size of the samples were investigated using X-ray diffraction (XRD) analysis. The measurements were carried out with a PANalytical EMPYREAN diffractometer employing Cu Kα radiation (λ = 1.5405 nm). Data collection was performed in $\theta/2\theta$ scanning geometry over the 20–100° angular range, with a step size of 0.02° and a scanning rate of 1° per minute. The incident angle was fixed at 3°, and all analyses were conducted at room temperature [12].

A Varian 640-IR Fourier-transform infrared spectrometer (FTIR) was employed to investigate the chemical bonding and functional groups in zirconium diboride (ZrB_2) powders subjected to gamma irradiation and subsequent thermal treatment [13]. For sample preparation, ZrB_2 was thoroughly mixed with potassium bromide (KBr) in a mass ratio of 1:300, and pellets with a thickness of 3–7 μm and dimensions of 8.0 × 30 mm² were formed at room temperature under a pressure of 6.0 × 10^4 N/m². The FTIR measurements were carried out over a spectral range up to 1800 cm^{-1}. All data were acquired under controlled experimental conditions, and the resulting spectra were systematically analyzed to evaluate structural modifications induced by gamma irradiation and thermal exposure.

Positron lifetime measurements were carried out using a fast–fast coincidence spectrometer equipped with BaF_2 scintillation detectors. The instrument provided a time resolution of 260 ps (FWHM). A ^{22}Na positron source with an activity of 6.5 μCi, encapsulated in a 7 μm thick titanium foil, was placed between two identical specimens in a sandwich-like arrangement. This configuration was positioned in front of the detectors of the lifetime spectrometer. To ensure sufficient statistical accuracy, data acquisition was performed over a 24-hour period, yielding more than ~3 × 10^6 counts. The recorded spectra were analyzed using the LT software package [14].

For Doppler broadening investigations, a slow positron beam system derived from a positron injector component was utilized. The experimental setup was installed and operated at the Joint Institute for Nuclear Research. Doppler Broadening Spectroscopy (DBS) measurements were conducted using a high-purity germanium (HPGe) detector with an energy resolution of about 511 ±

1.2 keV, enabling accurate detection of annihilation gamma photons. Signal processing was supported by a preamplifier and amplifier chain. The Doppler spectra were evaluated in terms of the S and W shape parameters, and the obtained data were calibrated with the SP-SE software [15].

3. Results and Discussion

3.1. Effect of gamma irradiation on the crystal structure of zirconium diboride

Figure 1 presents the X-ray diffraction patterns of ZrB_2 nanocrystals subjected to gamma irradiation at different absorbed doses. Comparative analysis of the spectra indicates that although some changes occur in the crystal structure with increasing absorbed dose, no formation of new phases or oxide phases is observed. This demonstrates the high radiation resistance of the material. Structural analysis performed using the Rietveld method determined the lattice parameters of ZrB_2 nanocrystals as a = 3.16846 Å, c = 3.53042 Å, and the unit cell volume V = 30.694 Å^3. The obtained results are in good agreement with literature data, confirming the high crystallinity of the synthesized material [16]. A more detailed analysis of the diffraction peaks shows that, particularly for the peaks indexed to the (101) plane, small but systematic shifts along the abscissa axis occur with increasing absorbed dose. Such shifts are associated with changes in lattice parameters and indicate the formation of local distortions in the crystal lattice under irradiation. These local deformations cause partial degradation in the columnar structural elements, leading to the onset of a weak amorphization process in the material. Calculations reveal that at absorbed doses of 300 kGy, 1000 kGy, 1500 kGy, and 3000 kGy, the maximum degree of amorphization is approximately 1.2%. This implies that the material largely preserves its crystalline structure, with disorder appearing only in limited regions [17].

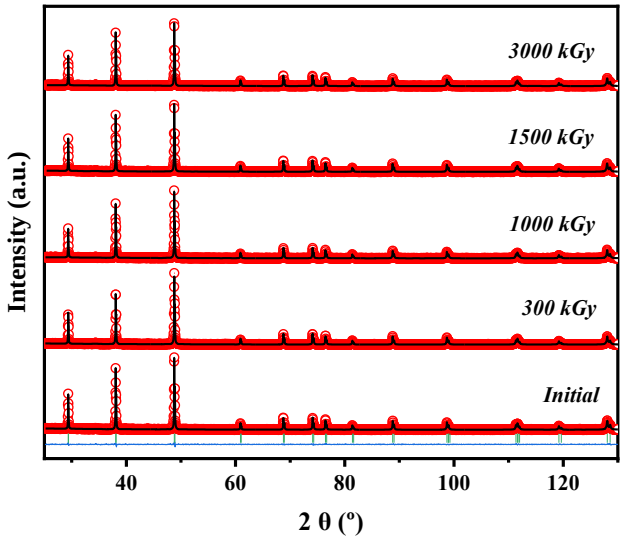

Fig. 1. Diffraction spectra of ZrB_2 nanocrystals irradiated at different absorbed doses. The lattice parameters of the ZrB_2 nanocrystal were determined as a = 3.16846 Å, c = 3.53042 Å, and V = 30.694 Å^3

On the other hand, internal stresses generated within the lattice due to gamma irradiation lead to an expansion of the crystal structure. Analysis of the lattice volume variation shows that at a dose of 300 kGy, the volume remains nearly stable. However, at doses of 1000 kGy and 1500 kGy, a sharp increase in volume is observed. At a higher dose of 3000 kGy, this increase ceases and reaches a stationary state (Fig. 2). This behavior is characteristic of ceramic-based materials and can be explained by the fact that lattice expansion under radiation reaches a maximum and then stabilizes [18]. For ZrB_2 nanocrystals, the maximum lattice volume expansion was determined to be $\Delta V = 0.011$ Å^3. These results indicate that even under high-dose irradiation conditions, the material largely maintains its structural integrity, undergoing only minor structural modifications.

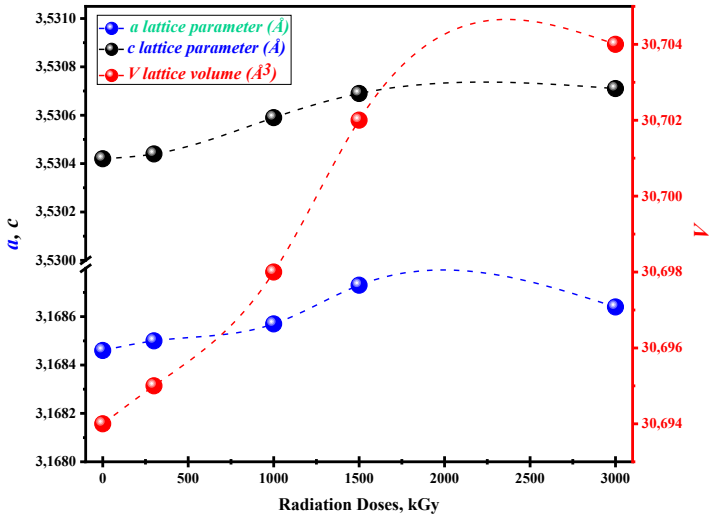

Fig. 2. Variation behavior of lattice parameters in zirconium diboride nanocrystals under gamma irradiation

These XRD results indicate that gamma irradiation does not induce phase transformation in ZrB_2, but it produces slight lattice distortions and limited disorder within the crystal structure. However, XRD mainly reflects long-range structural changes; therefore, to better understand irradiation-induced modifications in surface bonding and local chemical states, FTIR analysis was performed.

3.2. FTIR analysis of zirconium diboride under high gamma irradiation and after thermal annealing

Figure 3 presents the FTIR spectra of zirconium diboride samples before and after thermal treatment at 1173 K, following irradiation at doses of 1500 and 3000 kGy. In the spectrum of the non-irradiated ZrB_2 ceramic, vibrational modes corresponding to chemical bonds are detected at wavenumbers of approximately 650 cm^{-1}, 750 cm^{-1}, 838 cm^{-1}, and 3435 cm^{-1}. These observations are in good agreement with previously reported FTIR studies on ZrB_2-based composites and materials synthesized via sol–gel and carbothermal reduction methods [19], [20].

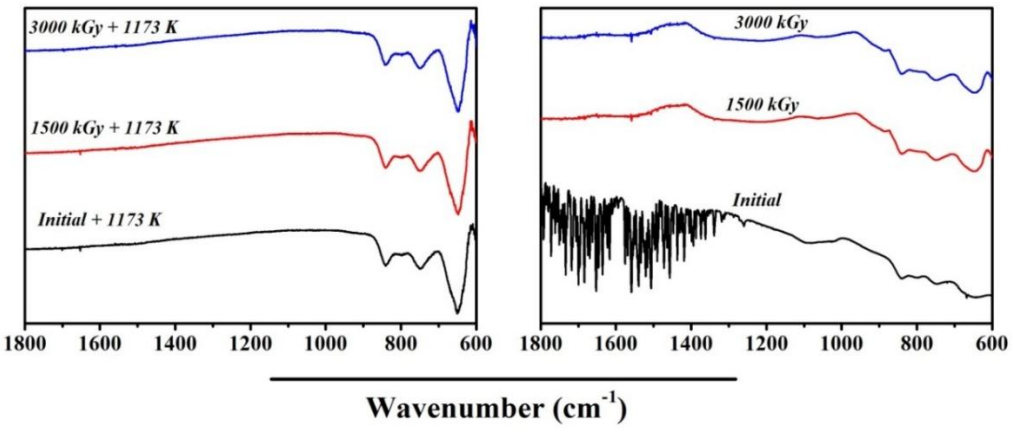

Fig. 3. Fourier transform infrared spectroscopy spectra of the ZrB_2 crystal at different gamma absorption doses and thermal annealing

With increasing irradiation dose (1500 and 3000 kGy), a noticeable enhancement in the intensity of all identified vibrational bands is observed. The FTIR analysis suggests that gamma irradiation promotes the formation of active sites on the surface of zirconium diboride, facilitating

the development of additional oxide-related centers. Furthermore, the results indicate the effective decomposition of hydroxyl and other functional groups present on the surface.

At an irradiation dose of 3000 kGy, the intensities of all peaks in the treated sample become nearly uniform. In unirradiated ZrB_2, the band at ~646 cm^{-1} is assigned to symmetric Zr–O–Zr stretching, while the peak at ~754 cm^{-1} corresponds to asymmetric vibrations. Zr–O bonds are typically observed within the 400–700 cm^{-1} range, although overlapping modes such as ν(Zr–O) + ν(Zr–N) and π(C–CH_3) + ν(Zr–O) with ring distortion may also contribute in this region [21]. The band near 839 cm^{-1} is attributed to ν(Zr–O–C) stretching [22], and the peak at 1287 cm^{-1} corresponds to ν(B=O) vibrations. Since the samples were irradiated under ambient conditions, surface transformations are likely to occur through several mechanisms.

$$ZrB_2(active\ surface) \xrightarrow{\gamma\ radiation} ZrB^{n+}\ (active\ centers: H^{\cdot}, HO^{\cdot}, O^{\cdot}) + H_2O \times B(OH)_3$$

The mechanism of decomposition of water molecules absorbed by the surface of the sample as a result of the action of gamma radiation is given in the following equations.

$$H_2O \times B(OH)_3 \xrightarrow{\gamma\ radiation} B(OH)_4^+ + H^- + B - O$$

$$H_2O \xrightarrow{\gamma\ radiation} H_2O^{\cdot +} + e^-$$

Following thermal treatment, the FTIR spectra exhibit increased intensities at 650, 750, and 838 cm^{-1}, indicating enhanced bond vibrations along with the complete decomposition of hydroxyl and related functional groups. Oxygen species interacting with active Zr sites lead to the formation of Zr–O–Zr and Zr–O–C bonds, confirming surface oxidation. Under ambient irradiation conditions, free radicals facilitate the generation of oxidized functional groups, whose concentration increases with higher gamma radiation doses.

The unchanged vertical slope of the “shoulder” in the broadened peaks across all frequencies suggests a uniform interaction between the active surface and oxygen. Additionally, the concentration of oxide centers on the ZrB_2 surface increases with increasing radiation dose. The FTIR results complement the XRD findings by showing that, although the bulk crystal structure remains preserved, irradiation promotes surface-related chemical modification and oxidation-related bond formation. Since these structural and chemical changes are expected to affect vacancy-type defects and local electron-density distribution, positron annihilation techniques were further applied to examine the defect evolution in greater detail.

3.3. Effect of Gamma Irradiation on Positron Annihilation Parameters in ZrB_2

Positron annihilation lifetime spectroscopy (PALS) measurements were performed to conduct a comparative analysis of the samples before and after gamma irradiation. For each sample, two lifetime components (τ_1 and τ_2) along with their corresponding relative intensities (I_1 and I_2) were determined. Table 1 presents the lifetime components and their relative intensities obtained for zirconium diboride samples after gamma irradiation.

Table 1. Lifetime components and relative intensities of zirconium diboride samples after gamma irradiation

Parameters	initial	1500 kGy	3000 kGy
τ_{mean} (ns)	0.188	0.190	0.193
I_2 (%)	24.5	21.2	16.0
I_1 (%)	75.5	78.8	84.0
τ_2 (ns)	0.232	0.246	0.261
τ_1 (ns)	0.174	0.176	0.181

These lifetime components reflect different electronic environments and interaction mechanisms within the material. The PALS results indicate that these parameters provide important

information about defects, vacancies, and the overall electron density distribution in the crystal structure [23]. In general, the τ_1 component is mainly associated with bulk annihilation processes and small vacancy-type complexes. The increase of this component from 174±2 ps to 181±1 ps suggests that irradiation induces changes in the electron density and in positron–electron interaction conditions within the material. These variations can be explained by the formation of vacancy-type defects or the reconfiguration of pre-existing defect structures.

The τ_2 component is predominantly related to positron annihilation at grain boundaries and within vacancy clusters [24]. After gamma irradiation, this component increases from 232 ± 5 ps to 261 ± 8 ps, indicating the formation of larger defect complexes. At the same time, the decrease in the I_2 intensity from 24.5% to 16% suggests a change in the relative contribution of these defect-related states, which may be associated with a reduction in their population or a redistribution of defect structures. Within the framework of the single-defect trapping model, variations in I_2 are linked to structural changes reflected in the primary lifetime parameters τ_1 and τ_2. Conversely, I_1 increases from 75.5% to 84.0%, indicating a higher contribution of bulk-like or monovacancy-related states to the annihilation process. Overall, the results demonstrate that gamma irradiation significantly modifies the defect structure of ZrB_2 and leads to a redistribution of positron trapping centers within the material.

The effect of gamma irradiation was investigated using variable-energy positron beams, and the results are presented in Fig. 1 (see supplementary materials for details). In both unirradiated and irradiated samples, the S parameter decreases with increasing annihilation depth. An increase in gamma dose leads to a higher concentration of open-volume defects in ZrB_2. For low-energy positrons (0–5 keV, up to ~0.23 μm depth), the elevated S parameter is attributed to enhanced surface annihilation. At higher energies (>10 keV), most positrons annihilate within the bulk of the material. In general, the increase in the S parameter reflects the growing contribution of both surface and bulk defects, indicating an overall rise in defect density. The pronounced increase observed in the 5–10 keV range after a dose of 1500 kGy is likely associated with changes in the electronic structure related to boron vacancies.

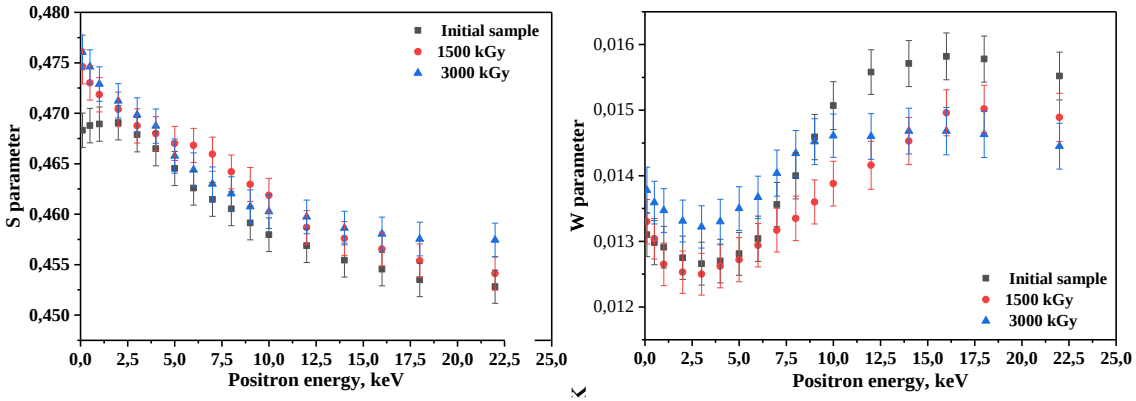

Fig. 4. Positron energy dependence of the S and W parameters for ZrB2 samples exposed to gamma radiation. On the left is the S-E dependence (S- characterizes the low momentum field), on the right is the W-E dependence (W- characterizes the high momentum field)

The combined analysis of the S and W parameters suggests that their variation may indicate positronium formation in regions with low electron density [25], [26]. According to the PLT results, in unannealed samples, the contribution of annihilation in intergranular regions increases with gamma dose, implying the possible formation of long-lived components. In contrast, annealed ZrB_2 samples tend to reach a more stable structural state at higher doses, approaching stoichiometric equilibrium.

This behavior indicates a transition toward a lower entropy state and suggests that, with annealing, the material can maintain its functional properties at gamma doses below 3000 kGy.

3.4. Electron Momentum Distribution in Gamma-Irradiated ZrB_2

The electron momentum distribution (EMD) spectra of gamma-irradiated ZrB_2 nanocrystals at a positron energy of 12 keV are presented in Figure 5. Preliminary analysis reveals the formation of approximately three main peaks corresponding to the degeneracy of electronic energy levels along the depth, with their intensities determined by the overlap of positron–electron wave functions. Similar peak structures have also been reported in other zirconium-based materials [27]. A comparison of peak positions shows that with increasing gamma irradiation dose, the peaks systematically shift toward higher momentum values (to the right). Specifically, the first peak, located at ~10.49×10^{-3} m_0c in the unirradiated sample, shifts to ~11×10^{-3} m_0c at the maximum dose, while the second peak moves from ~12.2×10^{-3} m_0c to ~13.4×10^{-3} m_0c. At an absorbed dose of 3000 kGy, a noticeable decrease in peak intensity is observed, which is associated with an increase in defect concentration [28].

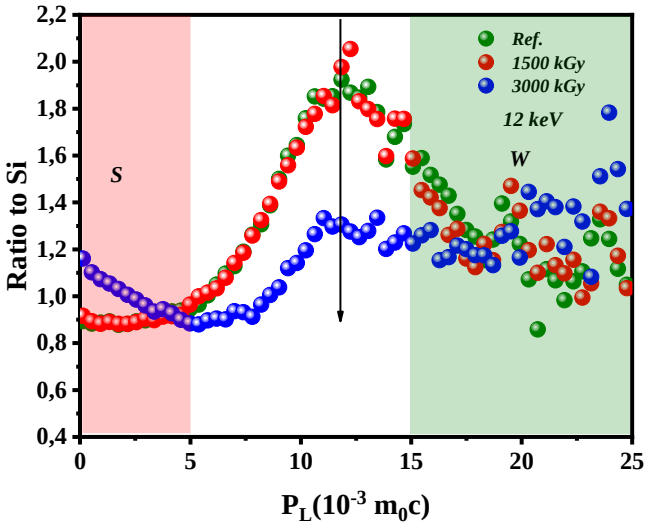

Fig. 5. Influence of gamma irradiation on the electron momentum distribution (EMD) spectra of zirconium diboride samples

Changes observed in the low-momentum region (~4×10^{-3} m_0c) are mainly attributed to open-volume defects acting as positron trapping centers, and the increase in intensity in this region indicates the formation of such defects [29]. The EMD spectra of ZrB_2 exhibit features characteristic of boron-based systems and are consistent with the results reported by Pujari et al. [30]. A significant fraction of positrons annihilates within the boron sublattice, which can be explained by the tendency of boron atoms to gain electrons from the metal matrix and become negatively charged [31]. From an electronic structure perspective, the overall electron density in the Zr–B system is mainly governed by the hybridization of Zr-4d and B-2p orbitals. However, irradiation-induced defects modify this interaction, leading to a redistribution of electronic states in both valence and core regions, which is reflected in the observed changes in the EMD spectra.

Overall, the combined results obtained from XRD, FTIR, PALS/DBS, and EMD demonstrate a consistent picture of irradiation-induced modification in ZrB_2. XRD shows that the material preserves its hexagonal phase with only minor lattice distortion and weak amorphization. FTIR reveals that these structural changes are accompanied by surface oxidation and bond rearrangement. Positron annihilation measurements confirm that gamma irradiation alters the concentration and nature of vacancy-type defects and positron trapping centers, while the EMD spectra indicate that these defects also affect the local electronic structure through redistribution of electron momentum. Therefore, all applied methods consistently show that gamma irradiation does not destroy the

structural framework of ZrB_2, but induces limited and measurable evolution at the crystallographic, defect, chemical, and electronic levels.

4. Conculusion. In this work, the influence of gamma irradiation and post-irradiation thermal annealing on zirconium diboride nanocrystals was comprehensively studied using XRD, FTIR, PALS, and DBS methods. The obtained results demonstrate that ZrB_2 retains its primary hexagonal crystalline structure even after exposure to high gamma doses, which confirms its high radiation resistance. No new phases or pronounced oxide phases were detected by XRD, although small peak shifts and slight lattice expansion indicated the presence of local lattice distortions and weak amorphization effects. FTIR analysis revealed dose-dependent enhancement of bands related to Zr–O–Zr, Zr–O, and Zr–O–C bonds, showing that irradiation promotes the formation of active surface oxidation-related centers. Positron annihilation spectroscopy confirmed substantial changes in the defect structure, including an increase in positron lifetime components and redistribution of trapping centers, which is associated with the formation and evolution of vacancy-type defects and intergranular defect regions. The S and W parameter trends, together with electron momentum distribution results, further supported the conclusion that gamma irradiation modifies both the defect concentration and the local electronic structure of ZrB_2. Thermal annealing contributed to structural stabilization and promoted a tendency toward a more equilibrium defect configuration. Therefore, zirconium diboride can be considered a structurally stable and radiation-tolerant ceramic material with strong potential for applications in environments exposed to high gamma radiation.

Author Contributions. S.S. (Samadov Samir) performed the formal analysis, prepared the original draft of the manuscript, reviewed and edited the manuscript, and supervised the research. N.M.T. (Nguyen Minh Trung) contributed to the validation of the results, data visualization, and preparation of the original draft of the manuscript. E.P. (Evgeni Popov) performed the formal analysis and contributed to the review and editing of the manuscript. A.S. (Anatoliy Sidorin) contributed to the preparation of the original draft, reviewed and edited the manuscript, provided research resources, supervised the study, and approved the final version of the manuscript. All authors have read and agreed to the published version of the manuscript.

Funding. Not applicable.

Data Availability. The data supporting the findings of this study are available from the corresponding author upon reasonable request.

Declarations

Conflict of Interest. The authors declare no conflict of interest.

Competing Interests. The authors declare that they have no competing interests.

Ethical Approval. This article does not involve studies with human participants or animals. Therefore, ethical approval was not required.

Informed Consent. Not applicable.

Acknowledgment. The authors gratefully acknowledge the support and research facilities provided by the Joint Institute for Nuclear Research (JINR), Dubna, Russian Federation.

References

[1] Monteverde F, Bellosi A, Scatteia L. Processing and properties of ultra-high temperature ceramics for space applications. Materials Science and Engineering A. 2008;485(1–2):415–421. https://doi.org/10.1016/j.msea.2007.08.054

[2] Kalavathi V, Bhuyan RK. A detailed study on zirconium and its applications in manufacturing process with combinations of other metals, oxides and alloys: A review. Materials Today: Proceedings. 2019;19:781–786. https://doi.org/10.1016/j.matpr.2019.08.130

[3] Li H, Zhang L, Zeng Q, Wang J, Cheng L, Ren H, Guan K. Crystal structure and elastic properties of ZrB compared with ZrB_2: A first-principles study. Computational Materials Science. 2010;49(4):814–819. https://doi.org/10.1016/j.commatsci.2010.06.027
[4] Loftus N, Olivares J, Crespillo M, Pérez EE, Watts J, Bohannan E, Hilmas GE, Fahrenholtz WG, Graham JM. Microstructural evolution of zirconium diboride irradiated with 5–10 MeV Au ions at room temperature and 570 °C. Journal of the European Ceramic Society. 2026;46:117902. DOI: to be assigned.
[5] Lin YR, Koyanagi T, Sprouster DJ, Petrie CM, Fahrenholtz WG, Hilmas GE, Katoh Y. Response of ^{11}B-enriched ZrB_2 ultra-high temperature ceramic to neutron irradiation at elevated temperatures. Acta Materialia. 2024;276:120111. DOI: to be assigned.
[6] Astecker T, Hosemann P, Balooch M, Lee AN, Crespillo ML, Hattar K, Liedke MO, Wagner A, Polcik P, Kirnbauer A, Mayrhofer PH. Influence of helium ion irradiation on the mechanical properties of high-entropy (Hf,Ta,Ti,V,Zr)-nitride, -carbide and -diboride thin films: A comparative study. Materials & Design. 2025;256:114223. DOI: to be assigned.
[7] Monteverde F, Guicciardi S, Bellosi A. Advances in microstructure and mechanical properties of zirconium diboride-based ceramics. Materials Science and Engineering A. 2003;346:310–319.
[8] Magnuson M, Tengdelius L, Greczynski G, Hultman L, Högberg H. Chemical bonding in epitaxial ZrB_2 studied by X-ray spectroscopy. Thin Solid Films. 2018;649:89–96.
[9] Paxton WA, Özdemir TE, Şavklıyıldız E. Anisotropic thermal expansion of zirconium diboride: An energy-dispersive X-ray diffraction study. Journal of Ceramics. 2016;2016:8346563.
[10] Zhang M, Ma X, Yin J, Zhang Y, Zhang L, Wen J, Dai L, Kuang R, Chen H, Weng X, Zhao X, Liang D, Xie J, Deng L. Microstructure, infrared optical properties and thermal stability of ZrB_2 and double-layer-structure Al_2O_3/ZrB_2 thin films by magnetron sputtering technique. Applied Surface Science. 2020;532:147280.
[11] Karwasz GP, Zecca A, Brusa RS, Pliszka D. Application of positron annihilation techniques for semiconductor studies. Journal of Alloys and Compounds. 2004;382(1–2):244–251. https://doi.org/10.1016/j.jallcom.2004.04.080
[12] Demir E, Mirzayev MN, Popov EP, Horodek P, Genov IG, Siemek K, Mirzayeva DM, Turchenko VA, Bulavin M, Beskrovnyi AI, Valizade AH, Akhundzada HV, Karaaslan SI. Effects of high-energetic $^3He^+$ ion irradiation on tungsten-based composites. Vacuum. 2021;184:109934. https://doi.org/10.1016/j.vacuum.2020.109934
[13] Mirzayev MN. High-flux neutron irradiation of boron trioxide analyzed with Raman and FTIR spectroscopy. International Journal of Modern Physics B. 2020;34(30):2050160. https://doi.org/10.1142/S0217979220501604
[14] Kansy J. Microcomputer program for analysis of positron annihilation lifetime spectra. Nuclear Instruments and Methods in Physics Research Section A. 1996;374(2):235–244. https://doi.org/10.1016/0168-9002(96)00075-7
[15] Dryzek J. Research activities on positron annihilation spectroscopy. Institute of Nuclear Physics, Polish Academy of Sciences (IFJ PAN). Available from: https://ifj.edu.pl
[16] Blumenthal H, Norton JT, Sindeband SJ. Structures of diborides of titanium, zirconium, columbium, tantalum and vanadium. Transactions of the American Institute of Mining, Metallurgical and Petroleum Engineers. 1949;185:749–751.
[17] Bao W, Robertson S, Zhao JW, Liu JX, Wu H, Zhang GJ, Xu F. Structural integrity and damage of ZrB_2 ceramics after 4 MeV Au ions irradiation. Journal of Materials Science & Technology. 2021;72:223–230. https://doi.org/10.1016/j.jmst.2020.08.058
[18] Abiyev AS, Huseynov EM, Hashimov RF. Gamma radiation-induced alterations in nanocrystalline titanium nitride (TiN) particles: A structural perspective. Radiation Physics and Chemistry. 2024;218:111638. https://doi.org/10.1016/j.radphyschem.2024.111638

[19] Han JS, An GS, Choi S. Synthesis of ZrB_2@SiC composite particles through sol–gel and carbothermal reduction. Materials Today Communications. 2022;33:104646. https://doi.org/10.1016/j.mtcomm.2022.104646
[20] Cheng YH, Qi Y, Hu P, Zhou S, Chen G, An J, Jin K, Han W. ZrB_2–SiC–G composite prepared by spark plasma sintering of in situ synthesized ZrB_2–SiC–C composite powders. Journal of the American Ceramic Society. 2016;99(6):2131–2137. https://doi.org/10.1111/jace.14207
[21] Li Y, Chen S, Ma X, et al. A simple way to prepare a precursor for ZrC–SiC ceramics. Journal of Materials Science. 2016;51:5160–5169. https://doi.org/10.1007/s10853-016-9807-3
[22] Bhaskar S, Awin EW, Kumar KCH, et al. Design of nanoscaled heterojunctions in precursor-derived t-ZrO_2/SiOC(N) nanocomposites: Transgressing the boundaries of catalytic activity from UV to visible light. Scientific Reports. 2020;10:430. https://doi.org/10.1038/s41598-019-57270-8
[23] Yabuuchi A, Tanaka M, Kinomura A. Radiation effects in materials studied by positron annihilation. Journal of Nuclear Materials. 2020;542:152473. https://doi.org/10.1016/j.jnucmat.2020.152473
[24] Stewart DM, Meulenberg RW, Lad RJ. Surface and interface studies in thin films. Thin Solid Films. 2015;596:155–159. https://doi.org/10.1016/j.tsf.2015.10.002
[25] Zhu Z, Yao M, Shi J, Yao C, Lu E, Cao X, Wang B, Wu Y. Radiation-induced defects in materials. Journal of Nuclear Materials. 2018;508:12–19. https://doi.org/10.1016/j.jnucmat.2018.05.022
[26] Brusa RS, Macchi C, Mariazzi S, Karwasz GP. Positron annihilation studies in materials science. Acta Physica Polonica A. 2005;107(5):702–711. https://doi.org/10.12693/APhysPolA.107.702
[27] Cizek J, Melikhova O, Prochazka I, Kuriplach J, Kuzel R, Brauer G, Anwand W, Konstantinova TE, Danilenko IA. Defect studies of nanocrystalline zirconia powders and sintered ceramics. Physical Review B. 2010;81:024116. https://doi.org/10.1103/PhysRevB.81.024116
[28] Tuomisto F, Makkonen I. Defect identification in semiconductors with positron annihilation: Experiment and theory. Reviews of Modern Physics. 2013;85(4):1583–1631. https://doi.org/10.1103/RevModPhys.85.1583
[29] Zhang S, Schut H, Brück E, van der Zwaag S, van Dijk NH. Effect of carbon on copper precipitation in deformed Fe-based alloys studied by positron annihilation spectroscopy. Journal of Physics: Conference Series. 2013;443:012027. https://doi.org/10.1088/1742-6596/443/1/012027
[30] Pujari PK, Sudarshan K, Goswami A, Manohar SB. Positron annihilation studies in the MgB_2 superconductor. Physical Review B. 2002;66:012518. https://doi.org/10.1103/PhysRevB.66.012518

https://doi.org/10.58225/sw.2026.1-25-33

ASSESSMENT OF LAND MANAGEMENT AND IMPLEMENTED PROJECTS IN THE MUGHAN PLAIN

Umbetova Sholpan[1*], Baymakhanova Zeynegul[2], Hasanov Farzali[3], Hasanova Arzu[4]
[1,2]Korkyt Ata Kyzylorda University, Kyzylorda, Kazakh*
[3,4]Azerbaijan University of Architecture and Construction, Baku, Azerbaijan
stanumbetova-37@mail.ru, baksy65@mail.ru, farzali.hasanov@azmiu.edu.az
arzu.hasanova@azmiu.edu.az

Abstract. The Mugan Plain is a vast, flat area of strategic and agricultural importance located in southeastern Azerbaijan, between the Kura and Araz rivers. This article analyzes the natural and geographical features of the Mugan Plain, including its topography, climate, soil, and water resources. It examines the large-scale land reclamation and water management projects implemented in the Mugan Plain, particularly during the tsarist period, to develop cotton production. Information is provided on the problem of soil salinization resulting from the rapid expansion of cultivated areas and on the construction of drainage systems to prevent it. The article also examines the construction and operation of the Jafarhan experimental station, as well as errors made in the design and implementation of collector and drainage systems. The Mugan-Salyan water supply system and its operating mode, the purpose of constructing the Main-Mil-Mugan collector, and the significance of these infrastructures in terms of water use regulation are discussed. The article also provides a detailed analysis of why irrigation and drainage systems have not performed as intended over the past 40 years. Finally, it provides extensive information on proposed measures to efficiently use arable land and water resources.

Keywords: canal, irrigation water, aquifers, collector, water yield, soil loss, efficient use

Key findings: The natural conditions of the Mugan Plain have made irrigated agriculture the dominant form of land use. Rapid agricultural expansion caused soil salinization due to inadequate drainage systems. Major water management infrastructure has played a key role in regulating water use, but has not functioned effectively for decades. The article examines the problems in detail and puts forward ideas and proposals for the sustainable use of land and water resources and the modernization of irrigation and drainage systems.

Cite this article as: *S. Umbetova, Z. Baymakhanova, F. Hasanov, and A. Hasanova, "ASSESSMENT OF LAND MANAGEMENT AND IMPLEMENTED PROJECTS IN THE MUGHAN PLAIN," SW AzUAC, vol. 1, 2026, doi:10.58225/sw.2026.1-25-33*
Article history: *Received: 05 December 2025 / Revised: 18 January 2026 / Accepted: 10 February 2026*

1. **Introduction:** The Mugan Plain covers the territory from the state border with the Islamic Republic of Iran, along the right bank of the lower reaches of the Kura and Araz rivers, to the Caspian Sea (Fig. 1). The territory is divided into the Talysh-South Mugan Plain, the North Mugan Plain, covering the vast delta of the Araz River, and the Salyan Plain near the mouth of the Kura River [1, 4]

Fig.1. Schematic plan of the Mugan Plain in 1869

On the Mugan Plain, the slope of the earth's surface decreases towards the Caspian Sea. On the Salyan Plain, it is about minus 22.0–28.0 m. In general, the height of the earth's surface on the Mugan Plain fluctuates between minus 28.0 m and plus 10.0 m.
The climate is of the semi-desert, dry-steppe type. The average monthly air temperature is 14.0–14.50 °C. The maximum temperature is 42.00 °C, and in frosty weather - minus 26.00 °C. The average annual precipitation is 250–300 mm, and the average annual evaporation is 1000–1200 mm (Table1).

Table 1. Natural and Geographical Features of the Mugan Plain

Parameters	**Indicaters**
Geographical Location:	Located in the southwestern part of the Kura-Araz Lowland
Area:	Approximately 450,000 hectares
Climate Type:	Dry subtropical (hot summers, mild winters)
Average Annual Precipitation	250–350 mm
Main Soil Types:	Gray-brown soils, gray soils, and solonchaks
Main Water Sources:	Kur and Araz Rivers, groundwater

Harvesting on the Mugan Plain without irrigation is impossible. Starting from the end of May, with warming, the normal development of plant root systems ceases due to a lack of water in the upper soil layer. If water does not reach the cultivated lands, fertile lands become unsuitable for human use. Arable lands are valuable when there is irrigation water [2,3,4].

Historians of the 19th century described the Mugan Plain as a green steppe and a sparsely populated region in the first spring months. Chroniclers who visited the Mugan and Mil Plains in the summer months called this region a desert. The Mugan Plain is a vast territory, the surface of which is so smooth that in summer you can see apples fallen on the ground from afar. In autumn and winter, the formation of a green cover turned it into a wintering place for people engaged in cattle breeding [1,2,3].

The Mugan Plain includes the territories of the Saatli, Sabirabad, Bilasuvar, Salyan, Neftchala and partly Imishli districts. Human food products are created when arable land comes into contact with water: “Soil + water = forage plants = wildlife = harvest.”

2. Materials and methods. The history of irrigation and land reclamation activities carried out by the population living mainly along the banks of the Araz and Kura rivers in the Mugan Plain dates back to ancient times. Local residents directed water into canals, which they drew during the

spring floods. Using the water reserves accumulated in the canals and ditches, they irrigated the crops they grew several times. These canals, which remained dry during the rest of the year, were called "dry ditches". In later years, water wheels installed on the rivers were used. Camels, horses and oxen were used to drive the wheels. In the second half of the 19th century, there were about 4,000 water wheels in the Mugan Plain [9,10].

Mechanical irrigation of the Kura River began in 1900 with a pump installed near the city of Salyan. In 1904, 5 pumping stations brought from Germany and England were located on the banks of the Kura River. In 1915, 50 thousand hectares of cultivated land were provided with irrigation water by about 100 pumping stations installed on the banks of the Kura River, of which 25 thousand hectares were used for growing cotton.

M. Avdiyev wrote in his work "Mugan-Salyan Plain", published in Baku in 1927: "In the 1860-1870s, there was not a single settlement in the middle part of the Mugan Plain where the population lived permanently. Lands suitable for cultivation served as a temporary place of residence for people engaged in cattle breeding in the winter months [2,3].

The Mugan Plain was annexed to the territory of the Russian state according to the Treaty of Gulistan, concluded between Tsarist Russia and the Islamic Republic of Iran in 1823. By the end of the 19th century, cotton, considered the main raw material for the textile industry developing in Tsarist Russia, was mainly purchased abroad. Beginning in 1861, the selling price of cotton in the world increased by about 4-5 times, and the Tsarist government, having assessed the current situation, began research and exploration work in Azerbaijan and the Central Asian regions in order to increase cotton production within the country [7,9].

Researchers assumed that the Mugan Plain had favorable natural conditions for cotton harvesting due to the receipt of water from the Araz River and the construction of canals.

Thus, in 1900, melioration and water works began to increase cotton production in Azerbaijan. In accordance with the colonial policy, priority was given to attracting labor, mainly from Russia, to the Mugan Plain, located on the border with the Iranian state. For the complete development of territories with fertile lands, a policy of settling Russians among the population of the same nationality was carried out [2,7,8,9].

In the Mugan Plain in 1900-1915, the main canals of Sabir (Upper Golistin), Mursalli (Lower Mugan), Narimanov (Middle Mugan) and Azizbekov (Upper Mugan) were built, through which water from the Araz River flowed (Fig. 2)

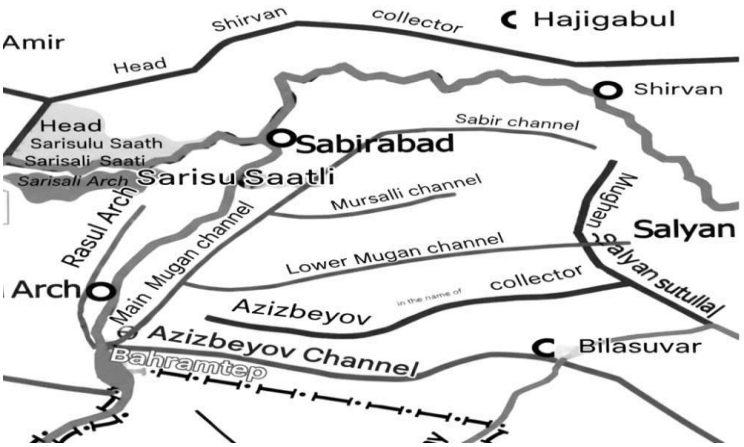

Fig.2. Schematic plan of the Mugan Plain in 1970

Under the influence of these canals, in 1917, 26.5 thousand hectares of cultivated land were provided with irrigation water for growing cotton. The total length of canals laid in the river bed was 297.2 km. The canals were laid mainly using manual labor and other tools, which was due to the

physical strength of the builders. New settlements and villages were created for the workers. In 1900-1915, 14 villages with a predominantly Russian population were built in Northern Mugani, and 20 in Southern Mugani, which were given Russian names [6,9,10,11].

It follows from the research that after the completion of the construction of 4 main canals, it was predicted that 162.3 thousand hectares of cultivated land would be provided with irrigation water in volumes corresponding to the need for water, but the harvest was only collected from 26.5 thousand hectares. Thus, the water level in the Araz River regularly rose during the summer months. Since the corresponding hydraulic structures were not built at the water intake points of the main canals, the entrances were temporarily closed with wood and other materials to prevent water from entering the canals. After the water level in the river dropped, it was necessary to clear the canal entrances from accumulated sediment. It took about 20-30 days to complete this work manually. Due to delays in the irrigation regime during cotton cultivation, problems arose in the development of crops. Crop plants were destroyed or seriously damaged at the initial stage, and the expected yield was very low. Lebedev N.A. In his work "Irrigation Management of Mugani", published in Tbilisi in 1918, he wrote about the Lower Mugan Main Canal (now Murselli): "The residents of the Lower Mugan main Canal's influence zone are dissatisfied and unhappy…, there is not enough water, the untimely provision of fields with irrigation water in the required volumes has become chronic, there has not been a single year when irrigation was carried out according to the norm" (Mustafayev *et al*., 2025; Ahmadova *et al*., 2025; Mustafayev, 2012; Mustafayev, 2015; Mustafayev *et al*., 2022; Zhapayev *et al*., 2023).

After the overthrow of the tsarist government in Russia in 1917, a certain part of the forcibly displaced Russians, taking advantage of the uncertainty that arose before 1920, returned to their native lands.

An average of 8 centners of crops were harvested from one hectare of cotton crops. In 1921, 552.7 thousand hectares of cultivated land were irrigated on the territory of the Republic of Azerbaijan. Cotton was grown on 124 thousand hectares of irrigated land, of which 36 thousand hectares were in the Mugan Plain, 35 thousand hectares in the Shirvan Plain, and 23 thousand hectares in the Mil-Karabakh Plain [2,3].

The foundations for the use of tractors on irrigated lands were laid in the Mugan Plain. In 1923-1925, 18 thousand hectares of land were cultivated by tractors imported from America, Germany, and Czechoslovakia. The first tractor base in the Soviet Union was created in Mugan. In 1926, the Mugan Land Reclamation Construction Department was created, which carried out land reclamation construction in Mugan.

3. Results and discussion. During the period of effective use of arable land in the Mugan Plain, that is, in the first years of the 20th century, a decrease in the yield of crops was observed from year to year. In 1901–1904, specially created commissions conducted ground research and established that the process of salt accumulation began in the upper part of the soil in cultivated areas used by plants. It was from these years that the term "soil salinization" began to be used in melioration. The main cause of soil salinization was the irrigation of cultivated areas. Under the influence of irrigation water supplied to cultivated areas in excess of the norm, infiltration waters from canals laid in the river bed, and water seeping into areas along the river during the spring flood, the process of salt accumulation in the plant layer began as a result of groundwater with a mineral content of 5–50 g/l, located at a depth of 3–4 meters from the surface of the earth, approaching the surface of the earth. Over the years, the degree of soil salinization has increased. As a result, the yield of cultivated plants decreased year after year [8,9].

Thus, a more complex problem arose – land reclamation in cotton-growing regions, the solution of which required large funds. To flush saline soils of salts, it was necessary to build collector-drainage systems and carry out large-scale flushing works.

Specialists of the tsarist government began implementing the project in Turkmenistan in 1912, and in 1914, in the territory of the village of Jafarhan, now the Saatli district. The implementation

of the project was suspended due to the First World War. In Soviet times, the construction of the Jafarhan drainage system station was completed in 1929-1931 (Fig.3).

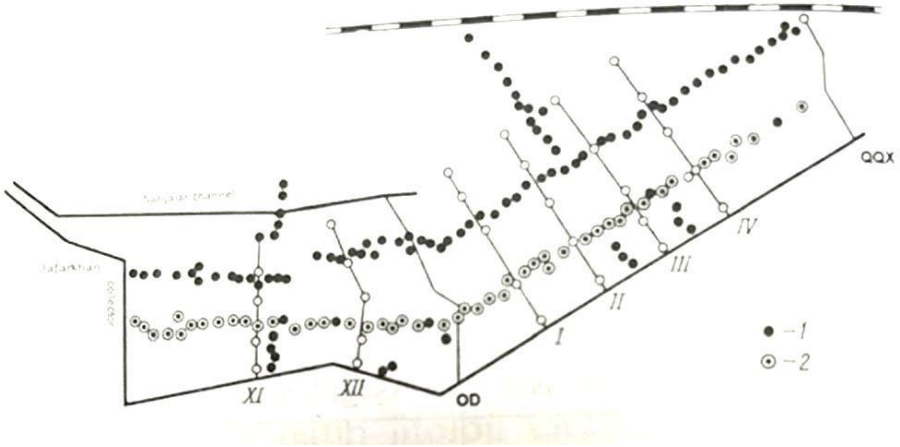

Fig.3. Schematic plan of the Cafarkhan experimental station

Based on the results of the research conducted at the Mugan experimental field, the construction of collector-drainage systems began throughout the Mugan Plain. It should be noted that mainly open-type drains were built on the plain

The results of numerous studies conducted in subsequent years showed that serious shortcomings were made during the capital flushing. Salt water collected from drains built in certain areas of Mugan was collected in collectors and discharged to neighboring areas. That is, in a certain part of the territory, the soil was cleared of salts, and in another part, it caused soil salinization. This process lasted from 1931 to 1953. The construction of the Mugan-Salyan water collection collector, which will discharge drainage water built on the Mugan Plain into the Caspian Sea, was carried out in 1950-1953 and was put into operation in 1953. The collector's impact area was 172 thousand hectares (Fig. 4).

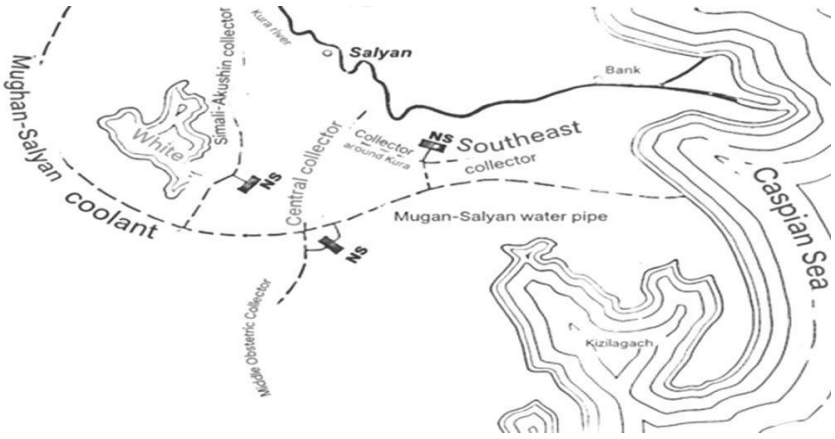

Fig.4. Schematic plan of collectors built on the Mugan-Salyan plains

The Mugan-Salyan watershed, starting from Northern Mugan, passes through the Middle Akushin Highlands and is discharged into the Caspian Sea by a pumping station built in the village of Sarygamysh in the Neftchala district.

The length of the watershed is 875 km, the water flow at the beginning is 21.0 m³/sec, at the mouth, 36.0 m³/sec. The total water flow at the pumping station is 21.0 m³/sec.

Since the watershed, 56 km long, up to the pumping station is semi-dugout and semi-fill, certain problems are observed in this section. Since 1970, the volume of melioration activities carried out on the Mugan Plain has increased from year to year, so the average annual flow rate at the pumping station was observed in 1954 at the level of 6.7 m3/sec, in 1959 - 12.3 m3/sec, in 1968 - 22.73 m3/sec, in 1970 - 27.19 m3/sec, in 1978 - 55.03 m3/sec. When considering the average observation data by month during the year, it becomes clear that in March 1968, the flow rate was 93.7 million m3, and the average monthly flow rate was 34.98 m3/sec, which is 60 percent more than the pumping station indicators (21.0 m3/sec). Since 1962, in the 3-4th months, the process of rising water level along the length of the reservoir towards the source was observed, as a result of which the reservoir did not operate in accordance with the design indicators. That is, the groundwater level in the adjacent territories rose. The process of soil salinization in the plant layer began on arable lands. Professor Alimov A.K. presented observation data on the average annual groundwater level and its mineralization in the territories affected by the Mugan-Salyan reservoir in the 1930s-1990s in tabular form.

When considering the indicators given in the table, it becomes clear that in 1930, the average depth of groundwater on the Mugan Plain was 3.84 m, average mineralization was 37.15 g/l, and in 1980 these indicators were 1.78 m in depth and 22.6 g/l in mineralization. That is, over the past 50 years, the depth of groundwater has increased by 2.0 m, and mineralization has decreased by 14.55 g/l.

Since 1930, the area of irrigated land on the Mugan Plain has increased, and the groundwater level has approached the surface due to the influence of irrigation water and filtration water from canals. The decrease in mineralization is due to the influence of drainage systems put into operation. Studies have shown the need to build a new collector on the Mugan Plain to discharge mineralized water collected from drainage systems into the Caspian Sea. Construction of the Main Mil-Mugan Collector began in 1984 (Fig.5).

Fig.5. Schematic plan of the section of the Main Mil-Mugan collector passing through the Mugan plain

It is planned that this collector will start in the Shamkir region on the right bank of the Kura River and will drain water from the collector-drainage systems of the Kura-Araz plain into the Caspian Sea.

The length of the collector in the upper reaches is 59 km: the first section was completed in 1994, to the Araz River, with a length of 52.7 km; the second section was completed in 2000, and the third section, with a length of 31.7 km, to the junction with the Mil-Karabakh collector, was put into operation in 2006

In connection with the connection of the Mugan-Salyan water pipeline to the Main Mil-Mugan collector in the upper reaches of the first section, the operation of the pumping station in this section was stopped. Thus, the consumption of electricity allocated to the pumping station ceased. The problem caused by the long-term rise in the water level in the upper section of the Mugan-Salyan aqueduct has also been eliminated (Table 2).

Table 2. The economic and environmental impact of the reclamation measures was assessed using the following indicators

Indicator	Before Project	After Project	Percent Change
Soil salinity level (g/L)	4.8	2.1	-56%
Groundwater depth (m)	1.2	2.4	+100%
Crop yield (c/ha)	18	32	+77%
Irrigation efficiency (%)	45	68	+23%

Since the beginning of the construction of the Main-Mil-Mugan collector (1984), its upper section has been in operation for 40 years. 25 years have passed since the construction of the section 20-30 years. Thus, the existing drains, culverts, and collectors in the influence zone of the Main-Mil-Mugan collector no longer function in accordance with the design parameters. Almost the majority of melioration structures built on the Mugan plain need reconstruction. Water losses from the canals of the existing irrigation systems amount to about 50 percent. Due to the fact that the irrigation and collector-drainage systems are built in an open way, the existing arable land is used inefficiently. 60-80% of the land in the cultivated areas is saline to varying degrees. The average depth of groundwater is about 1.2-1.5 m.

4. Conclusions. The conducted research and observations show that the technical condition and operation of the existing irrigation and collector-drainage systems in the Mugan Plain limit the possibilities for the efficient use of land resources. In this regard, to increase the productivity of cultivated lands and improve the melioration condition of the lands, it is proposed to implement the following measures:

Improvement of irrigation canals: To prevent water losses in open-type irrigation canals, it is necessary to reconstruct the main and field canals using modern technologies, and design field canals using a closed structure. It is necessary to limit the use of surface irrigation methods and expand the use of progressive irrigation technologies, such as drip and rain irrigation

Modernization of drainage systems: To effectively drain ground and surface water entering the territory, it is necessary to build drains and field culverts of a closed structure, which will create conditions for putting additional crop areas into operation.

Reconstruction of auxiliary hydraulic structures: Outdated hydraulic structures on existing collector-drainage and irrigation systems must be reconstructed in accordance with modern technical requirements, and control systems must be automated.

As a result of the implementation of these measures, more efficient use of arable lands of the Mugan Plain will be ensured, the melioration condition of the lands will be improved, and agricultural productivity will be increased.

Author Contributions. S.U. (Sholpan Umbetova) conceived the research idea, developed the conceptual framework of the study, designed the research methodology, supervised the investigation, analyzed and interpreted the data, and reviewed and edited the manuscript. Z.B. (Zeynegul Baymakhanova) collected the research materials, participated in the data analysis and interpretation, prepared the original draft of the manuscript, and contributed to the revision of the manuscript. F.H. (Farzali Hasanov) contributed to the interpretation of the results, reviewed and edited the manuscript, and provided scientific guidance. A.H. (Arzu Hasanova) assisted in data collection, validated the research findings, participated in manuscript editing, and approved the final version of the manuscript. All authors have read and agreed to the published version of the manuscript.

Funding. The authors received no financial support from any funding agency, commercial organization, or not-for-profit institution for the research, authorship, and/or publication of this article.

Data Availability. The data supporting the findings of this study are available from the corresponding author upon reasonable request.

Declarations

Conflict of Interest. The authors declare that they have no competing interests or conflicts of interest.

Ethical Approval. This article does not contain any studies involving human participants or animals performed by any of the authors.

Informed Consent. Not applicable.

References

[1] Volobuyev VR. *Mugan and Salyan Steppe*. Baku; 1951.

[2] Pashayev EP, Hasanov FH. *History and Development Path of the Azdovsuteslayiha Institute*. Baku; 2010.

[3] Pashayev EP, Hasanov FH. *Azdovsuteslayiha Institute – 80*. Baku: Sharq-Qarb; 2013.

[4] Hasanov FH, Agamamedova AB. Projects of melioration structures implemented on the Mugan Plain and the environmental situation. *Journal of Ecology and Water Management*. 2014;1:36–42.

[5] Hasanov FH, Bayramova AB, Kerimli BM. Study of land reclamation structures on the Mugan Plain and the situation after the construction of the Main Mil-Mugan Collector. *Journal of Ecology and Water Management*. 2019;2:49–55.

[6] Hasanov FH, Hasanova AK, Mamedova NF. Study of the operating mode of the Mugan-Salyan Reservoir. *Journal of Ecology and Water Management*. 2020;1:44–48.

[7] Akhmedzade AJ, Gashimov AJ. *History of the Creation of the Mugan Melioration Experimental Station and Its Role in the Development of Melioration Science*. Baku; 2014

[8] Hasanov FH, Khalilova AA, Valiyeva SA, Maharramova SY, Hasanova AX. Operational dynamics and environmental conditions of the reservoir-impacted region. *International Journal on Technical and Physical Problems of Engineering*. 2025:1–6.

[9] Mustafayev MG, Alizade SHV, Mustafayev FM, Akhundov AY, Hasanova AX. Anthropogenic impact on soil salinization and its management in irrigated areas of the Mughan Plains. *SABRAO Journal of Breeding and Genetics*. 2025;57(4):1688–1698.

[10] Mustafayev M. Water and physical characteristics of irrigated soils in the Mugan-Salyan Massif. *Journal of Water and Land Development*. 2012;17:61–67. https://doi.org/10.2478/v10025-012-0034-8

[11] Mustafayev M, Tukenova Z, Alimzhanova M, Ashimuly K, Mustafayev F. The influence of fertilisation on the water-salt regime in the conditions of the Mugan-Salyan Massif, Azerbaijan. *Journal of Water and Land Development*. 2022;55:276–285. https://doi.org/10.24425/jwld.2022.142330

[12] Mustafayev M. Criteria for the evaluation of the reclamation status of soils in the Mugan-Salyan Massif. *Journal of Water and Land Development*. 2015;24:21–26. https://doi.org/10.1515/jwld-2015-0003

[13] Zhapayev R, Kunypiyaeva G, Ospanbayev Z, Sembayeva A, Ibash N, Mustafayev M, Khidirov A. Structural-aggregate composition and soil water resistance based on tillage regimes in Southeast Kazakhstan. *SABRAO Journal of Breeding and Genetics*. 2023;55(5):1821–1830. https://doi.org/10.54910/sabrao2023.55.5.28

[14] Zhapayev R, Toderich K, Kunypiyaeva G, Kurmanbayeva M, Mustafayev M, Ospanbayev Z, Omarova A, Kusmang A. Screening of sweet and grain sorghum genotypes for green biomass production in different regions of Kazakhstan. *Journal of Water and Land Development*. 2023;56:118–126. https://doi.org/10.24425/jwld.2023.143723

[15] Mustafayev M, Sadigov R, Mirsalahov M, Gurbanov E, Jalilova L, Mustafayev M, Ahmadova A. Salts deposition and groundwater mineralization effect on soil salinization in the Shirvan Plain and Ganja-Gazakh Massif, Azerbaijan. *SABRAO Journal of Breeding and Genetics*. 2025;57(5):2147–2155. https://doi.org/10.54910/sabrao2025.57.5.35

https://doi.org/10.58225/sw.2026.1.34-43

THE ENVIRONMENTAL IMPACT OF AI-DRIVEN INNOVATION: EVIDENCE FROM THE UNITED STATES

Mukhtarov Shahriyar[1*], Kartal Mustafa Tevfik[2] ,Ayhan Fatih[3]
Vistula University, Warsaw, Poland Division of International Studies,
Korea University, Seoul, South Korea
Bandırma Onyedi Eylül University, Balıkesir, Türkiye
s.mukhtarov@vistula.edu.pl, mustafatevfikkartal@gmail.com, fayhan@bandirma.edu.tr

Abstract. This study investigates how Artificial Intelligence (AI)-related patents, income, trade openness, renewable energy generation and energy intensity influence carbon dioxide (CO_2) emissions in the United States. The empirical analysis is conducted using Canonical Cointegration Regression (CCR), Dynamic Ordinary Least Squares (DOLS), and Fully Modified Ordinary Least Squares (FMOLS) estimators. The empirical findings show that AI- related patents, income, trade openness, and energy intensity have positive and statistically significant effects on CO_2 emissions, whereas renewable energy generation contributes to reducing emissions. Furthermore, the interaction term between renewable energy generation and AI-related patents is negative and statistically significant, indicating that renewable energy generation moderates the emissions-increasing effect of AI-related technological innovation. This result suggests that the environmental implications of AI depend critically on the energy structure supporting its development and deployment. Accordingly, the study recommends that policymakers promote the integration of AI with renewable energy systems, reduce energy intensity in industry and transport through AI-enabled efficiency improvements, prioritize energy-efficient AI projects, and strengthen trade in AI-based green technologies. These measures are essential for ensuring that AI contributes to decarbonization rather than reinforcing carbon-intensive growth.

Keywords: US; CO2 Emissions; AI-related patents, Economic Growth; Renewable Energy Generation; Sustainable Development

Cite this article as: *S. Mukhtarov, M. T. Kartal, and F. Ayhan, "THE ENVIRONMENTAL IMPACT OF AI-DRIVEN INNOVATION: EVIDENCE FROM THE UNITED STATES," SW AzUAC, vol. 1, 2026, 10.58225/sw.2026.1-34-43*
Article history: *Received: 05 December 2025 / Revised: 18 January 2026 / Accepted: 10 February 2026*

1. Introduction. In recent years, the negative impacts of climate and environment related issues have increased. Accordingly, the interest of all countries and communities in environmental issues has been developing. In this context, the related parties have been considering a set of factors, including both economic and non-economic, to empirically understand the causes of negative progress over the years [1].

According to the current, both economic growth [2] and energy intensity [3] have been among the causes of environmental change. Also, some literature has considered the role of trade openness [4]. Although those factors have been used in the literature, contemporary literature has recently begun to consider the role of AI [5, 6] due to its growing prominence. However, the current use of AI algorithms is mainly driven by technological issues, leading to high energy consumption and harming the environment. On the other hand, AI-related patents have largely focused on environmental progress. Nevertheless, it is not certain whether the use of AI is beneficial or not for environmental progress.

Artificial intelligence (AI) is a set of technologies that enable computer systems to perform functions such as perception and reasoning, using machine learning, deep learning, and other techniques. As a result of these functions, AI is becoming capable of replacing some human tasks and

assisting in others [7]. In recent years, AI, which has significantly impacted life, not only increases productivity but also encourages complementary innovations [8]. From this perspective, the importance of AI cannot be ignored, and examining its fields of study is crucial. While the scope of artificial intelligence (AI) is broad today, its effects on the economy vary. Its impact on production processes, productivity, competitiveness, trade, energy, and labor creates both risks and opportunities in economic activity. AI, which has a general impact on growth and prosperity, can support growth by increasing production capacity, economies of scale, and the pace of innovation. According to UNCTAD [9], this situation also includes some drawbacks. The report emphasizes that because AI development is being undertaken by a small number of countries and companies, it may create inequality between countries. From this perspective, the greatest benefit is obtained by countries with strong digital infrastructure and high-tech investments. Globally, the inclusive role of artificial intelligence needs to be addressed through global cooperation. The WTO [10] highlights that artificial intelligence can increase trade in services and affect foreign trade by improving firms' international production-sharing and logistics processes. Artificial intelligence emerges as a key driver of international trade, reducing trade costs and increasing productivity through two main channels. AI-based tools can facilitate international trade by optimizing logistics, reducing language barriers, and automating customs procedures. Simulations conducted by the WTO suggest that AI can increase efficiency in international trade, potentially boosting global trade by 34% by 2040. Therefore, AI stands out as a crucial technology in international trade. In addition to production processes, efficiency, and international trade, the potential of artificial intelligence to transform the energy sector is a prominent issue. While it is well known that AI depends on energy, its development requires a cost-effective, sustainable electricity supply.

The IEA [11] report indicates that electricity consumption in data centers has increased by 12% from 2017 to the present. This shows that not only economic growth and efficiency, but also energy demand and infrastructure costs are affected. The report also states that different energy sources will be needed to meet the increasing electricity demand in data centers. It is predicted that renewable energy sources and systems, such as battery storage, will meet this increased electricity demand. Another prominent issue in the field of artificial intelligence and the energy sector is the use of AI to optimize energy and mineral supply, electricity generation, and consumption, thereby supporting energy efficiency [12]. However, alongside its potential benefits, the high electricity consumption of data centers raises concerns that AI will increase emissions and worsen environmental pollution [13,14]. Currently, data center emissions are estimated at 180 million tons of CO_2, and if current trends continue, this figure is projected to reach 300 million tons by 2035 [11]. From this perspective, the impacts of AI on emissions vary. Positive impacts depend on regulatory frameworks and the management of the impact of energy supply on carbon intensity.

The increase in carbon emissions, in addition to the environmental problems it creates in countries, also leads to significant problems such as global warming and climate change worldwide. Therefore, minimizing the environmental damage caused by carbon emissions generated to meet energy demands has become an important issue [15]. On a global scale, countries have also accepted the need to minimize environmental damage and have set targets to increase energy efficiency [16]. The literature contains widespread findings indicating that renewable energy sources reduce carbon emissions by decreasing dependence on fossil fuels [17-20]. Therefore, increasing the use of renewable energy sources in line with the Sustainable Development Goals is of great importance today [21].

Beyond their environmental significance, renewable energy sources also affect countries' production and foreign trade structures. In this context, renewable energy production and trade deficits become closely related issues [22]. Increasing renewable energy production reduces countries' dependence on energy imports, thereby reducing trade deficits and increasing competitiveness [23]. However, this may not always be the case. The transition to renewable energy, due to the high initial investment costs, may create dependence on imported technology and

equipment in the initial stages [24]. When both situations are considered together, the relationship between renewable energy and trade openness is shaped by countries' technological capacities and policies. At this point, artificial intelligence forms a common framework with its multifaceted impacts on international trade, the energy sector, production channels, and environmental sustainability.

Considering the rising critical importance of AI use in many areas, along with the aforementioned factors, this research aims to uncover the role of AI on CO_2 emissions. In doing so, the study focuses on the USA as the leading economy in the world, uses yearly data from 1985 to 2021, and applies cointegration-based regression methods (i.e., CCR, DOLS, & FMOLS) for empirical analysis. The results of the econometric estimations reveal that AI- related patents, income, trade openness, and energy intensity have a positive impact on CO_2 emissions in the USA. In contrast, the interaction between AI-related patents and REG has a negative impact. By considering these determinations, the study discusses various policy recommendations that can help the USA benefit from AI to support decarbonization.

The remaining parts of the study are as follows: Section 2 explains the methodology and data used; Section 3 presents the empirical results; and Section 4 concludes with policy recommendations.

2. **Materials and methods.** A large body of studies investigates the factors influencing CO_2 emissions, mostly using the Environmental Kuznets Curve (EKC) and STIRPAT frameworks, which primarily focus on income and population impacts. Yet these approaches face well-documented shortcomings, as noted by Ezzati et al. [25], Tisdell [26], Dinda [27], Brock and Taylor [28], and Berk et al. [29]. In light of these limitations, scholars such as Brock and Taylor [28], Criado et al. [30], and Berk et al. [29] argue for adopting broader, theoretically stronger modeling strategies. Recent empirical literature increasingly integrates AI into analytical frameworks. Notably, scholars such as Wang et al. [12, 16], Xia and Ahmad [31], Yang et al. [32], and Kartal et al. [33] systematically employ AI indicators to evaluate its environmental impacts.

AI technology alone may not necessarily lower or increase carbon emissions. The real impacts depend on several factors, including how and where the technology is used. AI technologies may make energy use much more efficient, but they also consume significant energy, particularly in data centers and cloud computing. If renewable sources primarily power the energy system, the growing energy demand for AI applications may not significantly increase carbon emissions. But if the energy system is heavily dependent on fossil fuels, the same AI technology may have the opposite effect, causing emissions to rise. Therefore, the incorporation of interaction terms is grounded in both theoretical and practical reasoning. Considering that the impact of AI patents on CO_2 emissions may depend on the level of renewable energy, an interactive model specification is proposed below. This model aims to empirically evaluate whether the impact of AI technologies on CO_2 emissions varies across energy structures. Additional economic, energy, and trade-related variables have also been included in this model. Considering the above-mentioned facts, the following model specification is proposed:

$$LCO2,t = \alpha 0 + \alpha 1 LAIPt + \alpha 2 LGDPt + \alpha 3 LTOt + \alpha 4 LEIt + \alpha_5 REG_t + \alpha_6 LREG_t * LAIP_t + \varepsilon_t \quad (1)$$

where CO_2 denotes emissions per capita, GDP denotes GDP per capita, OP denotes international oil price, REG denotes renewable energy generation, and εt is an error term of the econometric model. Given its status, the signs of $\alpha 1$, $\alpha 2$, $\alpha 3$, and $\alpha 4$ are anticipated to be positive for the United States while the sign of $\alpha 5$ is expected to be negative. In addition, the objective of this study is to empirically estimate whether the impact of AI technologies on CO_2 emissions varies across levels of renewable energy. Therefore, the sign of $\alpha 6$ is expected to be negative and statistically significant. This means that as the share of renewable energy increases, the emission-reducing impact of AI patents becomes stronger. Eq. (1) may be assessed using traditional econometric methods (see,

for example, Jin, [34]; Jin & Kim, [35]; Mukhtarov et al. [36]).

Specifically, the Canonical Cointegration Regression (CCR) [37], Dynamic Ordinary Least Squares (DOLS) [38, 39], and Fully Modified Ordinary Least Squares (FMOLS) [40, 41] were utilized.

The stationarity properties of the variables under investigation were analyzed through the Augmented Dickey-Fuller (ADF) test by Dickey and Fuller [42]. Furthermore, cointegration among the variables was assessed using the Engle-Granger cointegration test [43].

The study utilizes data from 1985 to 2021. CO_2 is measured in tons per person. The total number of AI-based patents indicates the presence of AIP. GDP is represented as gross domestic product per capita in US dollars at 2015 values. The REG represents the total amount of renewable energy production (trillion Btu). Trade Openness (TO) is the ratio of total trade to GDP. It is calculated as the sum of exports and imports, both expressed as proportions of GDP. Energy intensity (EI) is expressed as the ratio of total primary energy consumption to GDP (Btu per 2015 US $). Data on CO_2 emissions is sourced from Global Carbon Atlas [44] while REG and total primary energy consumption are sourced from the US Energy Information Administration [45]. The AIP data are collected from the OECD [46]. The GDP and TO are sourced from the World Bank database [47].

3. Results and discussion. Initially, the stationarity of the variables was evaluated using the Augmented Dickey-Fuller (ADF) test. The results of ADF are given in the Table 1. According to the unit root test results, all the variables under investigation became stationary after taking first differences.

Table 1. Unit root test results

	level	**1st difference**
CO2	1.528471	4.268422***
AIP	1.950514	-3.711620***
REG	0.708423	-4.662544***
GDP	-1.138991	-3.448411***
TO	-1.963913	-5.645272***
EI	0.084540	-6.173263***
AIP*REG	2.074959	-3.628488**

Notes: * and *** represent a rejection of the null hypothesis at 10% and 1% significance levels, respectively.

Hence, it becomes appropriate to assess the long-run relationships among these variables. To this end, the Engle-Granger cointegration test was employed, and the results are presented in the Table 2. The outcomes confirmed the existence of a long-run cointegrating relationship among the examined variables.

Table 2. Results of the Cointegration Test

Engle-Granger			
Tau-statistics	-6.434405 (0.020)	Z-statistics	-118.7638(0.000)
Notes: *p-values are in parenthesis.*			

Lastly, the Canonical Cointegration Regression (CCR), Dynamic Ordinary Least Squares (DOLS), and Fully Modified Ordinary Least Squares (FMOLS) methods were applied to estimate the long-run coefficients. The results obtained from these estimation techniques are presented in the Table 3.

Table 3. Findings of the Econometric Estimations

	CCR	**DOLS**	**FMOLS**
AIP	0.47^{***}	0.18^{***}	0.47^{***}
GDP	1.40^{***}	1.22^{***}	1.39^{***}
TO	0.01^{***}	0.01^{**}	0.01^{***}
REG	-0.20^{***}	-0.02^{***}	-0.20^{***}
EI	1.56^{***}	1.20^{***}	1.56^{***}
*REG*AIP*	-0.06^{**}	-0.02^{***}	-0.05^{***}
Constant	-14.7^{***}	-10.8^{***}	-14.6^{***}
Trend	-0.01^{***}	-0.01^{*}	-0.01^{***}

Notes: ****, **, and * display rejecting the null hypothesis at a 1%, 5%, and 5% significance level, respectively.*

The optimal lag length is determined using the Akaike information criterion (AIC). Table 3 demonstrates consistent results across all applied estimation methods, with parameters exhibiting similar signs and magnitudes. Specifically, the interaction term between renewable energy production and AI-related patents consistently shows a negative and statistically significant impact across methods. This means that when the share of renewable energy is high, the emission-reducing impact of AI patents is stronger. This evidence suggests that enhanced renewable energy deployment mitigates the sensitivity of the United States' CO_2 emissions to fluctuations in AI-related patents. This pattern demonstrates that the carbon-reduction potential of AI-based technologies is realized only when the energy system is sufficiently "green". In other words, technological advancement alone is not enough. Its environmental benefits are conditional on the sustainability of the underlying energy infrastructure. Moreover, AI-related patents, GDP, trade openness, and energy intensity individually exhibit positive and statistically significant impacts on CO_2 emissions, while REG has a negative impact on CO_2 emissions for the United States.

4. Conclusions. The findings of this study offer valuable insights into the complex relationships linking AI-related patents, GDP, trade openness, energy intensity, REG, and CO_2 emissions in the United States. Consistently, the results show that the interaction between AI-related patents and renewable energy production has a negative, statistically significant impact on CO_2 emissions. This notable finding underscores the potential of renewable energy production to mitigate the impact of AI technologies on CO_2 emissions. Furthermore, the study also detects a positive and statistically significant influence of AI-related patents, GDP, trade openness, and energy intensity on CO_2 emissions. On the other hand REG has a negative effect on CO_2 emissions.

Based on these results, the recent literature's findings suggesting that the environmental impacts of artificial intelligence are not one-sided are supported [48-50]. It is observed that if energy systems are not green, artificial intelligence technologies can increase environmental pollution due to their production processes, data processing infrastructure, and energy- intensive use, as well as the energy demand created by data centers. The relationship between carbon emissions and artificial intelligence is not direct; it varies depending on the application areas. When considered alongside green energy systems, artificial intelligence's ability to reduce carbon emissions underscores the importance of supporting energy systems with renewable resources. For the results of artificial intelligence to be positive, investments in renewable energy need to increase. The necessity of transitioning to green energy for artificial intelligence to effectively reduce environmental pollution is also consistent with the literature [51-53]. In this context, the results obtained show that artificial intelligence has a conditional role in reducing environmental pollution. If artificial intelligence applications are implemented within a fossil fuel-based system, the expected positive effect is reversed. Data centers, infrastructure, technologies that require high processing power, and digital networks increase carbon

emissions when powered by a fossil-fuel-based energy system.

Another subject of study, GDP, is associated with increased carbon emissions. This supports the literature's findings that increased production, consumption, and energy demand contribute to environmental pollution [54, 55]. In economies with high production capacity, such as the US, economic growth does not reduce environmental costs despite increased energy efficiency. While there are expectations that artificial intelligence will reduce carbon emissions, this needs to be supported by a transition to green energy. Therefore, to mitigate the environmental damage caused by economic growth, it must be supported by renewable energy use and energy efficiency policies.

Another variable underpinning this research is trade openness. The positive impact of trade openness on carbon emissions is noteworthy. The results show that increased trade openness can lead to higher carbon emissions due to larger production scale, greater energy use, and higher energy intensity in the global supply chain. There is no consensus in the literature regarding the environmental impact of trade openness. Reasons for this include differences between country groups, production structures, foreign trade content, and measurement differences [56]. However, pressure on carbon emissions is higher in areas where production growth comes from non-renewable energy sources, environmental regulations are weak, and especially where the export structure is based on energy-intensive sectors. The findings of this study are consistent with the literature, which provides evidence that trade openness increases carbon emissions [57-59].

Based on the obtained results, the following policy recommendations are proposed: a) As can be seen from the estimation results, AI technologies have an emission-reducing impact only when the energy system is "green". Therefore, AI applications should primarily be used in renewable energy infrastructure and energy management (e.g., smart grids and energy forecasting). In this context, AI strategies integrated with renewable energy should be developed. b) The finding that trade openness increases emissions indicates that the structure of imports and exports needs to be regulated. The transfer of AI-based technologies should be promoted jointly with green technologies. c) Green-oriented incentives should be provided for AI innovations. Specifically, government policies should prioritize support for energy- efficient and carbon-neutral AI projects. d) Considering the impact of energy intensity on CO_2 emissions, AI applications should be used to promote process optimization, reduce energy losses, and encourage automation.

Author Contributions. S.M. (Shahriyar Mukhtarov) conceived the research idea, developed the conceptual framework, designed the research methodology, performed the formal analysis, interpreted the findings, supervised the study, and reviewed and edited the manuscript. M.T.K. (Mustafa Tevfik Kartal) contributed to the study design, data collection, statistical and econometric analyses, interpretation of the results, and preparation of the original draft of the manuscript. F.A. (Fatih Ayhan) contributed to data validation, critically reviewed and edited the manuscript, participated in the discussion of the findings, and approved the final version of the manuscript. All authors have read and agreed to the published version of the manuscript.

Funding. The authors received no financial support from any funding agency, commercial organization, or not-for-profit institution for the research, authorship, and/or publication of this article.

Data Availability. The data supporting the findings of this study are available from the corresponding author upon reasonable request.

Acknowledgments. An earlier version of this article was presented at the Artificial Intelligence Technologies and Aerospace Problems–2025 Conference, held in Baku, Azerbaijan, on 8–9 June 2025, and was published in the conference proceedings. The present article has been substantially revised and expanded in light of the comments and suggestions received during the conference discussions, including improvements to the model specification and empirical analysis. The authors gratefully acknowledge the valuable feedback provided by the conference participants, which contributed to enhancing the quality, analytical scope, and methodological rigor of this study. The authors also acknowledge the use of generative artificial intelligence (AI) and AI-assisted technologies solely for improving the language, grammar, and readability of the manuscript. All scientific content, analyses, interpretations, and conclusions remain the sole responsibility of the authors.

Declarations

Conflict of Interest. The authors declare that they have no competing interests or conflicts of interest.

Ethical Approval. This article does not contain any studies involving human participants or animals performed by any of the authors.

Informed Consent. Not applicable.

References

[1] Ozcan B, Kılıç Depren S, Kartal MT. Impact of nuclear energy and hydroelectricity consumption in achieving environmental quality: Evidence from load capacity factor by quantile-based nonlinear approaches. *Gondwana Research*. 2024;129:412–424. https://doi.org/10.1016/j.gr.2024.02.018

[2] Ulussever T, Kartal MT, Kılıç Depren S. Effect of income, energy consumption, energy prices, political stability, and geopolitical risk on the environment: Evidence from GCC countries by novel quantile-based methods. *Energy & Environment*. 2025;36(2):979–1004. https://doi.org/10.1177/0958305X231220953

[3] Marra A, Colantonio E, Cucculelli M, Nissi E. The "complex" transition: Energy intensity and CO_2 emissions amidst technological and structural shifts—Evidence from OECD countries. *Energy Economics*. 2024;136:107702. https://doi.org/10.1016/j.eneco.2024.107702

[4] Arshad S, Joseph S, Rahman SU, Idress S, Shahid TA. Decarbonizing the future: A critical review of green energy, financial inclusion and trade openness on CO_2 emissions. *Bulletin of Business and Economics*. 2024;13(2):160–163.

[5] Dong M, Wang G, Han X. Impacts of artificial intelligence on carbon emissions in China: In terms of artificial intelligence type and regional differences. *Sustainable Cities and Society*. 2024;113:105682. https://doi.org/10.1016/j.scs.2024.105682

[6] Alatalo J, Heilimo E, Rantonen M, Väänänen O, Sipola T. Reducing emissions using artificial intelligence in the energy sector: A scoping review. *Applied Sciences*. 2025;15(2):999. https://doi.org/10.3390/app15020999

[7] Liu J, Liu L, Qian Y, Song S. The effect of artificial intelligence on carbon intensity: Evidence from China's industrial sector. *Socio-Economic Planning Sciences*. 2022;83:101002. https://doi.org/10.1016/j.seps.2021.101002

[8] Brynjolfsson E, Rock D, Syverson C. Artificial intelligence and the modern productivity paradox: A clash of expectations and statistics. NBER Working Paper No. 24001. Cambridge (MA): National Bureau of Economic Research; 2017. https://doi.org/10.3386/w24001

[9] United Nations Conference on Trade and Development (UNCTAD). *Technology and Innovation Report 2025: Inclusive Artificial Intelligence for Development*. Geneva: UNCTAD; 2025.

[10] World Trade Organization (WTO). *Making Trade and AI Work Together to the Benefit of All*. Geneva: World Trade Organization; 2025.

[11] International Energy Agency (IEA). *Energy and AI*. Paris: International Energy Agency; 2025.

[12] Wang Q, Li Y, Li R. Integrating artificial intelligence in energy transition: A comprehensive review. *Energy Strategy Reviews*. 2025;57:101600. https://doi.org/10.1016/j.esr.2025.101600

[13] Hankendi C, Coskun AK, Sovacool BK. Why transparency matters for sustainable data centers and carbon-neutral artificial intelligence (AI). *iScience*. 2025;28(11):112409. https://doi.org/10.1016/j.isci.2025.112409

[14] de Vries-Gao A. The carbon and water footprints of data centers and what this could mean for artificial intelligence. *Patterns*. 2026;7(1):101285. https://doi.org/10.1016/j.patter.2025.101285

[15] Aydin C, Cetintas Y. Does the level of renewable energy matter in the effect of economic growth on environmental pollution? New evidence from PSTR analysis. *Environmental Science and Pollution Research*. 2022;29(54):81624–81635. https://doi.org/10.1007/s11356-022-21491-9

[16] Wang Q, Zhang F, Li R, Sun J. Does artificial intelligence promote energy transition and curb carbon emissions? The role of trade openness. *Journal of Cleaner Production*. 2024;447:141298. https://doi.org/10.1016/j.jclepro.2024.141298
[17] Chen C, Pinar M, Stengos T. Renewable energy and CO_2 emissions: New evidence with the panel threshold model. *Renewable Energy*. 2022;194:117–128. https://doi.org/10.1016/j.renene.2022.05.060
[18] Kartal MT, Ayhan F, Sarıhan AY, Altaylar M. Examining a symmetric relationship of renewable energy, healthcare expenditures, and export with environmental degradation: Evidence from OECD countries by ARDL approaches. *Journal of Environmental Management*. 2025;390:126236. https://doi.org/10.1016/j.jenvman.2025.126236
[19] Jie W, Rabnawaz K. Renewable energy and CO_2 emissions in developing and developed nations: A panel estimate approach. *Frontiers in Environmental Science*. 2024;12:1405001. https://doi.org/10.3389/fenvs.2024.1405001
[20] Shaari MS, Abidin NZ, Karim ZA. The impact of renewable energy consumption and economic growth on CO_2 emissions: New evidence using panel ARDL study of selected countries. *International Journal of Energy Economics and Policy*. 2020;10(6):617–623. https://doi.org/10.32479/ijeep.10210
[21] Sebestyén V. Environmental impact networks of renewable energy power plants. *Renewable and Sustainable Energy Reviews*. 2021;151:111626. https://doi.org/10.1016/j.rser.2021.111626
[22] Jebli MB, Youssef SB. Output, renewable and non-renewable energy consumption and international trade: Evidence from a panel of 69 countries. *Renewable Energy*. 2015;83:799–808. https://doi.org/10.1016/j.renene.2015.04.061
[23] Zeren F, Akkuş HT. The relationship between renewable energy consumption and trade openness: New evidence from emerging economies. *Renewable Energy*. 2020;147:322–329. https://doi.org/10.1016/j.renene.2019.09.006
[24] Nouira R, Salem LB, Saafi S, Rault C. Renewable energy consumption and international trade: Does climate policy stringency matter? *Energy Policy*. 2025;206:114728. https://doi.org/10.1016/j.enpol.2025.114728
[25] Ezzati M, Singer BH, Kammen DM. Towards an integrated framework for development and environmental policy: The dynamics of environmental Kuznets curves. *World Development*. 2001;29(8):1421–1434. https://doi.org/10.1016/S0305-750X(01)00041-5
[26] Tisdell C. Globalization and sustainability: Environmental Kuznets curve and the WTO. *Ecological Economics*. 2001;39(2):185–196. https://doi.org/10.1016/S0921-8009(01)00244-1
[27] Dinda S. Environmental Kuznets curve hypothesis: A survey. *Ecological Economics*. 2004;49(4):431–455. https://doi.org/10.1016/j.ecolecon.2004.02.011
[28] Brock WA, Taylor MS. The green Solow model. *Journal of Economic Growth*. 2010;15(2):127–153. https://doi.org/10.1007/s10887-010-9051-0
[29] Berk I, Onater-Isberk E, Yetkiner H. A unified theory and evidence on CO_2 emissions convergence. *Environmental Science and Pollution Research*. 2022;29(14):20675–20693. https://doi.org/10.1007/s11356-021-17262-6
[30] Ordóñez J, Valente S, Stengos T. Growth and pollution convergence: Theory and evidence. *Journal of Environmental Economics and Management*. 2011;62(2):199–214. https://doi.org/10.1016/j.jeem.2011.03.002
[31] Xia Y, Ahmad M. Industrial robotics, resource efficiency, energy transition, and environmental quality: Designing a Sustainable Development Goals framework for G7 countries in the presence of geopolitical risk. *Sustainability*. 2025;17(5):1960. https://doi.org/10.3390/su17051960
[32] Yang X, Chen H, Li B, Jia D, Ahmad M. The relationship between artificial intelligence, geopolitical risk, and green growth: Exploring the moderating role of green finance and energy technology. *Technological Forecasting and Social Change*. 2025;217:124135. https://doi.org/10.1016/j.techfore.2025.124135

[33] Kartal MT, Kim E, Mukhtarov S, Taşkın D, Kirikkaleli D, Depren SK, Park J. Effect of AI-related patents, energy transition, environmental policy stringency, income, and energy consumption sub-types on environmental sustainability: Evidence from China by KRLS approach. *Journal of Environmental Management*. 2025;395:127924. https://doi.org/10.1016/j.jenvman.2025.127924
[34] Jin T. The effectiveness of combined heat and power (CHP) plants for carbon mitigation: Evidence from 47 countries using CHP plants. *Sustainable Energy Technologies and Assessments*. 2022;50:101809. https://doi.org/10.1016/j.seta.2021.101809
[35] Jin T, Kim D. The role of renewable energy in hedging against oil price risks: A study of OECD net oil importers. *Renewable Energy*. 2023;218:119325. https://doi.org/10.1016/j.renene.2023.119325
[36] Mukhtarov S, Azizov M, Kartal MT, Eynalov H. Catalyzing green transformation: Mitigating oil price impact on CO_2 emissions in Saudi Arabia via renewable energy transition. *Environmental Economics and Policy Studies*. 2024. https://doi.org/10.1007/s10018-024-00416-1
[37] Park JY. Canonical cointegrating regressions. *Econometrica*. 1992;60(1):119–143. https://doi.org/10.2307/2951679
[38] Saikkonen P. Estimation and testing of cointegrated systems by an autoregressive approximation. *Econometric Theory*. 1992;8(1):1–27. https://doi.org/10.1017/S0266466600010783
[39] Stock JH, Watson MW. A simple estimator of cointegrating vectors in higher order integrated systems. *Econometrica*. 1993;61(4):783–820. https://doi.org/10.2307/2951763
[40] Hansen BE. Efficient estimation and testing of cointegrating vectors in the presence of deterministic trends. *Journal of Econometrics*. 1992;53(1–3):87–121. https://doi.org/10.1016/0304-4076(92)90097-T
[41] Phillips PCB, Hansen BE. Statistical inference in instrumental variables regression with I(1) processes. *Review of Economic Studies*. 1990;57(1):99–125. https://doi.org/10.2307/2297545
[42] Dickey DA, Fuller WA. Likelihood ratio statistics for autoregressive time series with a unit root. *Econometrica*. 1981;49(4):1057–1072. https://doi.org/10.2307/1912517
[43] Engle RF, Granger CWJ. Co-integration and error correction: Representation, estimation, and testing. *Econometrica*. 1987;55(2):251–276. https://doi.org/10.2307/1913236
[44] Global Carbon Atlas. Carbon emissions. Global Carbon Atlas; 2025. Available from: https://globalcarbonatlas.org/emissions/carbon-emissions
[45] U.S. Energy Information Administration (EIA). Total Energy: Monthly Energy Review. Washington, DC: U.S. Energy Information Administration; 2025. Available from: https://www.eia.gov/totalenergy/data/monthly/index.php#renewable
[46] Organisation for Economic Co-operation and Development (OECD). Data Explorer: Environmental Policy Stringency (EPS) and AI-related patents. Paris: OECD; 2025. Available from: https://data-explorer.oecd.org
[47] World Bank. World Development Indicators. Washington, DC: World Bank; 2025. Available from: https://data.worldbank.org/indicator
[48] Cao Q, Chi C, Shan J. Can artificial intelligence technology reduce carbon emissions? A global perspective. *Energy Economics*. 2025;143:108285. https://doi.org/10.1016/j.eneco.2025.108285
[49] Qin M, Hu W, Qi X, Chang T. Do the benefits outweigh the disadvantages? Exploring the role of artificial intelligence in renewable energy. *Energy Economics*. 2024;131:107403. https://doi.org/10.1016/j.eneco.2024.107403
[50] Zhang W, Zeng M. Is artificial intelligence a curse or a blessing for enterprise energy intensity? Evidence from China. *Energy Economics*. 2024;134:107561. https://doi.org/10.1016/j.eneco.2024.107561
[51] Chishti MZ, Xia X, Dogan E. Understanding the effects of artificial intelligence on energy transition: The moderating role of the Paris Agreement. *Energy Economics*. 2024;131:107388. https://doi.org/10.1016/j.eneco.2024.107388

[52] Tao W, Weng S, Chen X, Alhussan FB, Song M. Artificial intelligence-driven transformations in low-carbon energy structure: Evidence from China. *Energy Economics*. 2024;136:107719. https://doi.org/10.1016/j.eneco.2024.107719
[53] Zhao C, Dong K, Wang K, Nepal R. How does artificial intelligence promote renewable energy development? The role of climate finance. *Energy Economics*. 2024;133:107493. https://doi.org/10.1016/j.eneco.2024.107493
[54] Salari M, Javid RJ, Noghanibehambari H. The nexus between CO_2 emissions, energy consumption, and economic growth in the US. *Economic Analysis and Policy*. 2021;69:182–194. https://doi.org/10.1016/j.eap.2020.12.007
[55] Sikder M, Wang C, Yao X, Huai X, Wu L, Kwame Yeboah F, et al. The integrated impact of GDP growth, industrialization, energy use, and urbanization on CO_2 emissions in developing countries: Evidence from the panel ARDL approach. *Science of the Total Environment*. 2022;837:155795. https://doi.org/10.1016/j.scitotenv.2022.155795
[56] Gozgor G. Does trade matter for carbon emissions in OECD countries? Evidence from a new trade openness measure. *Environmental Science and Pollution Research*. 2017;24(36):27813–27821. https://doi.org/10.1007/s11356-017-0441-z
[57] Chen F, Jiang G, Kitila GM. Trade openness and CO_2 emissions: The heterogeneous and mediating effects for the Belt and Road countries. *Sustainability*. 2021;13(4):1958. https://doi.org/10.3390/su13041958
[58] Derindag OF, Maydybura A, Kalra A, Wong WK, Chang BH. Carbon emissions and the rising effect of trade openness and foreign direct investment: Evidence from a threshold regression model. *Heliyon*. 2023;9(7). https://doi.org/10.1016/j.heliyon.2023.e17919
[59] Le TH, Chang Y, Park D. Trade openness and environmental quality: International evidence. *Energy Policy*. 2016;92:45–55. https://doi.org/10.1016/j.enpol.2016.01.030

https://doi.org/10.58225/sw.2026.1-44-52

GRAPHENE: 3D PRINTING FOR NEXT-GENERATION SUSTAINABLE AND SMART BUILDINGS

Imran Ali[1*], Al Arsh Basheer[2]
[1*]*Department of Chemistry, Jamia Millia Islamia, Jamia Nagar, New Delhi, India,*
[2]*Springhouse Drive, Pleasanton, USA drimran.chiral@gmail.com[1*], drimran_ali@yahoo.com[2]*

Abstract. Graphene 3D printing is an encouraging technology for sustainable and smart building construction. Graphene and its derivatives increase the thermal, mechanical, electrical, and rheological properties of printed cementitious and geopolymer materials. They increase interlayer bonding, printability, durability, crack resistance, and thermal performance while permitting the self-sensing competencies. This review describes important 3D printing methods, constructional applications, existing developments, and challenges, comprising rheological optimization, graphene dispersion, and standardization. Briefly, the graphene-based 3D printing delivers a strong prospect for durable, lightweight, energy-effective, and low-carbon future building construction.
Keywords: Graphene 3D printing, Nanomaterials, Sustainable construction, Smart buildings, Challenges anf future perspectives

Cite this article as: *I. Ali and A. A. Basheer, "GRAPHENE: 3D PRINTING FOR NEXT-GENERATION SUSTAINABLE AND SMART BUILDINGS", SW AzUAC, vol. 1, 2026, doi:10.58225/sw.2026.1-44-52*
Article history:*Received: 05 December 2025 / Revised: 20 January 2026 / Accepted: 10 February 2026*

1. Introduction. There is a great demand for sustainable, automated, earthquake protective and intelligent building systems globally [1]. The conventional construction methods utilise huge amounts of raw materials and energy. Besides, these methods release green gases and aerosols into the atmosphere. The cement production is only responsible for about 7-8% of global carbon dioxide emissions. Consequently, the increasing urbanization and infrastructure needs require stronger, faster, and more sustainable construction skills. Nowadays, 3D printing (C3DP) is gaining attention in manufacturing many small articles and commodities. Also, research is going on for fabricating buildings layer-by-layer directly by 3D printing. This technology provides many benefits comprising fast construction, no pollution, reduced labour, freedom of design, minimum material waste, and enhanced construction safety.

Of course, cementitious materials exhibit numerous qualities, but they cannot be used in 3D printing. For 3D printing, the material should be in liquid or paste form at the working temperature of the 3D printing machine. Therefore, the scientists and engineers are exploring suitable materials for this purpose. Nowadays, this is the era of nanotechnology and hence, nanomaterials have been explored for 3D printing purposes to construct buildings; to improve the performance of printable construction materials. Among many nanomaterials, graphene has been recognised as the best material for 3D printing to construct buildings; of course, in the initial stage at this time. Graphene has emerged as one of the most capable nanomaterials for building construction due to its unique features.

The use of graphene in 3D printing is gaining importance as an encouraging building construction material [2]. The research is going on in this area and no review is available on this topic. Therefore, attempts were made to describe the latest development in 3D printing using graphene for building construction. This review article broadly describes the recent developments in graphene 3D printing in building construction and identifies the future research directions for industrial applications.

Graphene as a building material. The graphene is considered the material of this century with remarkable properties. The graphene and its derivatives (Figure 1) are used for various applications. The graphene, graphene derivatives, and graphene-based composites are being

considered as the best 3D printing nanomaterial for building construction in the future. This is due to high specific surface area, good tensile strength (~130 GPa), Young's modulus (1.0 TPa), thermal, electrical, rheological, and thermal multifunctional properties (Table 1). Besides, graphene-based materials also increase rheological properties like viscosity, extensibility, and shape retention, which are important for stable 3D printing. Additionally, they enhanced the resistance against water infiltration, chloride attack, and chemical depletion. Furthermore, the graphene composites offer self-sensing ability for crack detection and structural health checking, making them appropriate for future smart and sustainable building materials. This is due to their electrical conductivity and piezoresistive behaviour [3].

Unlike conventional 3D-printed concrete, graphene did not show brittleness, shrinkage cracking, low tensile strength and weak interlayer bonding. In geopolymer or cementitious systems, graphene acted as a nano-reinforcement material, which increases load transfer, crack bridging, pore refinement, and interfacial bonding, thus refining toughness, durability, compressive strength, and interlayer adhesion. The graphene oxide is useful due to its oxygen having functional groups, which improve the dispersion and interactions with cement hydration products, giving denser microstructures. The graphene-based or mixed materials can considerably increase cement hydration, improve pore structure, decrease crack chances and reinforce the interfacial transition zone in cementitious matrices. Furthermore, the graphene-containing material introduces multifunctional features like self-sensing, thermal control, electromagnetic protection and structural health monitoring.

Several graphene derivatives are being utilized in construction materials. The most important is graphene oxide (GO), which contains oxygen functional groups like epoxy, hydroxyl, and carboxyl groups. These functional groups increase the dispersibility in water systems and expedite the interactions among the cement hydration products. The nest material is reduced graphene oxide (rGO), which possesses partially restored graphitic features and enhanced electrical conductivity compared to GO. The graphene nanoplatelets (GNPs) are multilayer graphene sheets. These have good mechanical reinforcement and lower production prices. The 3D graphene-based foams, aerogels, and sponges are used to provide lightweight porous constructions with improved mechanical stability features.

Graphene crystal

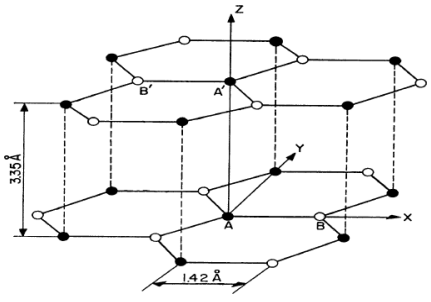

Graphene oxide

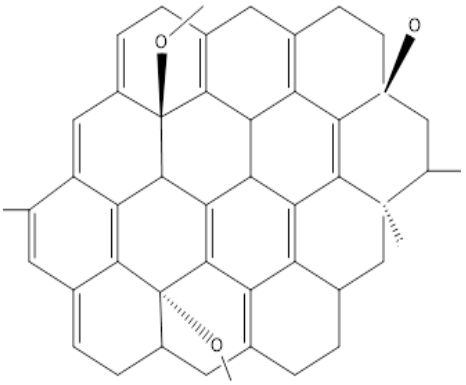

Reduced graphene oxide

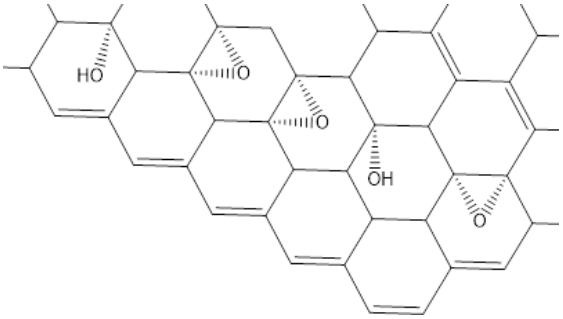

Fig.1. Structure of graphene and its compounds

Table 1. Graphene properties for 3D-printed building construction

Properties	Typical values	3D Printing construction benefits
Specific surface area	~2630 m^2/g	Increases interaction with cement hydration products
Thermal conductivity	3000–5000 W/m.K	Increases thermal management
Electrical conductivity	~10^6 S/m	Enables self-sensing and smart structures
Young's modulus	~1.0 TPa	Improves stiffness of printable composites
Tensile strength	~130 GPa	Progresses crack resistance and structural strength
Density	~2.2 g cm^{-3}	Gives lightweight structures
Impermeability	Nearly impermeable	Increase durability and water resistance
Tensile strength	~130 GPa	Increases crack resistance and structural strength

There are different types of printing techniques for graphene-based construction materials. The extrusion-based printing is the dominant technique for graphene-cement composites due to its scalability and simplicity [6]. The most important advantages are high material efficiency, continuous deposition and large-scale applicability. However, rheology control, nozzle clogging and dispersion stability remained the limitations. The direct ink writing (DIW) is a method of 3D printing. This allowed the precise deposition of graphene with controlled micro-structures. Recently, robotic additive manufacturing has gained attention in 3D printing construction. The robotic systems provided good flexibility for complex architectural designs, geometries and large-scale infrastructure construction. The major advantages of using graphene materials in 3D printing are given in Table 2. The printing, assembly, mechanism and constructed structures are shown in Figure 2.

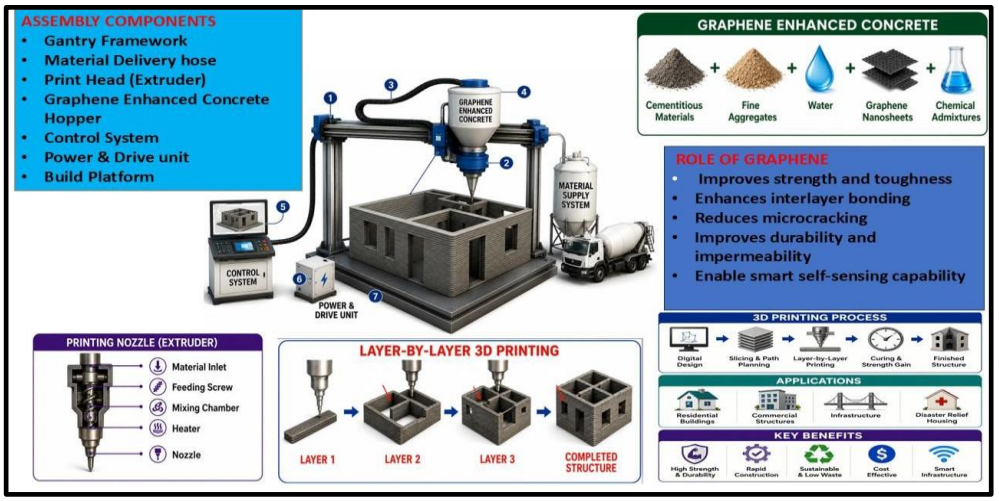

Fig.2. Printing, assembly, mechanism and constructed structures

Table 2. Advantages of using graphene materials in 3D printing

Advantages	**Effect on construction materials**
Pore alteration	Gives denser microstructure
Crack bridging	Decrease microcrack propagation
Improved interlayer bonding	Increases structural integrity
Better rheology	Increases printability and shape retention
Good thermal conductivity	Increases energy efficacy
Augmented durability	Good resistance against chemical attack
Good electrical conductivity	Permits structural health checking

2. Role of graphene in 3D printed construction materials. The use of graphene in construction materials is very important. The most important is rheological modification. This is due to the fact that the printable materials need optimized rheological properties. The most important properties are buildability, extrudability, pumpability and shape retention. For example, the GO nano-sheets can improve rheology because of their high surface area and interactions with water molecules [7,8]. Besides, GO enhanced the yield stress and viscosity, preserving the printability. The mechanical enhancement is another role of graphene in building materials. The graphene-based materials enhanced the mechanical strength. The several mechanisms involved are the pore refinement, crack bridging, load transfer enhancement, nucleation of hydration products and improved interfacial bonding. The studies have shown that the use has shown considerable increases in tensile, compressive, and flexural strength. The interlayer bonding improvement is an important additive construction. The graphene nano-sheets increase the interfacial cohesion by endorsing the hydration reactions and decreasing the void formation among the deposited layers. The graphene materials also provide good durability to the building. The durability is provided by refining pore structure, reducing permeability, improving freeze-thaw stability, increasing chemical resistance and reducing chloride penetration [9]. These are the features needed for long-term infrastructure applications.

3. Graphene-based materials. Generally, graphene and its compounds are mixed with the cementitious materials. The GO accelerated the cement hydration by performing as nucleation sites for calcium silicate hydrate (C-S-H) formation. The enhanced hydration kinetics resulted in denser micro-structures and greater strength development. The geopolymers are sustainable substitutes for Portland cement and the addition of graphene improved the material features. Most importantly, the geopolymer conductivity, strength, and crack resistance were reduced [10-12]. The graphene-based composites showed piezoresistive behavior, permitting the real-time structural fitness monitoring.

The different of graphene materials are given in Table 3, while Table 4 shows a comparison between conventional and graphene-enhanced printable concrete.

Table 3. Classes of graphene materials

Graphene materials	**Major characteristics**	**Construction applications**
Graphene oxide (GO)	Hydrophilic & oxygen functional groups	Improves dispersion and cement hydration
Reduced graphene oxide (rGO)	High electrical conductivity	Smart sensing infrastructure
Graphene nano-platelets (GNPs)	High mechanical strengthening	Strength enhancement
Graphene aerogels	Porous lightweight constructions	Thermal insulation
Graphene-polymer composites	Elastic and conductive	Smart building components

Table 4. Comparison between conventional and graphene-enhanced printable concrete

Properties	Conventional printable concrete	Graphene-based printable concrete
Crack resistance	Limited	Excellent
Tensile strength	Moderate	High
Interlayer bonding	Weak	Improved
Thermal performance	Moderate	Improved
Electrical conductivity	Low	Excellent
Self-sensing capability	Absent	Present
Durability	Moderate	High

4. Multifunctional applications of graphene in next-generation buildings. The graphene and its compounds are the choice in multifunctional applications to construct next-generation buildings. The smart graphene-based infrastructure provides stress sensing, self-monitoring ability, damage detection and real-time data acquisition. The thermal management is also controlled by the addition. The graphene also controls energy efficiency in buildings, decreasing heating and cooling needs. The electromagnetic interference shielding is another important benefit in new-generation buildings. This is achieved by protecting buildings from electromagnetic radiation and shocks. The light of this material allowed the fabrication of robust portable house systems to avoid any loss in earthquakes. This is the concept of sustainable housing, reducing cement use and carbon emissions. The detailed protocol of 3D printing of graphene and its material in building construction is given in Figure 3.

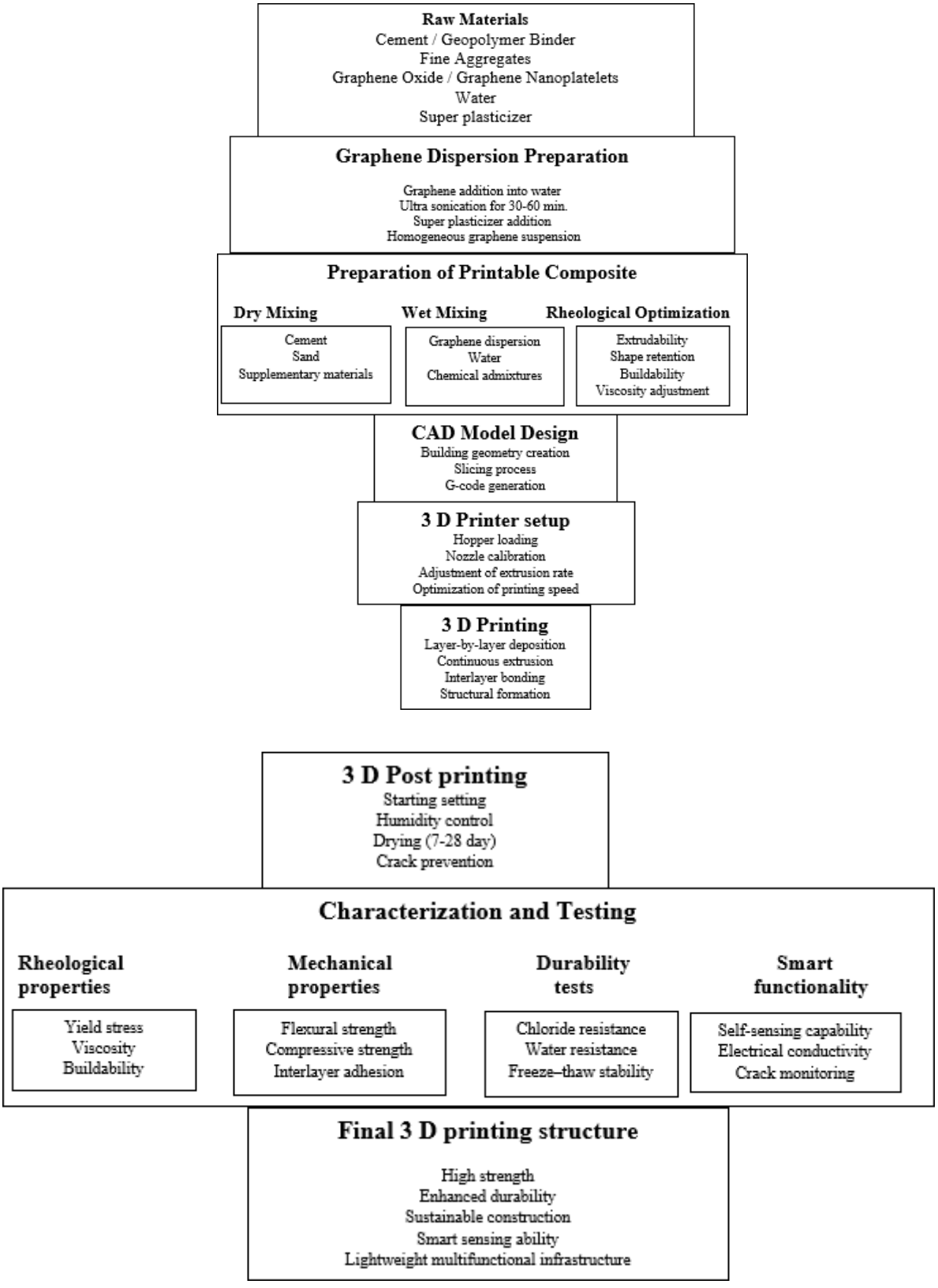

Fig. 3. Schematic illustration of graphene-based three-dimensional (3D) printing and material processing protocols for sustainable building construction

5. Current status of graphene in 3D-printed building construction. The 3D printing of graphene in building construction is in its development stage, as no example is available where graphene has been used as a 3D printing material for large industrial or community buildings.

However, the research is going on in this direction. Some lab batch and pilot-scale projects have shown the probability of graphene 3D printed construction. The Versarien (UK) prepared the "Lunar" pod using graphene-based Cementene™ concrete. The material is considered one of the first graphene 3D printed building structures. In this work, Cementene™ (a graphene cement additive) was used for concrete 3D printing for studios, office pods, leisure spaces and emergency shelters. These items showed good printability, strength, curing behaviour and sustainability. This project was the earliest graphene integration nanotechnology program.

Another program was started at the University of Virginia, Graphene-LC2 3D Printed Concrete. The researchers at the University of Virginia prepared a graphene printable concrete utilising limestone claimed clay cement (LC2). This showed 1% reduction in carbon emissions and about 23% increase in mechanical performance. The researchers at RMIT University also prepared GO-modified concrete for smart buildings. The GO-based material improved printability, electrical conductivity, crack sensing capability and stability of cementitious layers. It was realised that the material was useful for structural health monitoring, smart infrastructure for intelligent buildings and automatic maintenance systems. Some salient features of graphene-based 3D printing are given in Table 5.

Table 5. Key characteristics and performance attributes of graphene-based materials for three-dimensional (3D) printing in construction

Study/Project	Graphene Materials	Printing Method	Applications	Outcome
Versarien Lunar Pod	Graphene-based cement	Extrusion 3D printing	Buildings/pods	Improved strength&sustainability
Univ. Virginia concrete	Graphene with LC2 cement	Concrete extrusion printing	Sustainable buildings	31% low CO_2 emissions
RMIT Concrete	Graphene oxide	Additive concrete printing	Smart infrastructure	Crack sensing ability
Cement-Free Mortar	Graphene admixture	3D mortar printing	Sustainable architecture	Low cement consumption

6. Challenges. In spite of a bright future, there are some challenges to materialize the 3D printing technology for making houses using graphene and its compounds as building materials. The most important challenges are summarised below.

-Proper optimization of rheological properties due to increased viscosity and reduced printability by adding graphene to the materials.

-Nozzle blockage and extrusion instability may happen in 3D printing due to nanoparticle accumulation.

- Need to develop standard formulations, testing methods, and regulations.

-Potential health and environmental concerns associated with nanoparticle exposure.

-Limited knowledge of interlayer bonding mechanisms in graphene 3D printed structures.

A Summary of research gaps in 3D printing of graphene for building construction is given in Table 6.

Table 6. Research gaps, technical challenges, and future research directions in graphene-based three-dimensional (3D) printing for sustainable and smart buildings

Research Area	Current Limitation	Future Need
Dispersion of graphene	Accumulation	Large-scale dispersion methods
Optimization of rheology	Printability strength	AI-assisted formulation
Determination of durability	Limited long-term studies	Field-scale validation
Cost	Costly graphene synthesis	Low-cost production

Despite these challenges, the ongoing research is expected to overcome all these issues and 3D printed graphene buildings will be a reality in the coming years.

7. Future perspectives. The future of 3D printing with graphene materials in building construction is promising as it combines additive manufacturing, nanotechnology and smart infrastructure. This is due to the fact that graphene improves the durability, mechanical strength, thermal stability, and multi-functionality of the materials. The graphene-made composites light in weight, stronger, and more durable while decreasing cement use and environmental pollution. The development of smart self-sensing buildings is the future use of 3D printing with graphene. This will also support low-carbon and sustainable construction. The additive manufacturing decreases the material waste, while the addition will enhance low-carbon binders working and printable geopolymers. The future robotic additive systems will permit fast and automatic construction of houses, shelters, and remote infrastructures. Additionally, graphene-based materials will provide electromagnetic shielding, thermal insulation, and energy management to the buildings.

8. Conclusion. The graphene-based 3D printed building construction looks like a fascinating approach for next-generation sustainable buildings. Certainly, the 3D printing of graphene for buildings will improve the mechanical, electrical, rheological, thermal, and durability of the materials. The addition of graphene into construction material will enable the development of intelligent, energy-efficient, lightweight, and multifunctional building structures. The research in progress in this direction for removing several challenges. The continued interdisciplinary research comprising nanotechnology, civil engineering, robotics, and computational modelling will make the dream of sustainable buildings true soon. Briefly, the future of graphene-based 3D printing in building construction is quite bright. I hope that in some years time we shall see buildings and sky creepers around made of graphene and its materials using 3D printing.

Author Contributions. I.A. (Imran Ali) conceptualized the study, conducted the literature review, developed the manuscript framework, analyzed the current advances in graphene-based 3D printing technologies for sustainable and smart buildings, interpreted the findings, and wrote the original draft of the manuscript. A.A.B. (Al Arsh Basheer) contributed to the literature review, critically reviewed and edited the manuscript, validated the scientific content, improved the presentation of the work, and approved the final version of the manuscript. All authors have read and agreed to the published version of the manuscript.

Funding. The authors received no specific financial support from any funding agency, commercial organization, or not-for-profit institution for the research, authorship, and/or publication of this article.

Data Availability. No new datasets were generated or analyzed during the preparation of this review article. All information discussed in this manuscript is based on published literature cited in the References section.

Declarations

Conflict of Interest. The authors declare that they have no competing financial or personal interests that could have influenced the work reported in this manuscript.

Editorial Board Membership. Imran Ali is a member of the Editorial Board of this journal. To ensure an impartial and transparent editorial process, he had no involvement in the editorial handling of this manuscript, including reviewer selection, peer-review management, editorial decisions, or the final acceptance of the article. The manuscript was handled independently by another editor in accordance with the journal's editorial policies.

Ethical Approval. This article is a review study and does not involve experiments with human participants or animals. Therefore, ethical approval was not required.

Informed Consent. Not applicable.

References

[1]Narayan, J., & Bezborah, K. (2024). Recent advances in the functionalization, substitutional doping and applications of graphene/graphene composite nanomaterials. *RSC Advances*, **14**(19), 13413–13444. https://doi.org/10.1039/D3RA07072G

[2]Uddin, M. N., Bappy, M. A., Rab, M. F., Znidi, F., & Morsy, M. (2024). Recent progress on synthesis of 3D graphene, properties, and emerging applications. In *Chemistry of Graphene—Synthesis, Reactivity, Applications and Toxicities*. https://doi.org/10.5772/intechopen.114168

[3]Salah, H. A., Mutalib, A. A., Kaish, A. B., Syamsir, A., & Algaifi, H. A. (2023). Development of ultra-high-performance silica fume-based mortar incorporating graphene nanoplatelets for 3-dimensional concrete printing application. *Buildings*, **13**(8), 1949. https://doi.org/10.3390/buildings13081949

[4]Dubey, P. K., & Maurya, M. C. (2026). A comprehensive review of 3D printing in construction: Technology, materials, and digital workflow. *Innovative Infrastructure Solutions,* **11**(1), 51. DOI not available.

[5]Sovetova, M., & Calautit, J. K. (2024). Thermal and energy efficiency in 3D-printed buildings: Review of geometric design, materials and printing processes. *Energy and Buildings*, **323**, 114731. DOI not available.

[6]Guo, H., Lv, R., & Bai, S. (2019). Recent advances on 3D printing graphene-based composites. *Nano Materials Science*, **1**(2), 101–115. https://doi.org/10.1016/j.nanoms.2019.02.003

[7]Baytak, T., Gdeh, T., Jiang, Z., Arce, G., Colosi, L. M., & Ozbulut, O. E. (2024). Rheological, mechanical, and environmental performance of printable graphene-enhanced cementitious composites with limestone and calcined clay. *Journal of Building Engineering*, **97**, 110673. https://doi.org/10.1016/j.jobe.2024.110673

[8]Patil, R., & Alimperti, S. (2024). Graphene in 3D bioprinting. *Journal of Functional Biomaterials*, **15**(4), 82. https://doi.org/10.3390/jfb15040082

[9]Asim, N., Badiei, M., Samsudin, N. A., Mohammad, M., Razali, H., Soltani, S., & Amin, N. (2022). Application of graphene-based materials in developing sustainable infrastructure: An overview. *Composites Part B: Engineering*, **245**, 110188.
https://doi.org/10.1016/j.compositesb.2022.110188

[10] Chhetri, S., & Kuila, T. (2024). Polymer composites with 3D graphene architectures as high-performance EMI shielding materials: A review. *RSC Applied Polymers*, **2**(4), 507–533. https://doi.org/10.1039/D4LP00028A

[11] Guo, H., Lv, R., & Bai, S. (2019). Recent advances on 3D printing graphene-based composites.
Nano Materials Science, **1**(2), 101–115. https://doi.org/10.1016/j.nanoms.2019.02.003

[12] Narayan, J., & Bezborah, K. (2024). Recent advances in the functionalization, substitutional doping and applications of graphene/graphene composite nanomaterials. *RSC Advances*, **14**(19), 13413–13444. https://doi.org/10.1039/D3RA07072G

https://doi.org/10.58225/sw.2026.1-53-61

MODELING CONVERGENCE RATE ESTIMATES OF THE HEAVY BALL ALGORITHM VIA A RANDOM FOREST WITH SELF-ATTENTION

Daniil Miroshnichenko[1*], Majid Abbasov[2]
[1*,2]*St. Petersburg State University, Saint Petersburg, Russia*
miroshnichienko.daniil@gmail.com, m.abbasov@spbu.ru

Abstract. This paper addresses the problem of estimating convergence rates of iterative optimization algorithms, which is essential for analyzing and accelerating the training of modern machine learning models. Classical approaches to convergence rate estimation for momentum-based methods typically rely on analytical bounds derived under restrictive assumptions or on extensive empirical experimentation, both of which are computationally expensive and poorly scalable. As an alternative, we propose a data-driven framework for modeling convergence rate estimates using supervised machine learning. The proposed approach is demonstrated for the Heavy Ball optimization method applied to quadratic objective functions with heterogeneous curvature. A synthetic dataset is constructed by simulating Heavy Ball trajectories under randomly sampled objective parameters, optimization hyperparameters, and normalized initial conditions. The input features capture key characteristics of the optimization process, while the target variable represents a logarithmic estimate of the objective function decay along the trajectory, serving as a proxy for the convergence rate. To model nonlinear dependencies between optimization parameters and convergence behavior, we employ a Random Forest model augmented with a self-attention mechanism. This architecture enables adaptive weighting of feature interactions and improves predictive accuracy without requiring explicit analytical modeling of the underlying dynamics. Numerical experiments show that the proposed model achieves a coefficient of determination exceeding 0.8 when predicting convergence-related quantities, indicating strong agreement with empirically observed behavior. The results suggest that machine learning-based surrogate models can substantially simplify convergence rate estimation and that the proposed methodology is applicable to other optimization algorithms and objective classes.

Keywords: Convergence rate estimation, heavy ball method, momentum-based optimization, random Forest with self-attention, synthetic trajectory modeling, optimization dynamics

Cite this article as: *D. Miroshnichenko and M. Abbasov, "MODELING CONVERGENCE RATE ESTIMATES OF THE HEAVY BALL ALGORITHM VIA A RANDOM FOREST WITH SELF-ATTENTION", SW AzUAC, vol. 1, 2026, doi:10.58225/sw.2026.1-53-61*
Article history: *Received: 16 April 2026 / Revised: 13 June 2026 / Accepted: 23 June 2026*

1. Introduction. The analysis of convergence rates constitutes a fundamental problem in numerical optimization and plays a central role in the training of modern machine learning models. In large-scale learning settings, optimization algorithms are often executed for a very large number of iterations, and their convergence behavior directly determines computational cost, resource consumption, and overall training efficiency. Reliable estimates of convergence rates are therefore essential for selecting suitable optimization algorithms, tuning hyperparameters such as step sizes and momentum coefficients, and predicting the time required to reach a prescribed accuracy level. These considerations are especially important in neural network training, where optimization dynamics interact with high-dimensional parameter spaces and complex loss landscapes.

Traditionally, convergence rate estimates are obtained through either analytical derivations or empirical evaluation. Analytical approaches rely on structural assumptions on the objective function, such as Lipschitz continuity of the gradient and strong convexity, and provide worst-case bounds on the decay of the optimization error [1],[2]. While such results offer valuable theoretical insight, they

are often conservative and may not accurately reflect the behavior observed in practice. Moreover, deriving tight bounds for momentum-based methods remains challenging even for relatively simple objective classes. Empirical approaches typically involve repeated runs of the optimization algorithm followed by fitting convergence models to observed objective values or gradient norms, for instance via linear regression in logarithmic scale. Although more flexible, such procedures are computationally expensive, sensitive to noise, and difficult to automate or transfer across different problem settings.

These limitations motivate alternative approaches that avoid explicit analytical modeling of optimization dynamics. In this work, we adopt a data-driven perspective and treat the optimization algorithm as a black-box dynamical system whose convergence behavior can be learned from observed trajectories. Instead of deriving convergence rates from first principles, we propose to approximate them using supervised machine learning models trained on synthetically generated optimization data. This viewpoint is closely related to recent research on learning-based analysis and design of optimization algorithms, where machine learning techniques are used to predict performance characteristics or guide algorithmic decisions [3,4].

As a representative and technically challenging case study, we focus on the Heavy Ball method originally introduced by Polyak [1], which augments standard gradient descent with an inertial term in order to accelerate convergence. Unlike first-order methods without momentum, the Heavy Ball algorithm induces a second-order discrete-time dynamical system whose behavior is governed by the interaction between the step size, the momentum coefficient, and the curvature of the objective function. Even in the case of quadratic objectives, the resulting dynamics can exhibit oscillatory or underdamped regimes, as well as sensitivity to small perturbations in hyperparameter values. The convergence properties of the method are tightly linked to the spectral distribution of the Hessian matrix, leading to different convergence modes along distinct eigendirections and complicating the derivation of uniform convergence guarantees. Consequently, obtaining accurate convergence rate estimates for the Heavy Ball method requires careful analysis that goes beyond classical worst-case bounds and often remains analytically intractable in practice [5,6]. These characteristics make the Heavy Ball method a demanding yet informative testbed for data-driven convergence rate modeling, and a natural candidate for assessing the potential of machine learning-based surrogate models in the analysis of optimization dynamics.

The application of machine learning techniques to the analysis and enhancement of optimization algorithms has attracted increasing interest in recent years. A notable paradigm within this space is learning to optimize (L_2O), where machine learning models are trained to either design or improve optimization procedures based on empirical performance data. The comprehensive survey by Chen et al. describes this emerging paradigm and benchmarks multiple L_2O approaches, highlighting their ability to automate and adapt optimization strategies while also discussing limitations related to generalization beyond training distributions [7]. Unlike traditional theory-driven designs of optimization methods, which yield performance guarantees for specific classes of problems, data-driven optimization seeks to exploit patterns in empirical behavior to generate more efficient procedures.

In addition to L_2O, supervised machine learning models have been employed for performance prediction and algorithm selection. Trajanov et al. investigated explainable landscape analysis techniques for automated algorithm performance prediction, where the goal is to learn models that relate problem features to algorithm performance outcomes, thereby guiding the selection of the most suitable optimizer for new instances [8]. This line of research is conceptually aligned with the present work's objective of modeling convergence-related quantities, as both problems seek to approximate complex relationships between optimization settings and observed outcomes.

A broader context for surrogate modeling is found in engineering optimization, where surrogate-assisted optimization frameworks deploy machine learning regressors as approximations of expensive simulation models to accelerate design processes. In global antenna optimization, for

example, surrogate models such as kriging and variable-resolution approaches are used within iterative search schemes to reduce computation cost while preserving solution quality [9]. Reviews in this domain emphasize the trade-offs between surrogate fidelity and computational efficiency and underscore the importance of integrating surrogate predictions with optimization loops.

While surrogate modeling has a rich tradition in engineering contexts, general surrogate-assisted strategies have also been explored in automated history matching processes in reservoir engineering, where high-fidelity simulations are expensive and surrogate models reduce the costly runs required for optimization. These works review common surrogate model families including Gaussian processes, radial basis functions, and neural networks, illustrating the broad utility of data-driven approximations across different scientific domains.

Within the machine learning literature itself, ensemble methods such as random forests and boosting are widely studied for their predictive performance and generalization properties [10, 11]. However, classical ensemble models do not inherently capture structured relationships across samples or emphasize similarities driven by specific performance targets. This motivates the development of attention-augmented ensembles, such as the Self-Attention Forest framework utilized in this paper, which enriches tree-based models with data-dependent weighting mechanisms to better model complex regression targets. By grounding the proposed approach within this body of literature, the present work positions itself at the intersection of optimization analysis, performance prediction, and surrogate modeling, contributing a new perspective that combines these strands for learning convergence rate estimates.

1 Problem Statement and dataset. We consider the problem of estimating the convergence behavior of iterative optimization algorithms from observed optimization trajectories. Let $f:R^d \to R$ be a smooth objective function, and $\{x_k\}_{k\geq 0}$ denote the sequence of iterates generated by the Heavy Ball method with step size $\alpha > 0$ and momentum coefficient $\beta \in [0,1)$. Classical convergence analysis aims to characterize the rate at which $f(x_k)$ approaches its minimum value $f^\star$, typically by establishing bounds of the form $f(x_k)-f^\star \leq C\rho^k$ for some contraction factor $\rho \in (0,1)$. In this work, we adopt an empirical perspective and define a convergence rate estimate as a local, trajectory- dependent quantity that reflects the observed decay of the objective function along the optimization path rather than a global worst-case bound.

More specifically, given an initial point x_0 and the corresponding trajectory $\{x_k\}$, we define the target variable as a logarithmic estimate of the normalized objective value (1), computed as

$$\log_{10}\left(\frac{f(x_k)-f^\star}{f(x_0)-f^\star}\right) \tag{1}$$

at a given iteration index k. This quantity captures the effective contraction behavior of the algorithm and serves as a proxy for the convergence rate at different stages of the optimization process. The modeling task is then formulated as a supervised regression problem, where the goal is to predict this convergence-related quantity from a set of parameters characterizing the optimization dynamics.

The dataset used in this study is synthetically generated and constitutes a central component of the proposed methodology. Objective functions are chosen from a family of quadratic functions with heterogeneous curvature, parameterized by coefficients that control the conditioning of the problem. For each objective instance, Heavy Ball trajectories are simulated under randomly sampled optimization hyperparameters and normalized initial conditions. Each data sample corresponds to a randomly selected point along a stable optimization trajectory and is represented by a feature vector encoding the objective parameters, the Heavy Ball hyperparameters, the normalized initial state, and the relative iteration index. The associated target value reflects the observed logarithmic decay of the objective function at that point. This construction yields a diverse dataset that spans a wide range of dynamical regimes, including fast convergence, oscillatory behavior, and near-critical parameter settings. By explicitly modeling convergence-related quantities at the level of individual trajectory

samples, the dataset enables learning fine-grained relationships between optimization parameters and convergence behavior that are difficult to capture through analytical analysis alone.

The core object of study in this work is a supervised dataset that links a compact description of a Heavy Ball (HB) run to an empirical, trajectory-level proxy of convergence. We generate a synthetic regression dataset by repeatedly simulating HB dynamics on a two-dimensional quadratic objective of the form $f(x) = \frac{1}{2}(ax_1^2 + bx_2^2)$, where the curvature parameters $a$and $b$define the Hessian spectrum and, consequently, the conditioning of the problem. To ensure broad coverage of regimes, the pair $(a, b)$is drawn from four complementary sampling rules: highly ill-conditioned instances with small $a$and large b, isotropic instances with $a = b$, low-curvature instances with both coefficients near zero, and a wide-range regime where both coefficients vary up to large values. With 5000samples generated by the rule, the resulting dataset contains $N = 20000$labeled examples.

Each example corresponds to a single randomly chosen state along a stable HB trajectory and is represented by a seven-dimensional feature vector $(a, b, \alpha, \beta, x_{0,1}^{\text{norm}}, x_{0,2}^{\text{norm}}, k_{\text{norm}})$. The HB hyperparameters are sampled as $\beta \sim \mathcal{U}[0,0.999)$and $\alpha \sim \mathcal{U}(0, \alpha_{\max})$, where $\alpha_{\max} = \min\{0.95 \cdot 2(1+\beta)/L, 10\}$and $L = \max(a, b)$is the smoothness constant of the quadratic objective. This coupling between α, β, and $L$is a deliberate stability-oriented design choice: it concentrates sampling in parameter regions that are likely to produce meaningful trajectories while still allowing near-critical behavior. The initial point is generated by first sampling a radius $r \sim \mathcal{U}[10^{-3}, 20]$and then drawing $x_0$uniformly from the square $[-r, r]^2$; we store the normalized initialization $x_0^{\text{norm}} = x_0/r$, which lies in $[-1,1]^2$by construction and removes a trivial scaling degree of freedom. Trajectories are simulated for at most 300iterations, and early termination occurs when the gradient norm falls below 10^{-8}. To prevent numerical pathologies from contaminating the dataset, a run is rejected if the objective becomes non-finite or if $f(x_k)$exceeds $10^{12}\, f(x_0)$; when this happens, new (α, β)values are resampled up to 50attempts before drawing a new (a, b)pair. This rejection-resampling mechanism ensures that the final dataset consists of stable trajectories while still retaining challenging regimes close to instability.

The regression target is defined to reflect the observed objective decay along the trajectory in a scale-stable manner. Let $f_0 = \max\{f(x_0), 10^{-12}\}$denote a safeguarded initial objective value, and let $f_k = f(x_k)$be the objective at iteration k. We store $y = \log_{10}(f_k/f_0 + 10^{-30})$, which is typically non-positive and becomes more negative as the objective decreases. This target can be interpreted as a local, trajectory-dependent estimate of convergence progress at a particular stage of the run. In parallel, we record the normalized iteration index $k_{\text{norm}} = k/300$, which enables the learning model to represent time-varying behavior, including transient oscillations and phase transitions between fast initial decrease and slower asymptotic contraction. Because the quadratic Hessian is diagonal with eigenvalues $\{a, b\}$, the conditioning can be summarized by ratios such as b/a(when $a > 0$) or more robustly by $(\max(a, b) + \varepsilon)/(\min(a, b) + \varepsilon)$with a small ε, and our sampling rules explicitly produce both well-conditioned and ill-conditioned regimes. This diversity is important because momentum methods can exhibit qualitatively different convergence modes across eigendirections, and a dataset dominated by a single conditioning regime would lead to overly optimistic conclusions about generalization.

A key design decision is that each labeled example is obtained by sampling a random point along the trajectory rather than using only the final iterate or fitting a single global rate per run. This construction is intentional: Heavy Ball dynamics are not uniformly contracting at every iteration, and the observed decay may include oscillatory and nonmonotone segments even when the method eventually converges. By sampling along the trajectory, the dataset captures local regimes that are otherwise averaged out, allowing the model to learn how (α, β), curvature, and initialization jointly affect the instantaneous progress of optimization at different stages. Practically, this also increases the informativeness of the dataset because it exposes the learner to a wider range of convergence behaviors within a fixed simulation budget, enabling finer-grained prediction of convergence-related

quantities beyond what a single per-run summary statistic can provide. The appearance of the dataset is presented in table 1.

Table 1. Table captions should be placed above the tables

	a	b	alpha	beta	x0_1_norm	x0_2_norm	iter_norm	target_log10
0	3,75	385,21	0,01	0,73	-0,69	-0,88	0,29	-9,92
1	3,34	142,86	0,00	0,65	0,88	-1,00	0,92	-4,65
2	6,17	283,50	0,00	0,01	-0,20	-0,91	0,62	-3,13
3	3,66	236,82	0,00	0,78	0,18	-0,91	0,45	-10,63
4	1,71	119,52	0,03	0,95	-0,39	-0,80	0,30	-3,14
,,,	…	…	…	…	…	…	…	…
19995	458,77	311,31	0,00	0,17	-0,55	-0,58	0,08	-15,66
19996	295,70	116,68	0,00	0,93	0,09	0,06	0,18	-2,44
19997	334,71	120,41	0,00	0,36	0,15	0,31	0,05	-6,06
19998	89,13	181,54	0,00	0,59	0,53	0,27	0,06	-2,30
19999	161,28	113,63	0,00	0,89	-0,57	-0,41	0,34	-5,40

2. Model Training&Numerical Experiments. To model the relationship between optimization parameters and convergence behavior, we employ a tree-based ensemble method augmented with a self-attention mechanism. Random Forest–type models are particularly well suited for this task due to their ability to approximate highly nonlinear dependencies, robustness to feature scaling, and stability when trained on heterogeneous synthetic data. Unlike parametric models, ensemble trees do not impose restrictive assumptions on the functional form of the mapping between inputs and outputs, which is essential when modeling complex optimization dynamics driven by interacting hyperparameters and trajectory-dependent effects.

However, standard Random Forests treat all samples independently and lack an explicit mechanism for adaptively weighing feature interactions across the dataset. To address this limitation, we adopt the Self-Attention Forest framework proposed in [12], which extends classical tree ensembles by integrating an attention mechanism into the aggregation of individual estimators. In this framework, attention weights are computed based on similar relationships defined in the target space, allowing the model to dynamically reweigh tree contributions depending on the structure of the regression problem. In the context of convergence modeling, this mechanism enables the model to emphasize trajectory samples exhibiting similar objective decay patterns while reducing the influence of outliers arising from transient oscillations or near-critical parameter regimes. As a result, the architecture retains the interpretability and robustness of tree ensembles while incorporating a data-dependent aggregation strategy inspired by attention-based models.

The model is trained in a supervised regression setting using the synthetically generated dataset described in the previous section. Extra Trees are employed as base learners to increase variance reduction and improve generalization across diverse optimization regimes. Model hyperparameters, including the number of estimators, tree depth, and attention-related coefficients, are selected to balance expressive power and stability. Training is performed using a fixed random seed to ensure reproducibility, and all experiments are conducted without problem-specific tuning for individual objective functions.

To ensure that the reported results reflect genuine generalization rather than memorization of trajectory patterns, the dataset was randomly partitioned into training and validation subsets using an 80/20 split with a fixed random seed. The partitioning was performed after full dataset construction and shuffling, so that samples originating from different objective parameter regimes and trajectory segments were evenly distributed across both subsets. The model was trained exclusively on the training portion, while all quantitative and qualitative evaluations were conducted on the held-out

validation set. No resampling or reweighting strategies were applied, and the validation data were not used for hyperparameter tuning. This protocol ensures that the predictive performance reflects the model's ability to infer convergence behavior for previously unseen combinations of curvature parameters, hyperparameters, and trajectory stages.

Model performance is evaluated using the coefficient of determination R^2, which measures the agreement between predicted and empirically observed convergence-related quantities. In addition to global regression accuracy, qualitative agreement between predicted and true optimization trajectories is assessed by reconstructing objective decay curves from model predictions and comparing them to actual Heavy Ball trajectories. Numerical experiments are conducted on several benchmark objective functions, including the Rastrigin, Booth, and Himmelblau functions, which exhibit distinct landscape properties and convergence behaviors. Across all tested functions, the proposed model accurately captures the overall decay trend of the objective value, closely matching the empirical convergence profiles despite the presence of oscillations and nonmonotonic behavior in the true trajectories.

A complementary view of predictive performance is provided by the parity plot shown in Figure 4, where predicted values of the logarithmic decay measure are plotted against their empirical counterparts on the validation set. The concentration of points along the diagonal indicates a strong correspondence between predicted and observed convergence behavior across the full dynamic range of the target variable. Importantly, dispersion remains controlled even in the regime of large negative values, which correspond to late-stage convergence where objective values approach numerical precision limits. The absence of systematic bias in the central region and the preservation of monotonic structure across scales confirm that the model captures the dominant contraction patterns of the Heavy Ball dynamics rather than overfitting isolated trajectory segments.

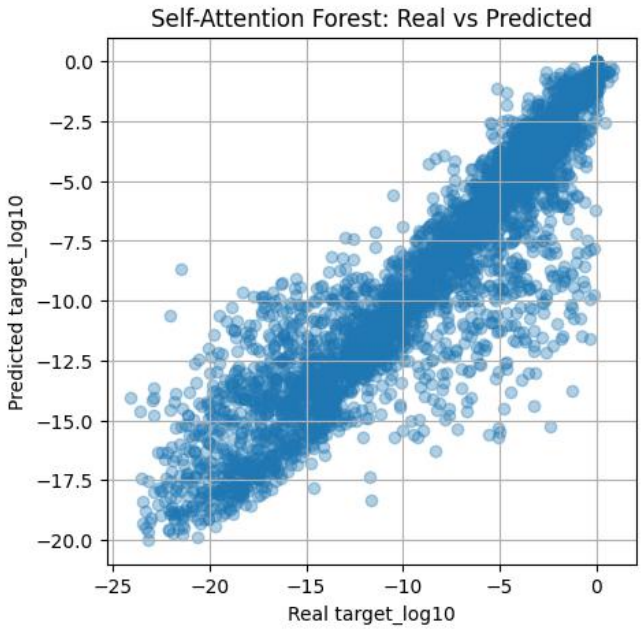

Fig. 1. Parity plot comparing the empirical logarithmic convergence measure with the corresponding predictions of the self-attention–augmented Random Forest on the validation set

The high R^2 values observed in these experiments indicate that the model successfully learns the underlying relationship between optimization parameters and convergence dynamics. These results demonstrate that self-attention–augmented tree ensembles provide an effective and flexible tool for modeling convergence rate estimates and can generalize across objective functions with substantially different structural properties. The results are presented on the figures 2-4.

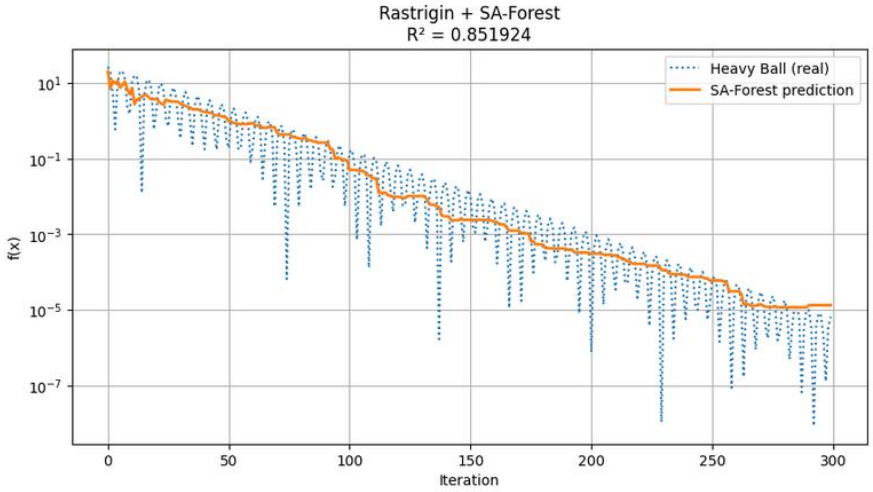

Fig. 2. Comparison between the true Heavy-Ball convergence trajectory and the trajectory predicted by the self-attention–augmented Random Forest for the Rastrigin function

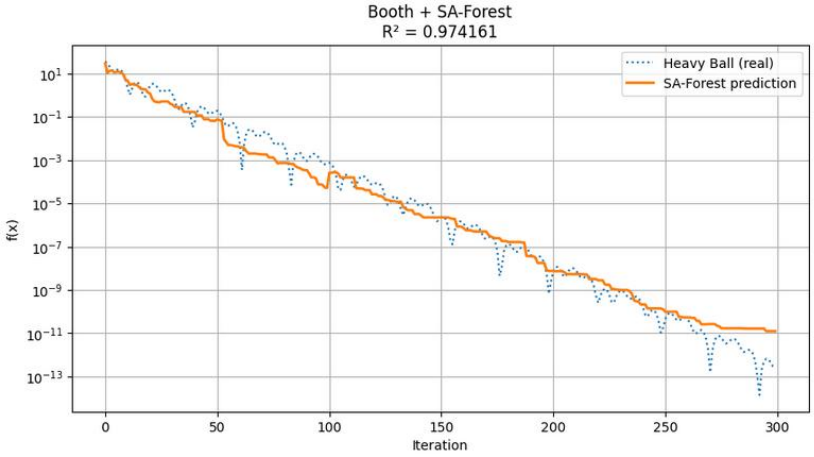

Fig. 3. Comparison of the true Heavy Ball convergence trajectory and the convergence profile predicted by the self-attention–augmented Random Forest for the Booth function

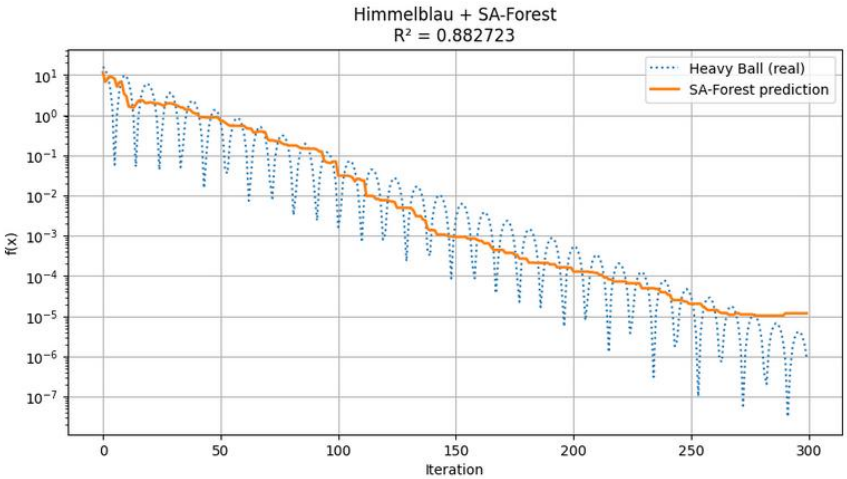

Fig. 4. Comparison of the true Heavy Ball convergence trajectory and the convergence profile predicted by the self-attention–augmented Random Forest for the Himmelblau function

3. Conclusion. This paper proposed a data-driven approach to modeling convergence rate estimates of iterative optimization methods, motivated by the fact that classical convergence analysis is often either overly conservative or impractical when applied to modern training pipelines. Instead of relying on closed-form bounds derived under restrictive assumptions, we treated the optimization algorithm as a dynamical system and learned a surrogate mapping from a compact description of the optimization setting to convergence-related quantities measured along trajectories. The Heavy Ball method was used as a technically demanding case study, since its inertial term induces oscillatory and regime-dependent behavior, and its performance is strongly influenced by the interaction between the step size, the momentum coefficient, and curvature properties of the objective.

A central contribution of the work is the construction of a synthetic dataset that explicitly targets convergence modeling. By simulating trajectories under diverse objective parameters, hyperparameters, and initial conditions, and by sampling states along stable runs, the dataset captures a broad spectrum of dynamical regimes, including fast contraction, transient oscillations, and near-critical configurations. This design allows the learning problem to focus on predicting empirically observed decay behavior rather than reproducing worst-case theoretical rates. Using this dataset, we trained a self-attention–augmented tree ensemble and demonstrated that the model can accurately predict convergence-related quantities and reconstruct objective value decay profiles across multiple benchmark functions. The obtained results indicate that the surrogate model captures the dominant convergence trends even when the underlying trajectory is nonmonotone, which is a typical feature of momentum-based optimization.

Beyond empirical accuracy, the proposed framework has methodological implications. First, it provides a practical alternative to repeated trial-and-error experimentation when selecting hyperparameters, since the surrogate can be queried to anticipate the likely convergence behavior for a given configuration. Second, it creates a pathway toward automated convergence analysis, where learned models can be used to compare optimizers, detect unstable regimes, and prioritize hyperparameter regions that yield favorable convergence profiles. Third, although the present study focuses on Heavy Ball dynamics, the same dataset-driven design can be extended to other optimization schemes. Momentum-accelerated methods such as Nesterov's acceleration exhibit similar second-order behavior and sensitivity to curvature, making them natural candidates for the same modeling pipeline. Adaptive methods such as Adam and RMSProp introduce additional state variables through moment estimates and coordinate-wise scaling; however, they can still be viewed within the same black-box dynamical perspective by expanding the feature representation to include algorithmic state summaries or statistics of gradient history. In this sense, the proposed methodology is not tied to a particular optimizer, but rather to the general principle of learning convergence behavior from trajectory data.

Finally, several directions remain for future work. Extending the approach from synthetic objectives to real training losses would require addressing stochastic gradients, minibatch noise, and nonstationarity, as well as defining convergence proxies that remain stable under stochastic dynamics. Another important direction is improving interpretability: while attention-enhanced tree ensembles offer some transparency, a deeper analysis of feature sensitivities could yield actionable insights into how curvature, momentum, and initialization jointly shape convergence regimes. Overall, the results of this study support the view that machine learning surrogates can substantially reduce the cost of convergence rate estimation, provide flexible tools for optimizer analysis, and serve as building blocks for automated systems that predict and improve optimization behavior in large-scale machine learning.

Author contributions D.M. (Daniil Miroshnichenko) conceptualized the study, developed the methodology, implemented the random forest with self-attention model, conducted the experiments, analyzed the results, prepared the figures, and wrote the original draft of the manuscript.M.A. (Majid Abbasov) supervised the research, contributed to the theoretical analysis and interpretation of the results, reviewed and edited the manuscript, validated the methodology, and approved the final version of the manuscript.All authors have read and agreed to the published version of the manuscript.
Funding. The authors received no financial support from any funding agency, commercial organization, or not-for-profit institution for the research, authorship, and/or publication of this article.
Data Availability. No datasets were generated or analyzed during the current study.
Declarations
Conflict of Interest. The authors declare that they have no competing interests or conflicts of interest.
Ethical Approval. This article does not contain any studies involving human participants or animals performed by any of the authors.
Informed Consent. Not applicable.

References

[1] Polyak, B. T. (1964). Some methods of speeding up the convergence of iteration methods. *USSR Computational Mathematics and Mathematical Physics, 4*(5), 1–17. https://doi.org/10.1016/0041-5553(64)90137-5
[2] Nesterov, Y. (2004). *Introductory lectures on convex optimization: A basic course*. Springer. https://doi.org/10.1007/978-1-4419-8853-9
[3] Bottou, L., Curtis, F. E., & Nocedal, J. (2018). Optimization methods for large-scale machine learning. *SIAM Review*, *60*(2), 223–311. https://doi.org/10.1137/16M1080173
[4] Andrychowicz, M., Denil, M., Gómez, S., Hoffman, M. W., Pfau, D., Schaul, T., Shillingford, B., & de Freitas, N. (2016). Learning to learn by gradient descent by gradient descent. In *Advances in Neural Information Processing Systems* (Vol. 29).
[5] Lessard, L., Recht, B., & Packard, A. (2016). Analysis and design of optimization algorithms via integral quadratic constraints. *SIAM Journal on Optimization, 26*(1), 57–95. https://doi.org/10.1137/15M1009597
[6] Su, W., Boyd, S., & Candès, E. J. (2016). A differential equation for modeling Nesterov's accelerated gradient method. *Journal of Machine Learning Research, 17*(153), 1–43.
[7] Chen, T., Chen, X., Chen, W., & Wang, Z. (2022). Learning to optimize: A primer and a benchmark. *Journal of Machine Learning Research, 23*, 1–59.
[8] Trajanov, R., Dimeski, S., Popovski, M., Korošec, P., & Eftimov, T. (2022). *Explainable landscape analysis in automated algorithm performance prediction*. arXiv:2203.11828.
[9] Pietrenko-Dąbrowska, A., et al. (2024). Variable resolution machine learning for global antenna optimization using sensitivity-analysis-based dimensionality reduction. *Scientific Reports, 14*, 28796. https://doi.org/10.1038/s41598-024-77367-w
[10] Zhao, Y., et al. (2024). A review on optimization algorithms and surrogate models. *Geoenergy Science and Engineering, 234*, 212554. https://doi.org/10.1016/j.geoen.2023.212554
[11] Rane, N. L., Choudhary, S., & Rane, J. (2024). Techniques and optimization algorithms in machine learning: A review. In *Machine Learning and Artificial Intelligence* (pp. 27–48). Deep Science Publishing. https://doi.org/10.70593/978-81-981271-4-3_2
[12] Utkin, L. V., & Konstantinov, A. V. (2022). *Self-Attention Forests*. arXiv:2207.04293.

https://doi.org/10.58225/sw.2026.1-62-72

t-BASICITY OF ROOT FUNCTIONS OF ONE NONLOCAL SPECTRAL PROBLEM FOR BOCHNER SPACE

Bilalov Bilal [1,2], Sadigova Sabina[2]
[1]*Yildiz Technical University, Istanbul, Turkiye*
[2]*Ministry of Science and Education, Baku, Azerbaijan*
bilalov.bilal@gmail.com, sadigova.sr@gmail.com

Abstract. We consider the system of functions, which are the root functions of one nonlocal spectral problem. It is introduced the concept of t-basis, induced by some tensor product. It is established the t-basisity of root functions for Bochner space $L_p(\mathcal{J};X)$, $1<p<+\infty$, if X is UMD (Unconditional Martingale Difference) space, where $\mathcal{J}=(0,2\pi)$. For this goal we firstly define the concept of t-Riesz property for classical trigonometric system and prove that if X is UMD space, then the trigonometric system has t-Riesz property in $L_p(\mathcal{J};X)$, $1<p<+\infty$.

Keywords: nonlocal spectral problem, t-basicity, t-Riesz property, Bochner space, Unconditional Martingale Difference property

Cite this article as: *B. Bilalov and S. Sadigova, "t-BASICITY OF ROOT FUNCTIONS OF ONE NONLOCAL SPECTRAL PROBLEM FOR BOCHNER SPACE," SW AzUAC, vol. 1, 2026, doi:10.58225/sw.2026.1-62-72*
Article history: *Received: 20 April 2026 / Revised: 22 June 2026 / Accepted: 30 June 2026*

1. Introduction. Banach valued differential equations have applications in various areas of mathematics such as partial differential equations, stochastic evolution equations, harmonic analysis, spectral theory of linear (in particular of differential) operators and etc. By this reason the interest to the X-valued differential equations very hight. This theory in one variable case sufficiently well developed (see, e.g. the monographs [1-7]). In connection with the development of analysis in Banach spaces it began to be studied solvability questions of X-valued differential equations in many variable case (see, e.g. the works [8-15, 19- 21]).

We consider the system of functions, which are the root functions of one nonlocal spectral problem. It is introduced the concept of t-basis, induced by some tensor product. It is established the t-basicity of root functions for Bochner space $L_p(\mathcal{J};X)$, $1<p<+\infty$, if X is UMD (Unconditional Martingale Difference) space, where $\mathcal{J}=(0,2\pi)$. For this goal we firstly define the concept of t-Riesz property for classical trigonometric system and prove that if X is UMD space, then the trigonometric system has t-Riesz property in $L_p(\mathcal{J};X)$, $1<p<+\infty$.

Note that UMD property for B-space X provides boundedness for many operators of harmonic analysis in Bochner spaces. And this in turn allows us to generalize the concept of a basis in the context of a Banach tensor product and to prove that the classical exponent system and their generalization Faber polynomials form basis for corresponding Bochner spaces in this sense. Using these results in works [16-18] it is given the X-valued analogues of Hardy and Smirnov classes of analytic functions and it is established some basic properties of these classes.

2. Preliminaries.

2.1. Notations. Accept the following notations. $\mathbb{N}$ – natural numbers; $\mathbb{Z}_+ = \{0\} \cup \mathbb{N}$; $\mathbb{R}$ – real numbers; $\mathbb{C}$ – complex numbers; $\mathcal{J} = (0,2\pi)$; $I = (-\pi,\pi)$. $L[M]$ is a linear span of M; $\overline{M}$ is a closure of M; B-space will be a Banach space. $\|\cdot\|_X$ will stand for the norm in X. By $[X;Y]$ we will denote a B-space of bounded (linear) operators from X to Y with $[X] = [X;X]$.

2.2. t-basis properties. t-basis from exponents. Let X, Y, Z be B-spaces and $t: X \times Y \to Z$ be a bilinear operator satisfying the following condition $\exists \delta > 0: \delta \| x \|_X \| y \|_Y \leq \| t(x;y) \|_Z \leq \delta^{-1} \| x \|_X \| y \|_Y$, $\forall (x;y) \in X \times Y$.

For simplicity, future presentation accepts the notation $xy := t(x;y)$ for every $(x;y) \in X \times Y$.

We denote t-span of M by $L_t[M]$ for the set $M \subset Y$ and define it as

$$L_t[M] = \{z \in Z: \exists \{(x_k;y_k)\}_1^{n_0} \subset X \times M \Rightarrow z = \sum_{k=1}^{n_0} x_k y_k\}.$$

Let $\tilde{y} \equiv \{y_k\}_{k\in\mathbb{N}} \subset Y$ be some system. Accept the following concepts.

System $\tilde{y}$ is t-complete in Z, if $\overline{L_t[\tilde{y}]} = Z$ (closure is taken in Z).

The system of operators $\{t_n\}_{n\in\mathbb{N}} \subset [Z;X]$ is called t-biorthogonal to $\tilde{y} \subset Y$, if $t_n(xy_k) = x\delta_{nk}$, $\forall x \in X \forall n,k \in \mathbb{N}$.

The system $\tilde{y} \subset Y$ forms t-basis for Z if $\forall z \in Z$ has a unique expansion in the form

$$z = \sum_{k=1}^{\infty} x_k y_k,$$

with $\{x_k\}_{k\in\mathbb{N}} \subset X$.

We call a triple $(X;Y;Z)$ be t_Y-invariant if $\{(x_k;\tilde{y}_k)\} \subset X \times Y: \sum_k x_k \tilde{y}_k = 0 \Rightarrow \sum_k \vartheta(\tilde{y}_k)x_k = 0$, $\forall \vartheta \in Y^*$.

Triple (X,Y,Z) is t-dense if $\overline{L[X \times Y]} = Z$ (closure is taken in Z).

The following criterion for t-basicity is valid.

Theorem 2.1 *Let the triple $(X;Y;Z)$ be t_Y-invariant and t-dense. Then the system $\tilde{y}$ forms a t-basis for Z if and only if the following assertions hold:*

- *(i) $\tilde{y}$ is t-complete in Z;*
- *(ii) $\tilde{y}$ has t-biorthogonal system $\{t_n\}_{n\in\mathbb{N}} \subset [Z;X]$;*
- *(iii) the projectors $\{P_m\}_{m\in\mathbb{N}}$:*

$$P_m(z) = \sum_{n=1}^{m} t_n(z)y_n, \qquad \forall z \in Z \forall m \in \mathbb{N},$$

are uniformly bounded, i.e. $\sup_m \| P_m \|_{[Z]} < \infty$.

We consider Z as the some Banach tensor product $X \overline{\otimes} Y$ of B-spaces X and Y. Denote the algebraic tensor product of XY by $X \otimes Y$ and the elementary tensor product of elements $x \in Xy \in Y$ by $x \otimes y$. In this case, it is obvious that the triple $(X;Y;Z)$ is $t-$ dense and $t_Y -$ invariant regarding the bilinear map $t(x,y) = x \otimes y$. Thus, according to the Theorem 2.1 we have the following

Corollary 2.2 *Let $X;Y$ be B-spaces and $Z = X \overline{\otimes} Y$. Then the system $\tilde{y} \subset Y$ forms $t-$ basis for Z if and only if the assertions $(i)-(iii)$ of Theorem 2.1 hold.*

2.3. Bochner Spaces and UMD Space. Let $(\mathcal{S}, \mathcal{A}, \mu)$ be a measure space and X be B-space. As usual, denote by $L_p(\mathcal{S}; X)$, $1 \leq p < +\infty$, the Bochner space generated by measure space $(\mathcal{S}; \mathcal{A}; \mu)$ with norm

$$\| f \|_{L_p(\mathcal{S};X)} = \left(\int_{\mathcal{S}} \| f \|_X^p \, d\mu\right)^{\frac{1}{p}}.$$

The Bochner space $L_p(\gamma; X)$ is defined similarly. We identify the segment I_0 and unit circle γ by mapping $e^{it}: I_0 \to \gamma$. This allows us to identify also the spaces $L_p(I_0; X)$ and $L_p(\gamma; X)$.
We provide the definition of the UMD property and the associated space.
Definition 2.3 *A Banach space X is said to have the property of UMD, if for all $p \in (1, \infty)$ there exists a finite constant $\beta \geq 0$ (depending on p and X) such that the following holds: whenever $(\mathcal{S}; \mathcal{A}; \mu)$ is a $\sigma - finite$ measure space, $\{\mathcal{F}_n\}_{n=0}^N$ is a $\sigma - finite$ filtration and $\{f_n\}_{n=0}^N$ is a finite martingale in $L_p(\mathcal{S}; X)$, then for all scalar $|\varepsilon_n| = 1$, $n = \overline{1, N}$; we have*

$$\| \sum_{n=1}^{N} \varepsilon_n df_n \|_{L_p(\mathcal{S};X)} \leq \beta \| \sum_{n=1}^{N} df_n \|_{L_p(\mathcal{S};X)}.$$

where $df_n = f_n - f_{n-1}$ is a martingale difference.
Let the set of all B-spaces that possess the UMD property be denoted by the symbol UMD.
To establish an analogous of the classical Fatou's theorem regarding harmonic functions on ω, we will need the following lemma from the monograph [21] (see p.127, Lemma 2.5.8).
Lemma 2.4 *[21] Let $g \in L_1^{loc}(\mathbb{R}; X)$ and $a \in \mathbb{R}$ and define $f: \mathbb{R} \to X$ by*

$$f(t) =: \int_a^t g(s) ds$$

Then the weak derivative ∂f and almost everywhere derivative f' of f both exist in $L_1^{loc}(\mathbb{R}; X)$ and are given by the $\partial f = f' = g$.
The set of all X-valued trigonometric polynomials $P_n: I_0 \to X$ of the form

$$P_n(t) = \sum_{k=-n}^{n} a_k e^{ikt},$$

with coefficients $\{a_k\} \subset X$, denote by $\mathcal{P}(X)$.
The following proposition is valid.
Proposition 2.5 *Let X be a B-space. Then $\overline{\mathcal{P}(X)} = L_p(I_0; X), 1 \leq p < \infty)$ (closure is taken in $L_p(I_0; X)$).*
We define on $\mathcal{P}(X)$ the multiplier operator $m: \mathcal{P}(X) \to L_p(I_0; X)$ by expression

$$(mP)(t) = \tilde{P}(t) = -i \sum_{k \in \mathbb{Z}} sign(k) a_k e^{ikt},$$

where

$$P(t) = \sum_{k \in \mathbb{Z}} a_k e^{ikt} \in \mathcal{P}(X),$$

and

$$sign(k) = \begin{cases} 1, & \text{if} k > 0, \\ 0, & \text{if} k = 0, \\ -1, & \text{if} k < 0. \end{cases}$$

We also consider the subspace $L_p^0(I_0;X)$ of $L_p(I_0;X)$ defined by

$$L_p^0(I_0;X) = \{f \in L_p(I_0;X): \int_{I_0} f(t)dt = 0\}.$$

Let H be the X-valued Hilbert transform on $\mathbb{R}$:

$$(Hf)(x) = \frac{1}{\pi}\int_{\mathbb{R}} \frac{f(y)}{x-y}dy, x \in \mathbb{R},$$

defined in a singular sense. The following H-characterization of UMD property is known.

Theorem 2.6 *[Burkholder-Bourgain] Let X be a B-space $p \in (1,\infty)$. The following assertions are equivalent:*

- $X \in$ UMD;
- $H \in [L_p(\mathbb{R};X)]$.

In future, we strongly will use the following proposition.

Proposition 2.7 *Let X be a B-space $p \in (1,\infty)$. If $H \in [L_p(\mathbb{R};X)]$, then $m \in [L_p^0(I_0;X)]m \in [L_p(I_0;X)]$.*

Further details regarding these and related results can be found, for example, in the monograph [21].

In what follows, for function $f \in L_1(I_0;X)$, we denote by $\{\hat{f}_k\}_{k\in\mathbb{Z}}$ (also written as $\{t_k(f)\}_{k\in\mathbb{Z}}$) the sequence of its X-valued Fourier coefficients, given by

$$\hat{f}_k := t_k(f) := \frac{1}{2\pi}\int_J f(t)e^{-ikt}dt, k \in \mathbb{Z}.$$

In work [6], the following theorem is proved.

Theorem 2.8 *[6] Let $X \in UMDp \in (1,\infty)$. Then the exponential system $\mathcal{E} = \{e^{int}\}_{n\in\mathbb{Z}}$ forms t-basis for $L_p(I_0;X)$, i.e. $\forall f \in L_p(I_0;X)$ has a unique expansion in the form*

$$f(t) = \sum_{n\in\mathbb{Z}} \hat{f}_n e^{int}, \quad (2.1)$$

in $L_p(I_0;X)$. Moreover, for $\forall m \in \mathbb{Z}$, the following series

$$(R_m^+ f)(t) = f_+(t) = \sum_{n=m}^{\infty} \hat{f}_n e^{int},$$

$$(R_m^- f)(t) = f_-(t) = \sum_{n=-\infty}^{m-1} \hat{f}_n e^{int},$$

also converges in $L_p(I_0;X)$ (so-called t-Riesz property) and $R_m^{\pm} \in [L_p(I_0;X)]$.

2.4 *t*-basicity of trigonometric system. *t*-Riesz property

Consider the following classical trigonometric system

$$\left\{\frac{1}{2}, \cos nx, \sin nx\right\}_{n\in\mathbb{N}}. \tag{2.2}$$

Let $f \in L_p(\mathcal{J};X)$. Denote by $\{\hat{f}_n^{\,c}, \hat{f}_n^{\,s}\}_{n\in\mathbb{Z}_+}$ the Fourier coefficients of f on (2.2):

$$\left.\begin{aligned} v_n^c(f) = \hat{f}_n^{\,c} &= \frac{1}{\pi}\int_0^{2\pi} f(t)\cos nt\, dt, \quad n \in \mathbb{Z}_+; \\ v_n^s(f) = \hat{f}_n^{\,s} &= \frac{1}{\pi}\int_0^{2\pi} f(t)\sin nt\, dt, \quad n \in \mathbb{N}. \end{aligned}\right\} \tag{2.3}$$

and denote by

$$S_n(f)(t) = \frac{1}{2}\hat{f}_0^{\,c} + \sum_{k=1}^{n}\left(\hat{f}_k^{\,c}\cos kt + \hat{f}_k^{\,s}\sin kt\right), \quad k \in \mathbb{N},$$

the Fourier sums of f. Paying attention to the expression

$$\hat{f}_k = \frac{1}{2\pi}\int_0^{2\pi} f(t)e^{-ikt}\, dt, \quad k \in \mathbb{Z},$$

we obtain

$$\tilde{S}_n(f)(t) = \sum_{k=-n}^{n}\hat{f}_k e^{ikt} = \hat{f}_0 + \sum_{k=1}^{n}\hat{f}_k(\cos kt + i\sin kt) + \sum_{k=1}^{n}\hat{f}_{-k}(\cos kt - i\sin kt)$$
$$= \hat{f}_0 + \sum_{k=1}^{n}[(\hat{f}_k + \hat{f}_{-k})\cos kt + i(\hat{f}_k - \hat{f}_{-k})\sin kt],$$

and in result it is true the relations between Fourier coefficients

$$\hat{f}_0^{\,c} = 2\hat{f}_0, \quad \hat{f}_k^{\,c} = \hat{f}_k + \hat{f}_{-k}, \quad \hat{f}_k^{\,s} = i(\hat{f}_k - \hat{f}_{-k}), \quad k \in \mathbb{N}.$$

Conversely, it holds

$$\hat{f}_0 = \frac{1}{2}\hat{f}_0^{\,c}, \quad \hat{f}_k = \frac{1}{2}\left(\hat{f}_k^{\,c} - i\hat{f}_k^{\,s}\right), \quad \hat{f}_{-k} = \frac{1}{2}\left(\hat{f}_k^{\,c} + i\hat{f}_k^{\,s}\right), \quad k \in \mathbb{N}.$$

Consequently, from these relations and from Theorem 2.8 follows the validity of the following

Proposition 2.9 *Let X be UMD space. Then the trigonometric system (2.2) forms t-basis for $L_p(\mathcal{J};X)$, $1 < p < +\infty$.*

It is obvious that $f(\cdot) \in L_p(I;X) \Leftrightarrow f(\cdot - \pi) \in L_p(\mathcal{J};X)$, and it holds

$$\| f(\cdot) \|_{L_p(I;X)} = \| f(\cdot - \pi) \|_{L_p(\mathcal{J};X)}.$$

Taking into account this relation we obtain that the Proposition 2.9 is equivalent to the following

Proposition 2.10 *Let X be UMD space. Then the exponential system $\mathcal{E}$ and at the same time the trigonometric system (2.2) forms t-basis for $L_p(I;X)$, $1 < p < +\infty$.*

Let the system (2.2) forms t-basis for $L_p(I;X)$. Assume

$$L_p^c(I;X) = \overline{L_t[\{\cos nt\}_{n\in\mathbb{Z}_+}]};$$

$$L_p^s(I;X) = \overline{L_t[\{\sin nt\}_{n\in\mathbb{N}}]}.$$

Take $\forall f \in L_p(I;X)$ and represent it in the form

$$f(t) = f^+(t) + f^-(t),$$

where

$$\left.\begin{aligned} f^+(t) &= \tfrac{f(t)+f(-t)}{2} \quad -\text{even},\\ f^-(t) &= \tfrac{f(t)-f(-t)}{2} \quad -\text{odd}, \end{aligned}\right\} \tag{2.4}$$

parts of f. It is evident that

$$f(\cdot) \in L_p(I;X) \Leftrightarrow f(-\cdot) \in L_p(I;X).$$

Paying attention to this relation from (2.4) follows $f^{\pm} \in L_p(I;X)$. Expanding $f(\cdot)$ on the basis (2.2) we have

$$f(t) = S(f) = \frac{1}{2}f_0{}^c + \sum_{k=1}^{\infty}(f_k{}^c \cos kt + f_k{}^s \sin kt).$$

Since $f^-(\cdot)$ is odd and $f^+(\cdot)$ is even functions we have

$$S_n^c(f) = \frac{1}{2}f_0{}^c + \sum_{k=1}^{n} f_k{}^c \cos kt = \frac{1}{2}v_0^c(f) + \sum_{k=1}^{n} v_k^c(f)\cos kt$$

$$= \frac{1}{2}v_0^c(f^+) + \sum_{k=1}^{n} v_k^c(f^+)\cos kt$$

$$+\frac{1}{2}v_0^c(f^-) + \sum_{k=1}^{n} v_k^c(f^-)\cos kt = v_0^c(f^+) + \sum_{k=1}^{n} v_k^c(f^+)\cos kt$$

$$= v_0^c(f^+) + \sum_{k=1}^{n}[v_k^c(f^+)\cos kt + v_k^s(f^+)\sin kt] = S_n(f^+), \quad \forall n \in \mathbb{Z}_+,$$

here we took into account that $v_k^s(f^+) = 0$, $\forall k \in \mathbb{N}$. From here we obtain the sequence $\{S_n^c(f)\}_{n\in\mathbb{Z}_+}$ converges in $L_p(I;X)$ (namely, $S_n^c(f) \to f^+$, $n \to \infty$).

Analogously, it follows

$$S_n^s(f)=\sum_{k=1}^{n} f_k^s \sin kt=\sum_{k=1}^{n} v_k^s(f)\sin kt=v_0^c(f^-)+\sum_{k=1}^{n} v_k^c(f^-)\cos kt+\sum_{k=1}^{n} v_k^s(f^-)\sin kt$$
$$=S_n(f^-),\quad \forall n\in\mathbb{N}$$

(where we took into account that $v_k^c(f^-)=0$, $\forall k\in\mathbb{Z}_+$). Consequently, $S_n^s(f)\to f^-$, $n\to\infty$, in $L_p(I;X)$, and let

$$S^c(f)=\frac{1}{2}v_0^c(f)+\sum_{k=1}^{\infty} v_k^c(f)\cos kt,$$

$$S^s(f)=\sum_{k=1}^{\infty} v_k^s(f)\sin kt.$$

So, it is true

$$f=S(f)=S^c(f)+S^s(f),\quad \forall f\in L_p(I;X). \tag{2.5}$$

It is not hard to see that $S^c(f)\in L_p^c(I;X)$ and $S^s(f)\in L_p^s(I;X)$. Moreover, it is true

$$L_p^c(I;X)\cap L_p^s(I;X)=\{0\}.$$

Then from (2.5) it follows that the subspaces $L_p^c(I;X)$ and $L_p^s(I;X)$ are complemented in $L_p(I;X)$ and it holds the direct sum

$$L_p(I;X)=L_p^c(I;X)\dotplus L_p^s(I;X). \tag{2.6}$$

Let's accept the following

Definition 2.11 *We will call that the t-basis (2.2) for $L_p(I;X)$ has t-Riesz property in $L_p(I;X)$, if there exists a constant $C>0$, such that*

$$\| S_n^c(f)\|_{L_p(I;X)}\le C\,\|f\|_{L_p(I;X)},$$

$$\| S_n^s(f)\|_{L_p(I;X)}\le C\,\|f\|_{L_p(I;X)},$$

$\forall f\in L_p(I;X)$, $\forall n\in\mathbb{N}$.

From above reasoning the following proposition follows.

Proposition 2.12 *Let X be UMD space. Then the t-basis (2.2) for $L_p(I;X)$, $1<p<+\infty$, has t-Riesz property in $L_p(I;X)$.*

3. Main results. Consider the following system

$$\{u_n^+(x);\ u_{n+1}^-(x)\}_{n\in\mathbb{Z}_+}, \tag{3.1}$$

where

$$u_n^+(x)=\cos nx,\quad u_{n+1}^-(x)=x\sin(n+1)x,\quad n\in\mathbb{Z}.$$

This system is a set of all root functions of the following nonlocal spectral problem

$$\left.\begin{aligned} u''(x)+\lambda^2 u(x)=0, \quad 0<x<2\pi, \\ u(0)=u(2\pi), \quad u'(0)=0. \end{aligned}\right\}$$

The main characteristic of this problem is that it has infinitely many associated functions. We will investigate t-basis properties of the system (3.1) in $L_p(\mathcal{J};X)$.

3.1 t-biorthogonality property of the system (3.1)

Let

$$\varphi_0^+(x)=\frac{2\pi-x}{2\pi^2}; \quad \varphi_k^+(x)=\frac{2\pi-x}{\pi^2}\cos kx;$$

$$\varphi_k^-(x)=\frac{1}{\pi}\sin kx, \quad k\in\mathbb{N}.$$

Consider the following operators

$$\left.\begin{aligned} t_k^+(f)=\int_0^{2\pi} f(x)\varphi_k^+(x)\,dx, \quad k\in\mathbb{Z}_+; \\ t_k^-(f)=\int_0^{2\pi} f(x)\varphi_k^-(x)\,dx, \quad k\in\mathbb{N}. \end{aligned}\right\} \tag{3.2}$$

It is obvious that there exist $C>0$, such that

$$\| t_k^{\pm}(f) \|_X \leq C \| f \|_{L_p(\mathcal{J};X)}, \quad \forall f\in L_p(\mathcal{J};X), \qquad \forall k.$$

From here immediately follows $\{t_k^{\pm}\}\subset[L_p(\mathcal{J};X);X]$. For elementary tensors of the form $f_n^{\pm}(\cdot)=u_n^{\pm}(\cdot)\otimes a$, $a\in X$, we have

$$t_k^+(f_n^+)=\delta_{kn}a; \quad t_k^+(f_{n-1}^-)=0, \quad \forall k,n\in\mathbb{Z}_+;$$

$$t_k^-(f_{n+1}^+)=0, \quad t_k^-(f_n^-)=\delta_{kn}a, \quad \forall k,n\in\mathbb{N}.$$

Consequently, the system of operators $\{t_k^+;\ t_{k+1}^-\}_{k\in\mathbb{N}}$ is a t-biorthogonal to the system $\{u_k^+;\ u_{k+1}^-\}_{k\in\mathbb{N}}$, i.e. it is valid

Lemma 3.1 *The system of operators* $\{t_k^+,;\ t_{k+1}^-\}_{k\in\mathbb{N}}$ *and* $\{u_k^+;\ u_{k-1}^-\}_{k\in\mathbb{N}}$ *are t-biorthogonal systems with respect to* $L_p(\mathcal{J};X)$.

3.2 t-Completeness. From Proposition 2.5 follows that the algebraic product $C_0^\infty(\mathcal{J})\otimes X$ is dense in $L_p(\mathcal{J};X)$. Thus, it is sufficient to prove that every elementary tensor $g(\cdot)\otimes a$, where $g\in C_0^\infty(\mathcal{J})$ & $a\in X$, can be approximated by t-linear combination of the system (3.1) in $L_p(\mathcal{J};X)$. In turn, for this it is sufficient to prove that $g\in\overline{L[(3.1)]}$ (the closure is taken in $L_p(\mathcal{J})$). And this immediately follows from the results of the works [22, 23]. So, it is valid the following

Lemma 3.2 *The system* (3.1) *is t-dense in* $L_p(\mathcal{J};X)$, $1\leq p<+\infty$.

3.3 t-basicity of the system (3.1). And now, let's prove the following main theorem.

Theorem 3.3 *Let X be UMD space. Then the system* (3.1) *forms t-basis for $L_p(\mathcal{J};X)$, $1<p<+\infty$.*

Proof. Paying attention to the Lemma 3.1 and Lemma 3.2, according to the t-basis criterion it is sufficient to prove that the projectors

$$P_{nm}(f)=\sum_{k=0}^{n} t_k^{+}(f)\cos kx+\sum_{k=1}^{m} t_k^{-}(f)\sin kx,$$

$\forall n\in\mathbb{Z}_+$, $\forall m\in\mathbb{N}$, are uniformly bounded, where the operators $\{t_k^{\pm}\}$ are defined by expressions (3.2). From these expressions we have

$$l_0^{+}(f)=\frac{1}{\pi^2}\vartheta_0^{c}(g),\quad l_k^{+}(f)=\frac{1}{\pi}\vartheta_k^{c}(g);$$

$$l_k^{-}(f)=\vartheta_k^{s}(f),\quad \forall k\in\mathbb{N},$$

where $g(x)=(2\pi-x)f(x)$, $x\in\mathcal{J}$, and $\{\vartheta_k^{c}(\cdot);\vartheta_k^{s}(\cdot)\}$ are Fourier coefficients on the system (2.2). Taking into account t-Riesz property of the system (2.2) in $L_p(\mathcal{J};X)$, we obtain

$$\| P_{nm}(f)\|_{L_p(\mathcal{J};X)}\le\frac{1}{\pi^2}\|\vartheta_0^{c}(g)\|_{L_p(\mathcal{J};X)}$$
$$+\frac{1}{\pi}\left\|\sum_{k=1}^{n}\vartheta_k^{c}(g)\cos kx\right\|_{L_p(\mathcal{J};X)}+\left\|\sum_{k=1}^{n}\vartheta_k^{s}(f)\sin kx\right\|_{L_p(\mathcal{J};X)}$$
$$\le \text{const}\,(\|g\|_{L_p(\mathcal{J};X)}+\|f\|_{L_p(\mathcal{J};X)})\le \text{const}\,\|f\|_{L_p(\mathcal{J};X)},\quad \forall n\in\mathbb{Z}_+,\qquad \forall m\in\mathbb{N}.$$

Acknowledgments
The authors would like to thank the Azerbaijan Science Foundation for supporting this research under Grant No. AEF-MGC-2024-2(50)-16/02/1-M16 02.

Funding
This work was supported by the Azerbaijan Science Foundation under Grant No. AEF-MGC-2024-2(50)-16/02/1-M16 02.

Data availability
No datasets were generated or analyzed during the current study.

Declarations

Conflict of interest
Bilal Bilalov is a member of the Editorial Board of this journal. He was not involved in the editorial handling, peer review, or decision-making process of this manuscript. The editorial process was handled independently. The authors declare no conflict of interest.

Author contributions
B.B. (Bilalov Bilal) and S.S. (Sadigova Sabina) jointly conceptualized the study, developed the methodology, conducted the investigation, analyzed the results, and contributed to writing and revising the manuscript. B.B. prepared the figures and performed the primary analysis, while S.S. supervised the research and validated the findings. Both authors read and approved the final manuscript.

References

[1] Schwartz, L. *Analysis*, Vol. II. Moscow (1972).
[2] Trenogin, V. A. *Functional Analysis*. Moscow (1980).
[3] Dunford, N., Schwartz, J. T. *Linear Operators. Part I: General Theory*. Moscow (1962).
[4] Krein, S. G. *Linear Equations in Banach Spaces*. Moscow (1971).
[5] Krein, S. G. *Linear Differential Equations in Banach Spaces*. Moscow (1967).
[6] Hille, E., Phillips, R. S. *Functional Analysis and Semi-Groups*. Moscow (1962).
[7] Arendt, W., Batty, C. J. K., Hieber, M., Neubrander, F. *Vector-Valued Laplace Transforms and Cauchy Problems*. Birkhäuser, Basel (2011). https://doi.org/10.1007/978-3-0348-0087-7
[8] Kreuter, V. M. *Vector-Valued Elliptic Boundary Value Problems on Rough Domains*. PhD Thesis, Universität Ulm (2018). https://doi.org/10.18725/OPARU-11852
[9] Lorist, E. *Vector-Valued Harmonic Analysis with Applications to SPDEs*. PhD Dissertation, Delft University of Technology, Delft (2021).
[10] Kreuter, M. *Sobolev Spaces of Vector-Valued Functions*. Master's Thesis, Ulm University (2015).
[11] Arendt, W. Vector-valued holomorphic and harmonic functions. *Concrete Operators* **3**, 68–76 (2016). https://doi.org/10.1515/conop-2016-0006
[12] Amann, H. Elliptic operators with infinite dimensional state space. *Journal of Evolution Equations* **1**, 143–188 (2001). https://doi.org/10.1007/PL00001384
[13] Arendt, W., Nikolski, N. Vector-valued holomorphic functions revisited. *Mathematische Zeitschrift* 234**,** 777–805 (2000). https://doi.org/10.1007/PL00004722
[14] Arendt, W., Nikolski, N. Addendum: Vector-valued holomorphic functions revisited. *Mathematische Zeitschrift* 252**,** 687–689 (2006). https://doi.org/10.1007/s00209-005-0842-2
[15] Denk, R., Hieber, M., Prüss, J. *R-Boundedness, Fourier Multipliers and Problems of Elliptic and Parabolic Type*. American Mathematical Society, Providence, RI (2003). https://doi.org/10.1090/surv/166
[16] Bilalov, B. T., Sadigova, S. R. The concept of t-basis and vector-valued Hardy classes. *Turkish Journal of Mathematics* **49**, 261–286 (2025). https://doi.org/10.55730/1300-0098.3552
[17] Bilalov, B. T., Sadigova, S. R., Sezer, Y. Vector-valued grand Hardy classes. *Journal of Contemporary Applied Mathematics* **15**(1), 122–155 (2025).
[18] Bilalov, B. T., Buyukarslan, A., Nasibova, N. P., Sadigova, S. R. X-valued Smirnov classes and t-basicity of Faber polynomials. *Journal of Contemporary Applied Mathematics* **16**(1), 94–108 (2026).
[19] Bilalov, B. T., Sadigova, S. R., Sezer, Y. On local solvability of 2m-th order X-valued elliptic equations (submitted).
[20] Bilalov, B. T., Sadigova, S. R., Sezer, Y. Schauder type estimates up to the boundary for m-th order X-valued elliptic equations (submitted).
[21] Bilalov, B. T., Sadigova, S. R. Schauder type estimates for m-th order X-valued elliptic operators and some properties of X-valued Poisson integrals in Banach spaces (submitted).
[22] Bilalov, B. T., Nasibova, N. P., Alili, V. Q. On the strong solvability of a nonlocal boundary value problem for the Laplace equation in an unbounded domain. *Journal of Contemporary Applied Mathematics* **15**(1), 92–106 (2025).

[23] Mammadov, T. J. Strong solvability of a nonlocal problem for the Laplace equation in weighted grand Sobolev spaces. *Azerbaijan Journal of Mathematics* **13**(1), 188–204 (2023). https://doi.org/10.56181/ajm.2023.v13.n1.188

[24] Bilalov, B. T., Sezer, Y., Hagverdi, H. On the basicity of one trigonometric system in Orlicz spaces. *Transactions of the National Academy of Sciences of Azerbaijan, Series of Physical-Technical and Mathematical Sciences: Mathematics* 44(1), 31–40 (2024). https://doi.org/10.30546/2617-7900.44.1.2024.31

https://doi.org/10.58225/sw.2026.1-73-81

SEISMIC RISK ASSESSMENT FRAMEWORK, REGULATORY EVOLUTION, AND REGIONAL SEISMICITY OF SAMSUN, TÜRKIYE

Humberto Varum[1], Sevda Özdemir[2]
[1]*Department of Civil Engineering University of Porto, Porto Portugal*
[3] *Ministry of İnterior Disaster and Emergency Management Presidency*
hvarum@fe.up.pt

Abstract. This paper discusses the legal framework, rapid assessment methodologies, and regional seismicity concerning existing reinforced concrete (RC) buildings under earthquake risk, with a specific focus on Samsun Province. Given Türkiye's high seismicity, identifying vulnerable structures prior to a catastrophic event is a matter of public safety. This study highlights the necessity of first-level seismic risk assessment methods and argues for the prioritization of public buildings. Furthermore, the geological and seismotectonic characteristics of Samsun and its districts are analyzed alongside historical earthquake data to contextualize the regional risk.
Keywords: Seismic Risk Assessment, Reinforced Concrete Buildings, Rapid Visual Screening, Public Buildings, Samsun Seismicity, North Anatolian Fault Zone (NAFZ), Türkiye Earthquake Building Code (TBDY-2018)

Cite this article as: *H. Varum, S. Özdemir, "SEISMIC RISK ASSESSMENT FRAMEWORK, REGULATORY EVOLUTION, AND REGIONAL SEISMICITY OF SAMSUN, TÜRKİYE", SW AzUAC, vol. 1, 2026, https://doi.org/sw.2026.1-73-81*
Article history: *Received: 16 May 2026 / Revised: 20 June 2026 / Accepted: 04 July 2026*

1.Introduction. Located on active seismic zones, Türkiye relies heavily on laws and enforcement regulations during the structural design and planning phases. These legal frameworks play a paramount role in establishing the fundamental principles for transforming buildings in high-risk areas following their seismic evaluation. Minimizing the impact of ground motions—the timing and magnitude of which remain unpredictable—on structures depends strictly on the design parameters and structural requirements defined by these regulations. Furthermore, constructing cities to specific standards by keeping abreast of advancements in earthquake engineering and innovations in building technology is only possible through seismic codes; these codes comprehensively delineate the structural models used in structural system analysis and design, as well as analysis methods based on seismic performance [2,4].

The inaugural earthquake regulation in Türkiye was drafted following the aftermath of the 1939 Erzincan earthquake and entered into force in 1940, utilizing the Italian seismic code of that era as its basis. Since no study regarding the seismic hazard mapping of Türkiye had been conducted until that date, seismic calculations were performed uniformly across all regions, irrespective of the building's actual location. Following the preparation of the earthquake zones map for Türkiye in 1942, seismic regulations published from 1947 onward conditioned structural calculations upon the seismicity of the specific region where the building is located. The seismic code, which was substantially revised in 2007

for the purpose of evaluating and retrofitting existing buildings, underwent its final revision in 2018 and entered into force in 2019.

With the 2018 revision executed in the Earthquake Regulation, the seismic hazard and its correlation with soil parameters—which had previously been addressed superficially—were rendered more realistic through the introduction of the seismic hazard map concept.

Table 1. Historical Overview of Earthquake Regulations

Regulation Title	*Effective Date*
Italian Construction Code for Structures to be Built in Earthquake Zones	1940
Provisional Construction Code for Earthquake Zones	1944
Building Regulation for Earthquake Zones in Türkiye	1949
Regulation on Structures to be Built in Earthquake Zones	1953
Regulation on Structures to be Built in Disaster Areas	1962
Regulation on Structures to be Built in Disaster Areas	1968
Regulation on Structures to be Built in Disaster Areas	1975
Regulation on Structures to be Built in Disaster Areas	1998
Regulation on Buildings to be Built in Earthquake Zones	2007
Türkiye Building Earthquake Regulation	2019

2. First-Level Seismic Risk Assessment Framework and Regional Seismicity of Samsun

2.1. First-Level Seismic Risk Assessment Approach. Considering that a vast majority of the building stock in Türkiye, which approaches nearly 20 million structures, was constructed prior to the Earthquake Regulation that entered into force in 1998, was updated in 2018, and took effect in 2019, it is imperative to rapidly inspect the existing building stock and practically rank these buildings in terms of risk severity to mitigate potential loss of life and property in anticipated earthquakes. Conducting detailed, individual structural analyses for a building stock consisting of millions of structures is both highly time-consuming and cost-prohibitive. For this reason, Tiered Assessment Methods, which yield results more rapidly and require less data, should be utilized in the seismic evaluation of the building stock. The Tiered Assessment Method is a methodology that progressively evaluates structures, moving from a preliminary observational inspection toward a more detailed and comprehensive seismic analysis. The initial step of this methodology is the First-Level Assessment Method (FLA) [1,3].

While developing FLA method, the objective is not to reach a definitive conclusion regarding the seismic safety of the inspected buildings, but rather to provide a preliminary insight for subsequent decisions such as retrofitting, strengthening, or demolition. Furthermore, in cases where a high volume of buildings must be inspected, a practical screening and prioritization for seismic evaluation can be established owing to these FLA method. Through this approach, it is possible to identify the buildings that require detailed inspection and to foresee the order of priority in which these identified risky structures should be subjected to comprehensive analysis. With the FLA method, also referred to as the First-Level Assessment Method (Street Screening Method), the seismic risk assessments of buildings can

be rapidly completed using formulations constructed with various parameter values, either without entering the building or by incorporating a partial interior inspection. Consequently, structures requiring "immediate intervention" in terms of seismic safety can be identified within a short period.

Following the First-Level Assessment Method, the inspected buildings are ranked based on their risk scores for the Second-Level Assessment, which incorporates as-built architectural surveys (measured drawings) and structural system parameters [5,6]. Consequently, prior to the Third-Level Assessment—wherein detailed seismic evaluations are performed—the existing building stock is thoroughly screened by prioritizing minimum cost and time efficiency [7].

In the earthquakes that Türkiye has experienced, public structures have suffered severe damage and rendered unusable just like other buildings, despite being designed with high importance factors. Public structures such as hospitals, police stations, and dormitories utilized for health, education, administration, and security purposes are high-occupancy buildings that must remain resilient and operational in the aftermath of a potential earthquake; thus, they require seismic evaluation as a matter of priority.

The formulation of the first-level assessment method was established on a legal framework through the Principles Regarding the Identification of Risky Structures, which is embedded within the Implementing Regulation of the Law on the Transformation of Areas Under Disaster Risk that entered into force in 2013. Containing distinct parameters and inspection criteria for reinforced concrete and masonry structures, this method is utilized exclusively to determine the seismic risk prioritization of buildings and to generate regional seismic risk distribution maps. These data can also be utilized to identify priority areas within urban transformation planning.

2.2. Regional Seismic Characteristics of Samsun. With a surface area of 9,083 km^2, the province of Samsun is situated between the deltas where the Yeşilırmak and Kızılırmak rivers discharge into the Black Sea. Geographically, it is located between latitudes 40° 50’ and 41° 51’ N, and longitudes 34° 25’ and 37° 08’ E. The province of Samsun is divided into 17 districts, namely 19 Mayıs, Alaçam, Asarcık, Atakum, Ayvacık, Bafra, Canik, Çarşamba, Havza, İlkadım, Kavak, Lâdik, Salıpazarı, Tekkeköy, Terme, Vezirköprü, and Yakakent.

Fig.1. Samsun Province and Its Districts

In terms of landforms, the province of Samsun exhibits three distinct topographical features: the mountainous region in the south, the plateaus situated between this mountainous terrain and the coastline, and the coastal plains stretching between these plateaus and the Black Sea. The Bafra and Çarşamba plains are located along the coast, formed within the delta areas of the Kızılırmak and Yeşilırmak rivers. The Black Sea coastal areas of the province comprise lowlands, whereas the inland areas extending southward are covered by mountain ranges of moderate altitude. The region lies between the Black Sea coast and the high mountains running parallel to the coastline further inland. In the Ünye-Çarşamba sector, these mountains consist of the Canik and Çangal ranges, which follow an east-west orientation, while trending east-south and west-northwest in the Samsun-Bafra sector.

Fig.2. Map of Samsun Province

According to 1:100,000 scale studies conducted by the General Directorate of Mineral Research and Exploration (MTA), the following geological units have been observed in Samsun: Within the province of Samsun and its districts, the Kapanboğazı Formation (Kk), Yemişliçay Formation (Ky), Cankurtaran Formation (Kc), Akveren Formation (Kta), Atbaşı Formation (Ta), Kusuri Formation (Tk), Tekkeköy Formation (Tt), Sarıyurt Formation (Ts), Mahmurdağı Volcanites (Tmv), Samsun Formation (Ts), İlyas Member (Tsi), Karasamsun Member (Tsk), Palaeo-alluvium (Qe), Modern Floodplain Deposits (Qt), and Alluvium (Qal-Qa) are present (Yılmaz, 2012) [10].

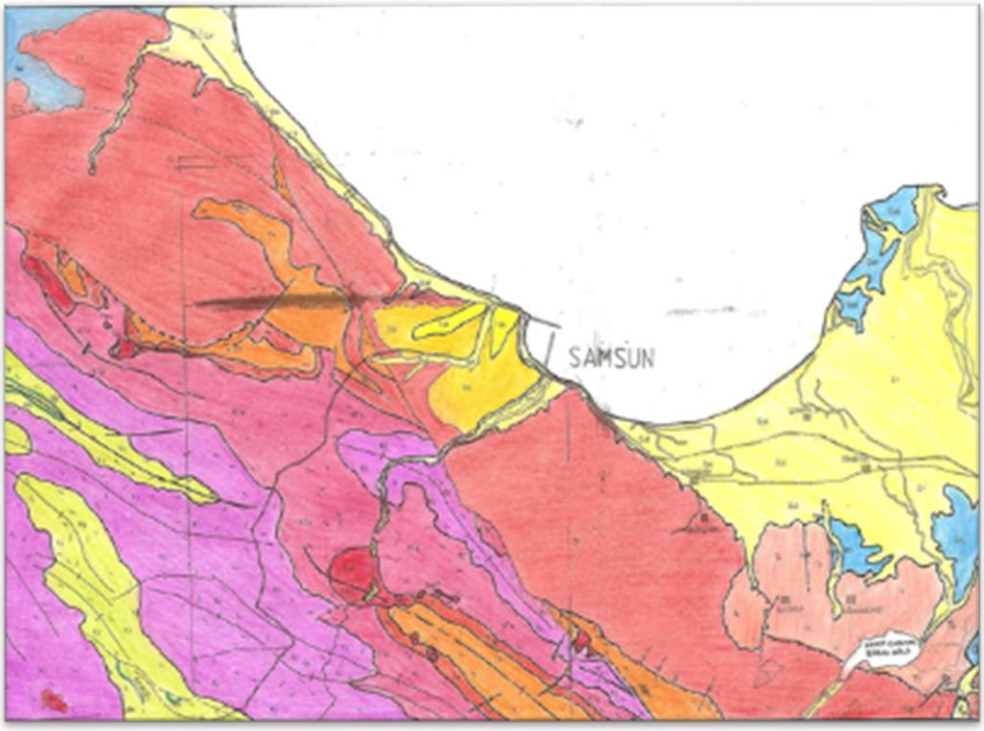

Fig.3. Geological structure of Samsun province (MTA)

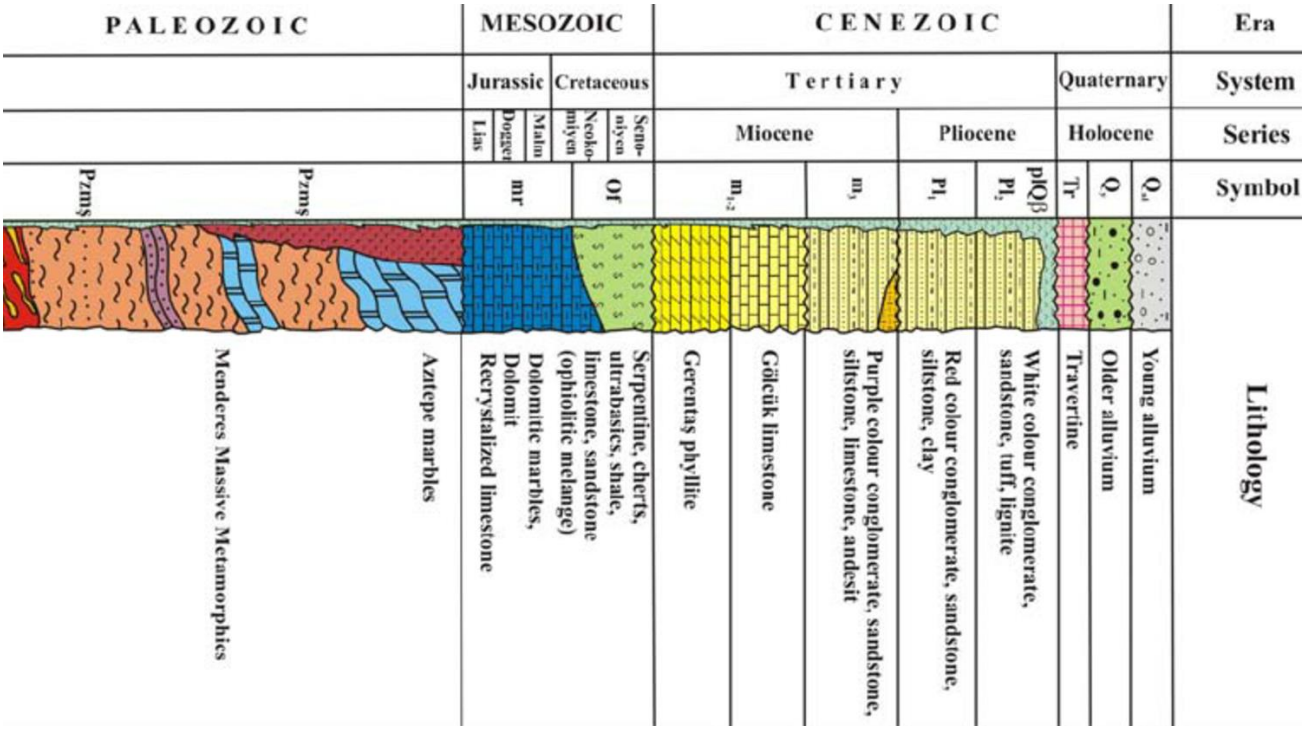

Fig.4. Stratigraphic columnar section template (MTA)

The geological framework for the city center of Samsun can be summarized as follows: alluvial extensions are prominent along the coastline, particularly on the Atakum beach and around Tekkeköy, whereas the center comprises gray-blue marine marl, gypsum, and clay interlayers within the Samsun Formation. The geological formations for the Samsun city center and all its districts have been detailed in Appendix 1.

Local soil conditions directly influence the characteristics of seismic motions and induce damage to structures built upon them. The earthquake zones of the Samsun city center and its districts are listed below.

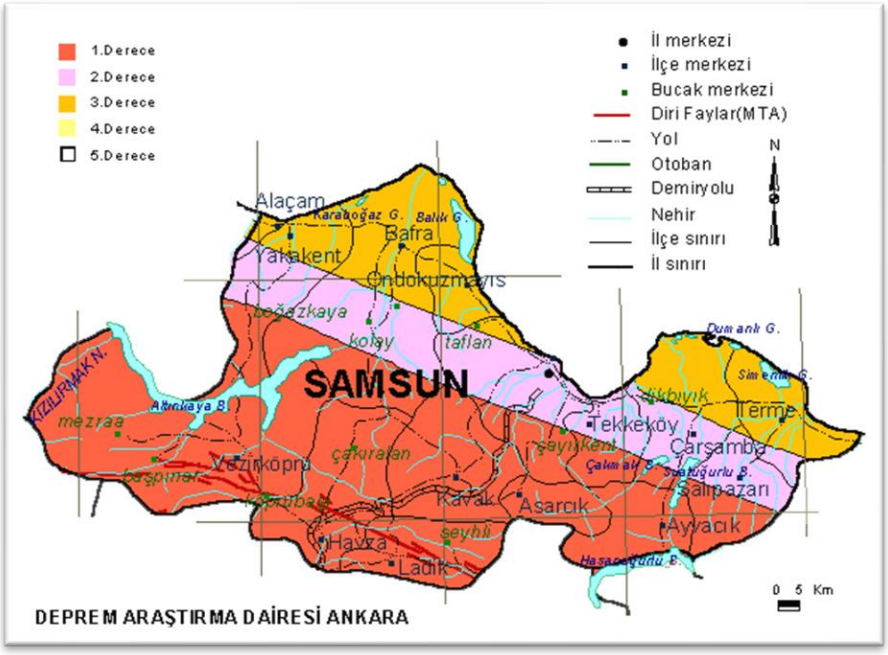

Fig.5. Earthquake map of Samsun province (2019)

According to the former Turkish Earthquake Zones Map, which was used before the implementation of the 2018 Türkiye Building Earthquake Regulation (TBDY-2018), the districts of Ayvacık, Asarcık, Kavak, Ladik, Havza, and Vezirköprü were classified as first-degree earthquake zones. The North Anatolian Fault (NAF) extends northwestward, passing through the northern margin of Lake Ladik and across the villages of Tatlıcak, Hasırcılar, and Aslantaş. This line passes 2.5 km north of the Akpınar Dam and immediately north of the dikes of Lake Ladik. On this right-lateral strike-slip fault, the foci of past and potential future earthquakes are shallow-seated. Consequently, the destructive impact of earthquakes in this region is substantially high. Due to tectonism, fractured formation structures are observed across the region. In addition to the North Anatolian Fault, the Erikli Reverse Fault, and the Ekinveren Fault, the thrust faults, reverse faults, vertical faults, and normal faults located in and around the province of Samsun are categorized and detailed below.

According to the former Turkish Earthquake Zones Map, the central districts of Samsun and the southern parts of Çarşamba were classified as second-degree earthquake zones, whereas the northern part of Çarşamba and the districts of Terme, Ondokuzmayıs, Bafra, Alaçam, and Yakakent were classified as third-degree earthquake zones. However, due to their specific soil characteristics, it is anticipated that the northern part of Çarşamba and the districts of Ondokuzmayıs, Bafra, and Terme will be more severely affected by an earthquake occurring along the North Anatolian Fault line compared to other regions.

A highly destructive earthquake with a magnitude of M_w=7.2 occurred along the North Anatolian Fault line between Ladik and Tosya on November 26, 1943. Centered in the Ladik district, this earthquake was effective across an area 300 km long and 20 km wide, extending from Erbaa in the west to Ilgaz in the east, and was strongly felt in neighboring towns and villages. In this earthquake, which caused catastrophic losses, 75% of the buildings collapsed, and extensive damage occurred along

highways and railway lines. Post-earthquake fires further compounded the loss of life and property. Approximately 2,300 citizens lost their lives, and 5,000 individuals were injured. The earthquake generated a 265 km long surface rupture; these fractures developed with a right-lateral strike-slip character, accompanied by a relative down-drop of the northern block (Özdoğan, 1993).

3. Conclusion. This study demonstrates that effective seismic risk mitigation in Samsun requires the integration of regulatory frameworks, rapid assessment methodologies, and regional seismotectonic evaluations. First-Level Seismic Risk Assessment methods provide a practical and cost-effective approach for prioritizing vulnerable reinforced concrete buildings, particularly critical public facilities requiring post-earthquake functionality. The seismic characteristics of Samsun indicate significant hazard variability, with fault-controlled strong ground motions in southern districts and soil-amplification effects in coastal alluvial regions. Therefore, combining rapid structural screening with site-specific seismic hazard assessments and modern earthquake-resistant design principles is essential for improving urban resilience and reducing future earthquake losses [8,9].

Author Contributions. H.V. (Humberto Varum) conceived and designed the study, contributed to the research methodology, supervised the research, interpreted the findings, critically revised the manuscript, and approved the final version for publication. S.Ö. (Sevda Özdemir) conducted the literature review, collected and analyzed the data, prepared the figures and tables, wrote the original draft of the manuscript, revised the manuscript, and approved the final version for publication.

Funding. The authors received no specific financial support from any funding agency, commercial organization, or not-for-profit institution for the research, authorship, and/or publication of this article.

Data Availability. The data supporting the findings of this study are available from the corresponding author upon reasonable request.

Declarations

Conflict of Interest. The authors declare that they have no competing interests or conflicts of interest related to this work.

Ethical Approval. This article does not involve studies with human participants or animals. Therefore, ethical approval was not required.

Informed Consent. Not applicable.

References

[1]Özdemir, S. (2019). *Seismic evaluation methods and applications of public buildings* (Master's thesis). Samsun, Türkiye.

[2]Kasimzade, A., Erdik, M., Kundu, T., Sucuoğlu, H., & Clemente, P. (Eds.). (2024). *Earthquake resistant design, protection, and performance assessment in earthquake engineering* (Vol. 54). Springer Nature. https://doi.org/10.1007/978-3-031-65407-7

[3]Kasımzade, A. A., Şafak, E., Ventura, E. C., Naeim, F., & Mukai, Y. (2018). *Seismic isolation, structural health monitoring, and performance based seismic design in earthquake engineering: Recent developments*. Springer.

[4]Kasimzade, A. A., et al. (2025). Economic evaluation of 2000 Baku earthquake impact in view of building features. *Construction Economics and Management, 32*(3), 191–206.

[5]Kasimzade, A. A., et al. (2025). System identification for non-destructive assessment of structures: Lessons learned. In *Communications in Computer and Information Science* (Vol. 2225, pp. 235–250). Springer Nature. https://doi.org/10.1007/978-3-031-73417-5_18

[6]Kasimzade, A. A., & Nematli, E. (2024). New structural seismic isolation system for tower structures. In *Geotechnical, Geological and Earthquake Engineering* (Vol. 54). Springer Nature. https://doi.org/10.1007/978-3-031-65407-7_1

[7]Kasimzade, A. A., et al. (2024). Novel approach on mathematical modelling and numerical evaluation of the seismic protection of structural dynamic systems. *Mathematical Methods in the Applied Sciences*. https://doi.org/10.1002/mma.

[8]Kasımzade, A. A., et al. (2024). The contribution of natural seismic base isolation on the durability of traditional Japanese structures. In *Geotechnical, Geological and Earthquake Engineering* (Vol. 54). Springer Nature. https://doi.org/10.1007/978-3-031-65407-7_3

[9]Kasimzade, A. A., et al. (2024). The new criterion on performance-based seismic design with application to high-rise building. In *Geotechnical, Geological and Earthquake Engineering* (Vol. 54). Springer Nature. https://doi.org/10.1007/978-3-031-65407-7_11

[10] Yılmaz, Y. G. (2012, May 11–12). *Samsun ilinin deprem riski ve alınabilecek önlemler sempozyumu*. In *Bildiri Özetleri Kitabı* (pp. 139–158). Samsun, Türkiye.

https://doi.org/10.58225/sw.2026.1-82-91

RENEWABLE BUILDING TECHNIQUES WITH IMPACT ON URBAN INFRASTRUCTURE SUSTAINABILITY

Mohit Yadav[1], Khushwant Singh[2], Vugar Hacimahmud Abdullayev[3], Fernando Moreira[4], Dheer Dhwaj Barak[5]*, Raj Kumar Sharma[2], Sunil Kumar[6], Deepak Kumar[7]

[1]Chandigarh University, Mohali 140413, India
[2]Guru Gobind Singh Indraprastha University, Dwarka, New Delhi, India
[3]Azerbaijan University of Architecture and Construction, Baku, Azerbaijan
[4]Universidade Portucalense, Porto, Portugal
[5]Maharshi Dayanand University, Rohtak, Haryana, India
[6]Central University of Haryana, India
[7]Lala Hansraj Phutela College of Law, Sirsa, India
mohit.e15793@cumail.in, erkhushwantsingh@gmail.com, abdulvugar@gmail.com,fmoreira@upt.pt, barakdheer410@gmail.com, profrksharma07@gmail.com, aggarwalsunil968@gmail.com, deepakpunia1000@gmail.com*

Abstract. The current work investigates the green technologies and their influence in promoting sustainable urban development in Bulgaria under both climate change and urbanization. Although eco-consciousness has increased, EEO adoption is hampered by institutional fragmentation, unstable support measures and scarce involvement of the private sector who owns 93% of the building stock (based on theoretical analysis and official Bulgarian and EU legislative documents). The difficulties are related to absence of long-term financing, change in conditions of the renovation programmer, and insufficient involvement from all actors. However, green technologies offer potential for cutting energy use, addressing climate risks and upgrading infrastructure. Instances include green roofs, passive heating, water conservation systems, smart HVAC and energy-saving facades all of which can reduce levels of energy consumption by 30–50% and CO_2 emissions by up to 40%. EU initiatives, such as the new Directive on Energy Efficiency of Buildings, are driving large scale renovation by 2033 providing additional opportunities. On the basis of a SWOT analysis it is concluded that due to standard policy support, social-justice-related aspects and integrated planning, green technologies can be established as one pillar for sustainable modernization in transition economies. Novelty The importance of the study can find expression in its theoretical rationalization of the relationship between construction greening and institutional factors, pointing out strategies directed toward policy, financing, and stakeholder cooperation.

Keywords: Opportunities and Obstacles, Construction, Sustainability, Environmental Adaptation, Energy Efficiency, Regulatory Compliance

Cite this article as: *M. Yadav, K. Singh, V. H. Abdullayev, F. Moreira, D. D. Barak, R. K. Sharma, S. Kumar, and D. Kumar, "RENEWABLE BUILDING TECHNIQUES WITH IMPACT ON URBAN INFRASTRUCTURE SUSTAINABILITY," SW AzUAC, vol. 1, 2026. https://doi.org/10.58225/sw.2026.1-82-91*
Article history: *Received: 20 May 2026 / Revised: 24 June 2026 / Accepted: 04 July 2026*

Introduction. Under the current global warming trend and rapid urbanization, the sustainable development of cities is increasingly a matter of concern. In 2050, it is estimated that nearly 70% of the world population will reside in urban agglomerations which currently use approximately 80% of energy produced on earth and produce about 75% of carbon dioxide [1]. In 2019, the construction industry represented one of the most important GHG contributors to global carbon emissions (about 39%) [2]. In this regard, active implementation of “green” technologies into construction industry is

regarded as a response to the challenges and an effective measure to ensure sustainable development goals and environmental burden mitigation, and thus interest in this question has grown relevant [3]. But the uneven development processes and legal tools governing "green" construction continue to hinder creativity. Furthermore, there is very little engagement and investment from the private sector in green projects which in turn hinders the dissemination of environmentally friendly solutions in the industry. Guo et al. performed an empirical analysis on the effect of smart city construction programs on energy preservation and CO_2 emission reduction in China, proving that the general realization of smart city programs can make a remarkable contribution to decreasing CO_2, raising urban infrastructure's comprehensive energy consumption performance [4]. "The move to a 'new digital normal' will be enabled through the combined benefit of digital energy management technologies, monitoring and predictive analytics," the researchers. The success of these programmes (will be) depends on the conditions and technological readiness to address a range of local regions suggesting in such environments, benefits long-term planning for sustainable development with their own territorial features. Consistent with these results and their study. Figure 1 depicts the applications of eco-friendly technology for sustainability.

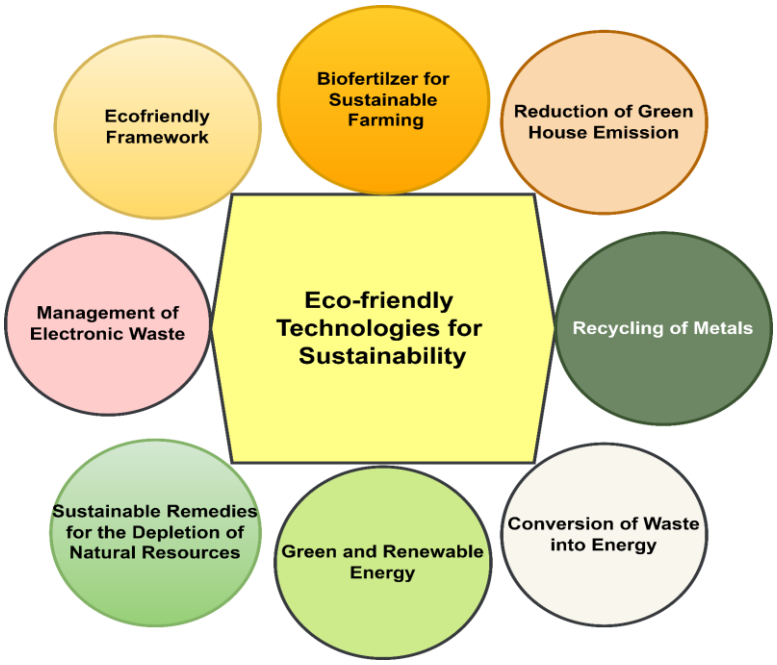

Fig.1. Applications of eco-friendly technology for sustainability

Researchers analyzed the influence of smart cities o n th e mo ve to wards green technological innovations. The researchers also proved that building of elements of wise city infrastructure contributes to the surge in environmentally sound technologies [5]. Guo et al. established that the progress of Smart cities influences positively in the adoption of green solutions and also stressed on regions with higher level of technological readiness, they are more attractive to smart city programs [6]. Gil-Ozoudeh et al., prospective of the technological design of green buildings in sustainable urban development had also been researched, the practicality of ecologically oriented architectural engineering was elaborated [7]. The researchers conclude that due to the above a further integration of green technologies in urban planning is needed to enable cities and settlements to adapt themselves better towards the challenges of climate change. The research of researchers analyzed the condition of green projects and initiatives in construction, while concentrating on the European Union (EU) countries experience, and the peculiarities when implementing environmental approaches in Bulgaria. Introduction The Scientists have studied the prospective of sustainable building development,

highlighting that the dissemination of green practices in emerging economies remains incipient. Researchers emphasized the need to apply foreign experience based on local specificity and to establish a national system of stimulation for green construction, which includes educational programs, preferential loans, and work on the development of standards to certify buildings. Other Bulgarian Rodrigues et al. carried out an extended study of the indicators for sustainable urban development in Bulgaria, and pointed out that the main problems remained with low building energy efficiency, irrational use of natural resources, limited access to renewable energy sources and lack of adequate reflection of sustainable solutions within the strategic planning for urban environment [8]. Furthermore, the scientists underlined the requirement for a complex approach to sustainable urban environment creation in particular through innovation construction materials insertion, local energy infrastructure formation, and deepening and spreading inter branch cooperation of public and private institutions. Thus, the aim of the present study was to a detailed theoretical study on the influence of green construction technologies on the sustainable construction of the city (Bulgarian urban environmental studies. practices and challenges). To achieve this goal, the tasks were formulated: to evaluate the role of green technologies in saving energy and infrastructure against climate risks; adaptation of urban environment to determine the institutional and financial constraints that inhibit the information spread on green technologies implementation; research into impact of different factors on stimulation promoting use of green construction, as well as their significance with regard to sustainable cities' development.

Materials and methods. The regulatory framework analysis enabled a systematized and conceptualized understanding of the key documents, strategies and projects that guide both climate and construction policy at national levels (in this case Bulgaria and Europe). The analysis of legislation also revealed the degree of legal consistency between European climate objectives and regulation inside construction in Bulgaria. In this way it was possible to consider the field of regulation as a dynamic system that changes and to examine its potential power towards eco-friendly construction practices. Institutional analysis was used as a tool to examine the structure and function of organizations that affect climate and construction policy at national level in Bulgaria. That provides a basis for measuring the degree of participation and influence among individuals from outside Europe but who still play key roles in reshaping industry rules. Such an approach also helps researchers to understand the institutional logic of decision-making: worse even figure mechanisms toward developing a sustainable construction society from managerial and control perspectives.

By means of systematic approach, the green technologies were viewed as parts in its urban complex integrating them into this broad framework of overall sustainable development.Grasping the processes in which architectural, engineering, or environmental measures affect a given urban milieu within a single sharp comprehensive way of thinking, this method achieved major savings and sharply accelerated its previous status. Fig.2 depicts the renewable building techniques with impact on urban infrastructure sustainability and Fig.3 depicts the flowchart of working model for sustainable infrastructure with renewable building techniques.

Fig.2. Renewable building techniques with impact on urban infrastructure sustainability

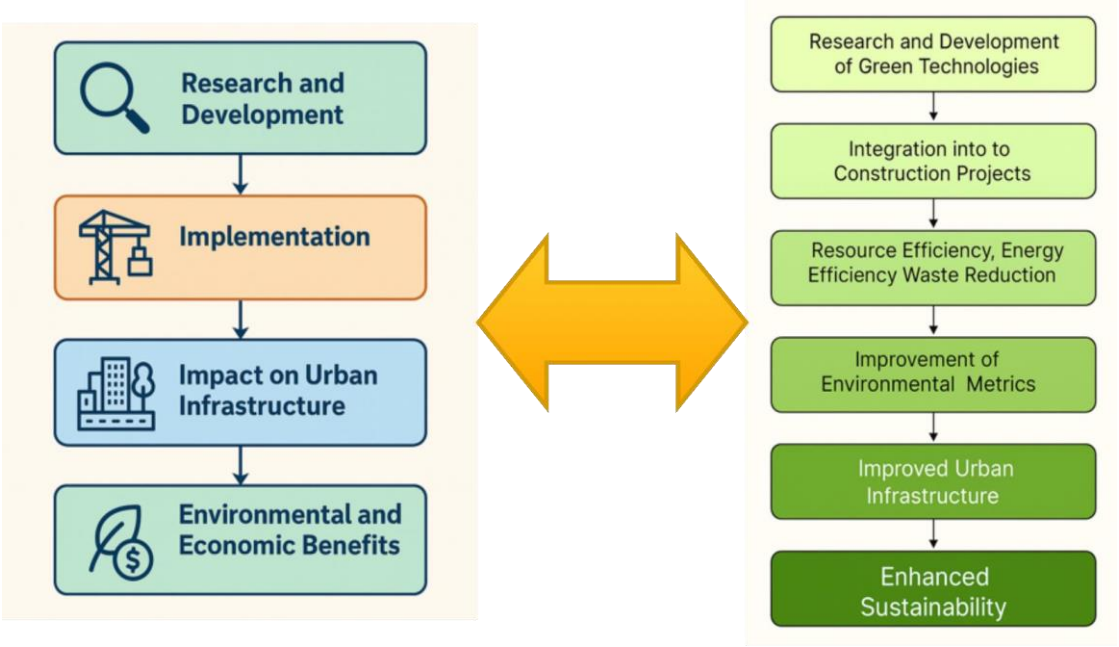

Fig.3. Flowchart of working model for sustainable infrastructure with renewable building techniques

This is similar in some respects to the previous item. Under this methodological lens, green technologies become three kinds of tools. They can be used to transform the energy, social and natural subsystems of the city.Therefore, taking strengths, weaknesses, opportunities and threats (SWOT) analysis about where to develop green technologies in construction technology as a guide for theoretical prediction analysis categorized the internal and external factors of construction sustainability that constitute a force. SWOT analysis looked at the way institutions, economy, technology and society interact, all affecting effectiveness of this sector's transition. This way it made possible a framework for studying and expressing in theory about risks and possibilities for the future of programmes that retrofit buildings.

The research team made use of domestic data to analyze the current situation and future outlook for green technology developments. The information about the energy efficiency of the existing residential building stock, how many cases have been realized and the profitability of certain technological areas had been translated. The approach taken by the study's researchers was perhaps

more utilitarian and down-to-earth than that of certain cozy, bureaucratic assessments. This is because with expert views indicating such things as is there a business environment for technology, where do institutional bottlenecks lie—among other empirical evidence gathered on site—the analysis became both down-to-earth and less prone to abstract reasoning. This approach, in turn, was applied to the final stages of theoretical work and made it possible to synthesize the results of various analytical methods into one overarching picture. Regulatory, institutional, systemic and empirical data were integrated through this method, facilitating combined conceptualization of different approaches towards evaluating green technologies ' contributions in modernizing the building sector. And so with the synthetic method, the theoretical construction was coherent and the analysis presented as a whole possessed logical rigor.

Results and discussion. Construction progress of green technology is becoming one of the key forces in the sustainable urban environment development, in rapid developing countries in general where city boom. Bulgaria, which is in the phase of the construction industry conversion and European environmental acclimation, is evincing a trend to promote interest in the environment oriented approaches. By early 2025, there are elements of-proof or more in and the construction industry in Bulgaria showing a slow, adoption of green techniques, even existence though their diffusion remains fragmented. For instance, there are as of there are only 54 green buildings in Bulgaria. Architectural Researchers have managed projects that use energy-saving materials, solar water and insulation structures commercial and residential sectors in large cities. The role of environmental certification limited, and it is most frequently used buildings) more from foreign investors than domestic developers. Certification companies that underestimate English Green building certification in Bulgaria The first and only green building certification system currently available in Bulgaria is the English BRE Global and the Building Research Establishment Environmental Assessment Method (BREEAM) standard in the German Council for Sustainable Building. with the DGNB standardisation system, and the counts Studio project among its few members. employs the DGNB scheme.

Construction regulations are experiencing revision and realignment with European standards. This has made methods of construction application of technologies for buildings variable and nonuniform. In keeping with this trend, Bulgaria has ratified a "Long-range national policy to aid recovery of the country's stock of residential and other buildings by 2050", as well as it is carrying out an "Integrated energy and climate plan for the Republic of Bulgaria 2021–2030". These papers all incorporate measures designed to reform construction law and energy-saving standards and support renewable energy sources. While, both the academic and professional communities are only gradually piecing together a unified understanding of green principles in architecture. By 24, according to the National Program for Energy Efficiency in Residential Buildings in Bulgaria, 270 apartments in three multifamily blocks of flats in

Sofia were renovated. Launched in 2015, this project which is entrusted to Ministry of Regional Development and Public Works has now completed the repair of a total 1, 968 units across the country at its close in 24o 'clock . These actions have reduced household heating bills and cut the amount of CO_2 given off, thus raising substantially environmental quality. The program emphasized improving structures, especially older ones, via energy conservation methods like insulation, new windows and higher-efficiency heating systems. The National Program extends full grant assistance to condominium associations of multi-family buildings built before 1990, creating a warm relaxing interior environment and enhanced energy efficiency. More than 2,022 sites have now received finance agreements under this program, with roughly two-thirds completed and the rest underway. Beneficial results seen include improved indoor comfort, lower energy bills, and increased satisfaction of the their occupants. Hurdles to its wider adoption include the regulation of homeowner associations and financial frameworks suitable for widespread use.

The outlays for this will be considerable: already in the pipeline are about 200 million leva (over 100 million euros) allocated through 2024 by regional development projects for the energy-

saving renovation of multi-family residential buildings unkindly sited in Bulgaria's coal regions as the country shifts its energy These investments aim at reducing energy use and removing energy poverty as an example by insulation, strengthening the heating system, and a variety of energy-efficient modifications to form a green living environment. At a broader level, the EU program Horizon 2020 provides abundant funding for energy-saving technologies and green solutions in virtually all industries, residential building. Evaluations of energy efficiency investments at EU level suggest strong paybacks over a number of years. Reports often show returns considerably greater than the original investment in terms ofenergy savings and environmental gains. For example, according toa report from the European Institute of Banking and Finance, home-insulation measures offered a payback time as low as two years on average in many countries.

This fact adds more sustainability to the infrastructure. How green buildings can reduce impact of climate fluctuations and heat waves and floods, in particular overheating states of urban cores.The use of green roofs (that decreases air temperature of cities lower by 1-3 degrees Celsius and stormwater storage volume can be reduced by Landscaping & Natural Screens(50-80%): Vertical landscaping & natural screens help make sure you follow us on our social media platforms. restore biological connections within the urban environment favorable to reduced thermal pollution and making densely populated areas more habitable. Such solutions are also some of the adaptation components of cities to climate change, preparing them for climate change without radically restructuring existing structures. The green technologies aesthetic and recreation potential results in a positive impact on the social level, increasing the identity of citizens with their residential location and promoting the growth of local communities.

Regarding the environmental factor, green usage The variety of technologies in construction sector provides a harmonised The foundation helps in integrating the economic development with the natural environment of the global climate agreements being implemented . Focusing on energy savings and renewables According to informaiton, in an effort to limit the harmful impact of the former, Bulgarians are striving to mitigate the negative effects of the latter. construction. The development of sustainable construction practices and encouraging of renewable energy source on the directly decrease the environmental performance of the city (lower gaseous emissions, assist to minimize the ecological footprint).

For Bulgaria, reaching this objective is a technical and institutional challenge. Under the new legislation, there is a requirement that all (whatever their ownership or purpose and regardless of date of construction) buildings are brought up to standard by 2033. This goes for both residential, public and commercial money. The first priority (common action) is to be accorded to the best-performing buildings in terms of energy efficiency, which will require immediate action on improving the thermal performance of these buildings with a particular focus on introduction of electrical heat pumps and electrification of heating systems, despite their continuing high costs and low availability throughout the EU. Among the obligations arising from the directive, Bulgaria, like other EU member states is to develop and submit a national building renovation plan by 2040: a concerted strategy for modernising building stock setting out long-term national glass-by-glass repair mechanisms as well as criteria for choice of buildings and financing sources.

From this, it can be concluded that, notwithstanding its ambitious. targets for modernising the building stock or achieving climate neutrality, the renovation schedule programs faces fundamental systemic limitations. As can fb as one can observe, although a need for green technologies, financial constraint and unwillingness to full Government's support lead to reduction in their active implementation. Furthermore, the absence of a stable government) regulation and planning tools, and a clear 78 influence of the segmentaare mesopolitical levels. professional talent, provide another shortage of talents for professionals. complexity.

Also, the incorporation of green-GIT green construction technologies- embodied energy address representing construction GDP (Germany) and measure of construction activity (UK), high levels of capital intensity, particularly at the design. specialised materials and engineering

procurement equipment of facilities. Thus, energy-efficient all-encompassing buildings, smart HVAC systems, solar AND photocatalytic facades, geothermal installations, and other innovative solutions require significant investments. For resource scarce economies such opposed to countries that have few domestic investment resources, such as well as Bulgaria, it is a crucial barrier to renovation in mass and climate-related moderisation of the building stock.

In this sense it is of fundamental importance supporting technological and building measures with social support, through the promotion of information campaigns, subsidies and technical assistance programmes as well as flexible financing instruments. Green technologies will only be part of sustainable and inclusive urban development when we uphold the principles of social justice.

By analysing the innovations of energy-efficient technologies in construction, it was proved that they are based on common political and economic objectives and related to certain consequences of the COVID-19 pandemic. The researchers say the EGD is more than environmental regulation instruments- but a comprehensive recipe for sustainable growth, economic incentives and political backing. The research verified these findings and became more pragmatic with the case of Bulgaria – without contextual adjustment of pan-European objectives to the national level, taking into account construction fund peculiarities, PPP interaction specifics or a long-term financing model establishment, green edifice transformation decelerates. Hence, if Bongardt and Torres concentrated on the institutional architecture of the EU -the study demonstrated how these macroeconomic tendencies are reflected in urban infrastructure (in an institutionally volatile country with a transition economy).

Furthermore, where the effectiveness of an individual technological implementation is concerned, empirical analysis of the effect of specific technical solutions on urban sustainability is also an area on which there has traditionally been a scientific interest. The research conducted by Muntean compared the processes of infrastructure construction in Germany, Romania and Bulgaria and particularly emphasised the effects on their economies. The scholar stressed that the sustainability of infrastructure depends on the quality of management and the level of integration between sectors. Thus, this paper elaborated on the latter finding and provided evidence that in countries with low capital, such as Bulgaria, “Institution-based view” of IHaRM would place significant attention on an ability to create institutional infrastructure for securing sustainable form of rules of the game, access to finance and longterm support measures for different renovation programmes. The Case study: a contribution to the future In conclusion the analysis process in this paper, we indicated that private sector (shareholder enterprises), which is superstructure part of socialist market system and has created most housing stock so far as well play an important role in structuring based our past from socioeconomic analysis; it can help us expand and complement the results with systemic measurement of the factors determining building industry’s sustainable development in transition economy.

Yarova et al. evaluated economic benefits of green technologies in Ukraine and indicated the significant energy efficiency (EE) enhancement and CO2 reduction that can be achieved by the state support for sustainable development[9]. The Ukrainian example tows the line of Bulgaria’s present situation concerning the prospect of developing a sound green building sector. Private sector participation in sustainable building is limited in both countries and government intervention is critical. Unlike Ukraine, where the government has supported energy efficiency more strongly, in Bulgaria disarranged legisiation framework and unveiled govenmental support have left a heavy industry footprint on green technologies. According to Yarova et al. Bulgaria could increase green technology adoption by enhancing private sector participation with financial incentives and green certification mechanisms.

Hasanov et al. analysed the permanent link between human development and environmental sustainability in Azerbaijan based on CO_2 emissions, and socioeconomic indicators[10]. Azeriinducerat tillväxtgreen, green growth policy increasingly focuses on energy efficient technologies in building, like green in Bulgaria. In terms of reducing energy consumption for building

construction in Azerbaijan, the development and promotion of order‟s green certificates like Green Zoom were successful in commercial buildings but not in residential spaces in Bulgaria. Both face institutional impediments; yet, Azerbaijan's focus on energy-efficient buildings could inform Bulgaria's strategies, especially in urban areas where the commercial properties can be more receptive to refurbishment with sustainable technologies.

Verdiyeva et al. represent the green growth strategy for Azerbaijan based on sustainable economic growth, with the integration of a green technology[11]. What Azerbaijan is actually experiencing matches the aspirations of Bulgaria, where they are trying to modernise their infrastructure with its sustainable development. Azerbaijan has benefitted economically from this plan, making effective use of green technology within commercial real estate. Bulgaria faces significant financial barriers including high start-up costs and limited public private partnerships. Therefore, the results of Verdiyeva et al. for Decision reiterate the call for an effective financing mechanism, one of the chief recommendations regarding Bulgaria s modernisation efforts particularly related to participation[1215].

In many cases, the scope of studies concerning green building in the area of technology energysaving systems, heat recovery system, green roofs into buildings and facade with photocatalysis etc.) however did not go beyond the object only to see them only as example technical solution for green technology or catechize how to encourage construction industry take advantage from new technologies[16-18]. Finally, the scrutiny of green innovations' effectiveness in terms of lowering carbon footprint and raising energy efficiency is a steady point on today's scientific agenda, particularly when considering global climate objectives. But how-to do green technologies in transition economy, where diffusion is confronted to classical and not so stable institutions, remains little known. The study was intended to contribute new knowledge in this respect by providing theoretical analysis backed up with regulatory data from Bulgaria and EU, as well as empirical evidence on existing renovation programmes. This methodological tool enables to connect macroeconomic model of sustainable development with the particular programmes of urban infrastructure modernizing, determine systemic barriers and propose mechanisms ensuring their overcoming.

Overall, the research conducted is a extension of the existing framework, conceptually. adding to the analysis of green technology not purely technical, institutional, and their ratio oflengths thanwhere6. economic and social factors that condition their adoption in the Bulgarian construction industry. This interdisciplinary perspective makes it possible to take into account green as part of an overall system of technologies sustainable urban development, where successful is feasible only when all relevant factors are considered.

Conclusions. The main aspects of the development and impact of green technologies on the sustainable development of urban infrastructure were determined based on the study. The results showed that green building applications have a great opportunity in enhancing the energy performance of buildings and contributing to reduce the CO_2 emission and climate change. The significance of these solutions is particularly high in middle- and low-income countries with a large share of old housing stock, and where building renovation represents the primary means of raising the resilience of urban areas. In this optic the example of green technologies introduction in Republic of Bulgaria was chosen as an analytical basis. The review of the legal framework has revealed that driving towards mass renovations through the construction fund in Bulgaria is hindered by various institutional issues such as fragmented legislation, missing holistic climate roadmap and unstable financing schemes. In spite of the presence of European directives and support programmes, their transposition to the domestic level is slow and unequal. In addition, the poor participation of the private sector is still a major constraint. These are slowing the translation of climate pledges into action and impede the deployment of new solutions in reality. The SWOT analysis helped to arrange the internal and external factors that contribute for the success or failure of green technologies implementation. Strengths (potential for energy cost reduction, institutional support at EU level,

environmental impact) and weaknesses (institutional fragmentation, high initial economic expenses, lack of specialists) have been pointed out. Key investment opportunities found include increase in availability of capital, growth in sustainable building demand from international investors and potential to establish local production facilities for energy efficient products. Risks were expressed by non-fulfilment of renovation targets, increasing mistrust from the population and increased social division in terms of different opportunities for participation in support programmes. These considerations highlight the compulsion for indivisible solutions, paradise management systems where architectural, engineering and social dimensions formed a single approach for modernising the city environment. This study has several methodological limitations and especially theoretical dependence and secondary data that may not fully illustrate the practical obstacles of implementation of green technologies in Bulgaria. Multi-method research (combining policy analysis with empirical investigations such as surveys, energy audits and case studies) may provide deeper insights into the real effects of green technologies and investigate whether they really meet their goals on a broad scale. Furthermore, panel studies and empirical evidence may contribute to a better assessment of the effectiveness of policies in comparison to social and economic effects on green construction.

Author Contributions. All authors contributed to the conception and design of the study, literature review, methodology, data collection and analysis, manuscript preparation, revision, and approval of the final version of the manuscript.
Funding. The authors received no specific financial support from any funding agency, commercial organization, or not-for-profit institution for the research, authorship, and/or publication of this article.
Data Availability. The data supporting the findings of this study are available from the corresponding author upon reasonable request.
Declarations
Conflict of Interest. The authors declare that they have no competing interests or conflicts of interest related to this work.
Ethical Approval. This article does not involve studies with human participants or animals. Therefore, ethical approval was not required.
Informed Consent. Not applicable.

References

[1]Li, G., Zhang, X., Mirzaei, P. A., Zhang, J., & Zhao, Z. (2018). *Urban heat island effect of a typical valley city in China: Responds to the global warming and rapid urbanization*. *Sustainable Cities and Society, 38*, 736–745. https://doi.org/10.1016/j.scs.2018.01.033
[2]Ahmed Ali, K., Ahmad, M. I., & Yusup, Y. (2020). *Issues, impacts, and mitigations of carbon dioxide emissions in the building sector*. *Sustainability, 12*(18), 7427. https://doi.org/10.3390/su12187427
[3]Fei, W., Opoku, A., Agyekum, K., Oppon, J. A., Ahmed, V., Chen, C., & Lok, K. L. (2021). *The critical role of the construction industry in achieving the sustainable development goals (SDGs): Delivering projects for the common good*. *Sustainability, 13*(16), 9112. https://doi.org/10.3390/su13169112
[4]Guo, Q., Wang, Y., & Dong, X. (2022). *Effects of smart city construction on energy saving and CO_2 emission reduction: Evidence from China*. *Applied Energy, 313*, 118879. https://doi.org/10.1016/j.apenergy.2022.118879
[5]Ma, X., Li, J., Guo, Z., & Wan, Z. (2024). *Role of big data and technological advancements in monitoring and development of smart cities*. *Heliyon, 10*(15). https://doi.org/10.1016/j.heliyon.2024.e10852

[6]Guo, M., & Zhou, Y. (2025). *Boosting sustainable urban development: How smart cities improve emergency management—Evidence from 275 Chinese cities*. *Sustainability, 17*(15), 6851. https://doi.org/10.3390/su17156851

[7]Gil-Ozoudeh, I., Iwuanyanwu, O., Okwandu, A. C., & Ike, C. S. (2022). *The role of passive design strategies in enhancing energy efficiency in green buildings*. *Engineering Science & Technology Journal*, *3*(2), 71–91.

[8]Rodrigues, M., Franco, M., Filipova, H., Silva, R. J., Kazandzhieva, V., Nacheva, R., ... & Antonova, K. (2024). *Profile of urban sustainability in Bulgaria*. *Environment, Development and Sustainability*, 1–39. https://doi.org/10.1007/s10668-024-05657-4

[9]Yarova, N., Lipych, L., Gutsul, T., Zhurba, O., & Novytskyi, V. (2025). *Economic benefits of green technologies: Ukrainian experience*. *International Journal of Economics and Financial Issues, 15*(1), 412. https://doi.org/10.32479/ijefi.17624

[10] Hasanov, R. I., Giyasova, Z., Azizova, R., Huseynova, S., & Zemri, B. E. (2024). *Long-term dynamics between human development and environmental sustainability: An empirical analysis of CO_2 emissions in Azerbaijan*. *Challenges in Sustainability, 12*(4), 273–280. https://doi.org/10.56578/cis120403

[11] Verdiyeva, P., Dadashova, J., Bayramov, V., & Aliyeva, R. (2025). *Green Growth Strategies for Sustainable Economic Development*. https://doi.org/10.62844/jerf.20

[12] Lata, K., Singh, P., Saini, S., & Cenkeramaddi, L. R. (2024). *Deep learning-based brain tumor detection in privacy-preserving smart health care systems*. *IEEE Access*. https://doi.org/10.1109/ACCESS.2024.3456599

[13] Singh, K., Yadav, M., Barak, D., & Moreira, F. (2025). *Machine-learning-based frameworks for reliable and sustainable crop forecasting*. *Sustainability, 17*(10), 4711. https://doi.org/10.3390/su17104711

[14] Singh, K., Yadav, M., & Yadav, R. K. (2024). *IoT-based automated dust bins and improved waste optimization techniques for smart city*. In *Revolutionizing Automated Waste Treatment Systems: IoT and Bioelectronics* (pp. 167–194). IGI Global Scientific Publishing. https://doi.org/10.4018/979-8-3693-6016-3.ch012

[15] Hajimahmud, V. A., Singh, Y., & Yadav, M. (2024). *Using a smart trash can sensor for trash disposal*. In *Revolutionizing Automated Waste Treatment Systems: IoT and Bioelectronics* (pp. 311–319). IGI Global Scientific Publishing. https://doi.org/10.4018/979-8-3693-6016-3.ch020

[16] Yadav, M., Hajimahmud, V. A., Singh, K., & Singh, Y. (2024). *Convert waste into energy using a low-capacity igniter*. In *Revolutionizing Automated Waste Treatment Systems: IoT and Bioelectronics* (pp. 301–310). IGI Global Scientific Publishing. https://doi.org/10.4018/979-8-3693-6016-3.ch019

[17] Singh, K., Yadav, M., Singh, Y., & Barak, D. (2024). *Finding security gaps and vulnerabilities in IoT devices*. In *Revolutionizing Automated Waste Treatment Systems: IoT and Bioelectronics* (pp. 379–395). IGI Global Scientific Publishing. https://doi.org/10.4018/979-8-3693-6016-3.ch023

https://doi.org/10.58225/sw.2026.1-92-100

A COMPREHENSIVE ANALYSIS OF MACHINE LEARNING-BASED RETENTION OF STAFF MEMBERS

Mohit Yadav[1], Khushwant Singh[2], Vugar Hacimahmud Abdullayev[3], Fernando Moreira[4], Dheer Dhwaj Barak[5]*, Raj Kumar Sharma[2], Sunil Kumar[6], Deepak Kumar[7]

[1]Chandigarh University, Mohali 140413, India
[2]Guru Gobind Singh Indraprastha University, Dwarka, New Delhi, India
[3]Azerbaijan University of Architecture and Construction, Baku, Azerbaijan
[4]Universidade Portucalense, Porto, Portugal
[5]Maharshi Dayanand University, Rohtak, Haryana, India
[6]Central University of Haryana, India
[7]Lala Hansraj Phutela College of Law, Sirsa, India
mohit.e15793@cumail.in, erkhushwantsingh@gmail.com, abdulvugar@gmail.com,fmoreira@upt.pt, barakdheer410@gmail.com, profrksharma07@gmail.com, aggarwalsunil968@gmail.com, deepakpunia1000@gmail.com*

Abstract. In the hypercompetitive business environment, retaining employees remains a top challenge for companies trying to maintain stability, productivity and lower costs associated with turnover. An attempt to ascertain different factors that influence retention such as corporate culture, employee empowerment, organizational learning, talent development strategies, entrepreneurship education adoption of cultural intelligence and application technology like artificial intelligence and machine learning. This study synthesizes literature review along with empirical evidences. Many predictive modeling approaches including Random Forests, deep learning and Stacking-Based Transfer Learning, and Logistic Regression have a high degree of potential to predict turnover, find critical reasons for attrition, and lead proactive retention strategies. The mediating and moderating roles of job engagement, socialization tactics, organization size, and protean career orientations in predicting retention outcomes are examined across diverse organizational contexts (e.g., banks, startups, global work context). The findings emphasize the importance of integrating data-driven analytics and human-oriented strategies, offering HR practitioners beneficial advice on developing focused interventions to enhance employee satisfaction and sustainable stability in modern, multilingual work settings.

Keywords: Deep learning, Random Forest, Stacking-Based Transfer Learning, Human Resource Management

Cite this article as: *M. Yadav, K. Singh, V. H. Abdullayev, F. Moreira, D. D. Barak, R. K. Sharma, S. Kumar, and D. Kumar, "A COMPREHENSIVE ANALYSIS OF MACHINE LEARNING-BASED RETENTION OF STAFF MEMBERS", SW AzUAC, vol. 1, 2026, https://doi.org/10.58225/sw.2026.1-92-100*
Article history: *Received: 20 May 2026 / Revised: 24 June 2026 / Accepted: 04 July 2026*

Introduction. Supervisor employee turnover as the bottleneck of human resource management is gradually paid attention [1]. The cycle of employee turnover phenomena has become a chronic phenomenon in modern corporate operations, because of rapid development and increased competition in the market economy [2,3]. Cultural dose as enterprises of competitive base and spiritual appease, having its special value tendency and behavior observing, simultaneously be also

kind of important means to create harmonious environment [4]. Not only is this culture story able to attract talent, it creates job satisfaction which leads to enhanced work engagement and increased belonging in staff so that's not all it is doing a fairly good job of retaining the talent that enter our doors [5]. Employee retention is still a significant concern for HR departments that are trying to maintain organizational stability and reduce the costs associated with high turnover [6]. The forecast accuracy of traditional management approaches is often constrained by their poor ability to effectively incorporate information from multiple databases [7]. Employee satisfaction depends, as is commonly recognized, on more than just financial compensation [8]. A solution is not determined solely by whether one's language has an official status in a given administrative area, but satisfaction also depends on other factors including fair distribution of workloads, respectful treatment, prizes and awards and welfare benefits, or amicable management practices [9,10]. Conversely, motivation, retention, commitment and goal achievement at work are all strongly linked to employee happiness. The present study aims to explore the following: 1) A focus on improving organizational commitment and employee happiness has gained increasing attention. Sexual environment in it, whether sexual harassment occurs, will make a difference in organizational commitment and job satisfaction [11-13]. Level of job satisfaction and organizational commitment due to their increased importance as strategic resources. Satisfaction is also a predictor of employee commitment. For the purpose of this descriptive and empirical study approach purposive sampling technique is employed. Primary data was collected by 75 respondents who completed a structured questionnaire and was analyzed using percentage methods. The results show that staff commitment and management are significantly impacted by employee satisfaction. Contributing factors that can affect motivation and satisfaction include incentives, salary, leave policies, stressors, and rewards. High employee turnover is a deadly problem that managers are grappling with and managers can attest that this is more than just an issue of productivity and the bottom line in terms of morale. The study is focused on more accurate forecast models constructed and analyzed on the basis of data to obtain a better turnover forecasting [14]. Machine learning models are utilized in the search of the key causes that cause attrition by considering employee related data such as demographic, job attribute and performance. The whole aim is to identify the best predicting model that may serve as a guiding tool to produce useful retention policies. On the whole, the findings can be applied to more proactive strategies that can decrease employee turnover and enhance the planning of the work-force [15]. Level of Analysis: Job and Worker __ Random Forest, Logistic Regression Although most of the HR analytic approaches, in the present study, are grounded on the normative tools only, we deploy other types of normative power against the traditional ones. LR is particularly widespread being used as a candidate approach to reveal valuable HR information due to its interpretability. Nonetheless, to make better predictions, we found out that a machine learning model such as Random Forest was in fact highly effective at predicting a complex, non-linear pattern of employee behavior [16]. These models take the place of a useful complement of models to facilitate the design of targeted and data-driven retention interventions on the basis of consistency in prediction quality and more informative understanding of key reasons of attrition. To generate more accurate predictions on likely turnover trends, the proposed method relies on big data analytics for in-depth analysis of the multi-faceted signals like employee behavior, business performance parameters and cultural factors. Given a laboratory validation, the model is more accurate and reliable for predicting retention results to help firms that wish to follow proactive and analytical workforce management approaches in order to be supported for better decisions.

Materials and methods. In addition to the Triangle model concentrating on employee retention prediction, we also investigate how deep learning technology can be applied to make use HR strategy as well. The model is a deep feedforward neural network developed from feeding various trends (engagement levels, dozens of job performance measures, demographic information and turnover histories) into a few thousand large companies. In order to ensure scientific rigor, as well as practical relevance of the study, a multimethod design is used providing quantitative predictive modelling and

qualitative input from HR experts and employees. According to results, deep learning can provide substantially higher employee turnover prediction performance than traditional predictive models because it obtains better accuracy, precision, recall and F1- score. All this proves, how deep learning can transform HR analytics and allow corporations to generate more precise predictions at a reduced duration of time which can transform retention strategy into a reactive instead of a proactive approach. There are many ethical implications of such complex algorithms though the most significant of them apply to algorithmic transparency and data privacy. These elements are well represented in the article and the article takes an effort to underscore the fact that companies must be responsible AI-enabled consumers of HR solutions. The policies of big data have impaired the HR analytics of employee retention and talent management. The ability to anticipate hazards at workplaces is central to the minimization of turn over and enhancement of employee performance in the present hyper competitive business environment. The study is about the search of talent, and retention agents of the high potential employees through foresight-based HR analytics. Figure 1 depicts the flowchart of the working model. Figure 2 represents the comprehensive analysis of working model.

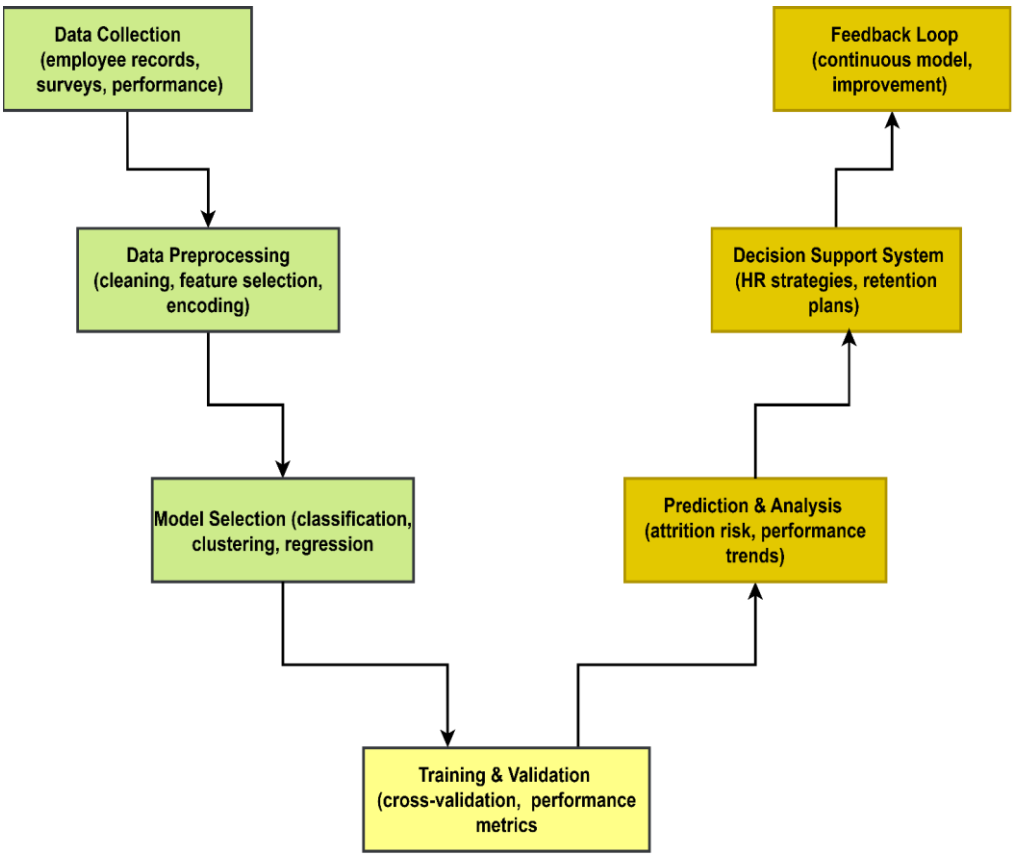

Fig.1. Flowchart of proposed model

There are also predictive models related to staff churn, and for predicting new hires who will be successful if we give them additional help in progressing through their professions. The flavor of the work is about crunching data sets which include demographics, years on job for employees, how people performed and whether they churned (that is left employment). Data collection part collect employeerelated data (attendance, questionnaires, and performance indicators). Preprocessing involves cleaning and preparing data for ML models. Model selection part select appropriate machine learning methods (e.g., decision trees for attrition prediction and clustering for staff grouping). Training and validation part validate correctness and train models. Predict and analyze potential

employee turnover, performance trends, and workload difficulties. Decision support part provide HR with practical insights for retention initiatives. Feedback loop part continuously improve models with new data.

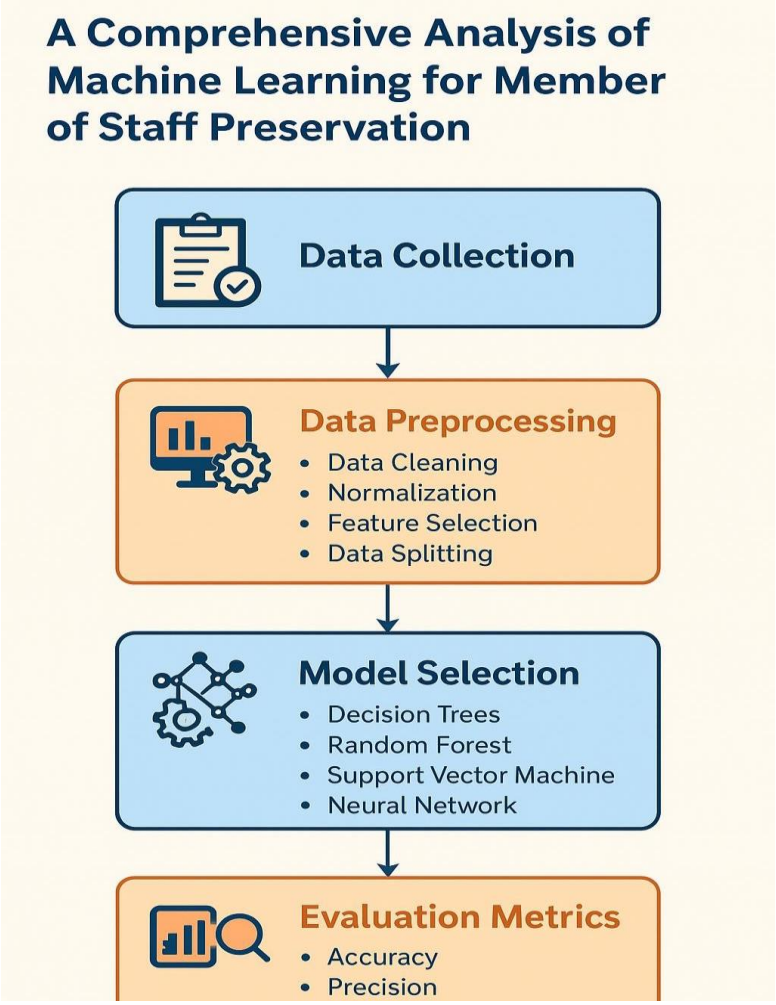

Fig.2. Comprehensive analysis of working model

Random Forests and logistic regression are machine learning methods applied to discover the factors critical to turnovers. To sum up these results indicate that HR predictive analytics can confidently predict employee exits and decisions to leave work by predicting promotion opportunities, receiving recognition reporting and overall satisfaction from the job reporting; all of which may be part of retention improvement efforts. From those numbers, companies can work to reduce turnover costs and retain their high-value employees over the longer-run by building customized retention plans. If there's one fly in the ointment of today's fast-moving workplace, it is keeping employees. Business-level and personal efforts to retain good talent in an organization are cropping up here and there. In this light, studies of EI measurement have never been as important as far as retention strategies are concerned. The purpose of the study is to determine the impact of AI and EI on employee retention. An extensive literature review was conducted to learn about this association. It was estimated that available literature always confirms the relationship between AI and EI, justifies their role to attain improved employee retention outcomes. It would not make you wrong to have an idea of why people leave, in a world where most jobs are cutthroat and insane, if you are a company that wants to retain top talent over a long period of time. The quality and level of

products, services, and workforce is preserved with the help of retention. those garmens are insights into the new people before they even start to work) is important information about the culture and the flow of a company. The proposal suggests a method of testing the significance of Employee turn over variables using IBM HR Analytics Employee Attrition and Performance dataset. The strategy incorporates data visualization, machine-learned attrition predictive models, and SHAP (SHapley Additive exPlanation) feature importance analysis into the workflow to discard major drivers of attrition. In addition, they propose an advice system, where userbased collaborative filtering technique is used to give individualized retention strategy with various risk indicators to each employee. It also develops forward looking measures to avert or be in a better position to anticipate employee turnover in case of prescriptive modeling and reasonable counsel are combined. Retaining employees has proved to be a massive challenge to businesses in the highly competitive business world in the contemporary times. In addition to being a mere issue of maintaining a productive office, loss of star players can also translate to the failure of the company in the long term. In an effort to predict turnover flow behaviour and identify what the main predictors are of absence, scholars have consequently been becoming increasingly interested in machine learning models. There are many factors that contribute to employee retention and analysts frequently face difficulties in making sense of potentially confusing information in personnel data. Feature selection has gained an important role to enhance analytical quality and to identify the most relevant features. The work presents an innovative methodology called the Enriched Employee Retention Analysis System (EERAS), which is a novel framework that combines feature selection and machine learning methods. The two primary objectives of system design are: (1) to find out and rank the critical reasons causing employee attrition, and (2) to propose important factors in retaining staff. Four feature selection methods, including MRMR, Chi-2, ANOVA and Kruskal applied to various classifiers in a large employee dataset empirical study: Decision tree, linear regression, Na\"ive Bayes, Support vector machine, XGBoost source data set that was randomly divided. The results presented in this paper indicate that the feature selection reduces the training time and enhances the classification accuracy. Furthermore, EERAS provides some practical examples of what HR policies could contain to make them more supportive of long-term staff retentions plans. Foreseeing layoffs and finding employees already is a major concern for all businesses and industries, especially those that experience high levels of employee churn or seasona changes in labor needs. The work [8] measures the efficiency of two models XGBoost a supervised classification and KMeans, an unsupervised method of clustering to predict employee retention rate and possibility of laying off staff members. It assesses the model's accuracy, interpretability and predictive power against metrics such as employee tenure, performance reviews and engagement scores. The results demonstrate that in binary classification, XGBoost is better at providing a clear “yes” or “no”. and fairly practical HR decision-making-relevant predictions. KMeans, however, helps in discovering patterns and wine sowing workers into separate clusters also gives insights on traits of the workforce. According to the comparative research, XGBoost with statistical local texture descriptors is the best model for precise layoff prediction, and KMeans can help understand employee clustering and their behavior patterns. These findings illustrate how machine learning could enhance predictive workforce management and offer insight for strategic HR planning and policy formulation.

Results and discussion. In [9] a Stacking Based Transfer Learning (TL) is presented in order to reduce the risk of employee retention. We construct a hierarchical stacking ensemble of deep learning models where we combine the domain specific data and pre-trained representations (BERT for textual, ResNet for numerical). The algorithm is exploited to offer retention estimates by fusing number values and textual data. Experimental results based on a publicly employee retention dataset verify the effectiveness of our proposed strategy. The use of Stacking-Based TL framework outperforms the offthe-shelf models such as Random Forest (88.3%) and Support Vector Machine (85.7%), which achieves an accuracy of 92.5%. Also, 17% of prediction error is decreased by the

model when compared to baseline methods. Generative AI (or GAI, a type of artificial intelligence) is one of the most rapidly expanding innovators in talent and HR technology. The review [10] addresses the utilization of GAI in talent management, particularly with regard to its role in employee engagement and retention initiatives. It also considers the wider implications of costs and benefits on implementing the GAI into practice. A literature overview on usage and applications in performance evaluation, as well as hiring/ training & talent identification discovery is provided. The findings indicate that the benefits of using GAI in HR practices can be seen as a number of direct and significant positive effects, such as efficiency, individuality of employee experiences, improved quality decision-making based on data-driven action reports, and so on. However, also implementing GAI provides serious doubts, whether in terms of ethical decision-making and algorithmic biases, or privacy threats and accelerated change that HR professionals will be forced to adapt to with these systems. It is a curious insight into the revolutionary nature of GAI, in regard to retention, employee engagement and HR administration, in the current digital environment that is rapidly evolving. Considering the increased globalization and the incessant connectivity, there has been a trend nowadays with many businesses around the world attempting to establish methods of effectively attracting and retaining multicultural talent in their workforce due to emerging diversity. This paper examines interactions between the cultural intelligence (CQ) of a supervisor and subordinate and job engagement as well as intention to stay in multicultural workgroups. After this call, we carried out two empirical studies, which were based on leader member exchange (LMX) theory and engagement with work. Like in Study 1 (m170 matched), supervisor CQ moderates an employee CQ that leads to job engagement. Study 2 (matching data 161) confirmed the findings and also indicates the importance of job engagement on the intentions of the employees to remain. A 2CQ CQ study, whereby the dual gain approach is employed to enhance the supervisor and the TC-workers CQ, would be added to theory and practice of retention/performance in multicultural work groups. The research article under discussion contributes to the existing body of knowledge by assuming that the organizational learning and employee empowerment are the mediating variables between employee retention intentions and talent development strategies. The findings provide useful management implications to the banking sector in Bangladesh, indicating that the development of organizational learning potential and employee empowerment could benefit the retention performance.. A questionnaire on 5-points Likert scale was distributed to 378 employees of private banks. Replies were analyzed using SmartPLS software and the proposed links were tested. This study's findings indicated that the link between talent development strategies and employees' retention intention is mediated by organizational learning and employee empowerment processes. Effects of University-Based Entrepreneurship Education 85 The study investigates time the extent to which university-based entrepreneurship education influences employee retention in Chinese start-up businesses. University-level entrepreneurship education may, however, help shape students' omporting people's professional attitudes and behaviour, which will influence their entire career over time. This is grounded in the attraction, selection and attrition model and social learning theory. To investigate A two-stage web-based and onsite survey was conducted among employees from startups in three entrepreneurial incubators in China. The hierarchical multiple regression and bootstrapping (n = 274) was conducted with the final sample. The results indicate that entrepreneurship education substantially enlarges employees' willingness to remain in the firm and protean career attitudes have a mediating role between the two. Further, this mediating relationship was found to be reinforced by socializing tactics. These findings provide long-term yet salient benefits of how entrepreneurship education at university contributes to the graduates' employment and thus useful lessons for the design of university's entrepreneurship curriculum and people management in startups. Focusing on influences that impact workers' propensity to stay and commitment, the study investigates employee retention in SMEs and large corporations. Size of the firm doesn't matter; retention is highly influenced by such factors as nature of work, benefits, relationships with co-workers, normative

commitment and organizational commitment based on a partial least squares structural equation modeling analysis of 511 employee responses. While the models certainly succeed in highlighting organizational differences, a more focused examination is needed for homogeneous groups of employees. The findings suggest that companies need to focus less on bringing in new subscription services or take-out food and more on improving workplace connections, perks and job happiness if they want a high number of people to stay. By adopting the moderating role of organization size and using a holistic point of view, this study helps in better understanding employee retention, as well as the joint influences of multiple constructs. The research is on how corporate intrapreneurship influences employee retention in Nigerian banks with emphasis on characteristics such as initiative, innovation, decision making, strategic change and company growth. The data was obtained purposively from the eight (8) banks on Nigeria Stock Exchange. Results: The results demonstrate that corporate intrapreneurship has a significant influence on employee retention, resulting in a positive and statistically significant effect in initiative, company growth, decision-making, and creativity. Among them, initiative was the most important factor (coefficient = 0.557077, p-value < 0.05), followed by decision-making (coefficient = 0.1632493, p-value < 0.05), business development (co-efficient = 0.4497637, p-value < 0.05) and creativity (co-efficient = 0.1185839, p-value < 00:05). In the other hand, there was no significant difference due to strategic change (p-value = 0.090). The study reveals that Corporate intrapreneurship is a very strong predictor of employee retention in Nigerian banks, especially as they prompt novel initiative and expansion oriented strategy. To encourage a spirit of risk taking, proactive decision making and utilization of competitive opportunities and reduce turnover - HR Director It is the quality of employees and managers that it recommends organizations focus on developing, by working to build an organizational culture that embraces risk, encourages proactive decision making and leverages competitive opportunities. The findings add to knowledge by introducing intrapreneurial strategies as a strategic tool for achieving workforce stability in the banking industry. The HRM practices of South Indian self-financed institutions were also investigated in the study. Topics reviewed included recruitment and selection, initial training, supervision, training and career development. Data were procured from faculty through surveying. The results indicate that satisfaction with prospects for career advancement, and satisfaction with the quality of work life were not high while feeling valued by management was high among faculty members. What they did also find, though, were unusually high stress levels and rather low job security.

Conclusions. The fact that employee retention management is the catchphrase of any organization in the industry, is simply because an ordinary person would desire a workforce that is stable and thus will result in high productivity and low turnover-cost. The paper highlights the multi-dimensional aspect of retention in its correlation between human aspect variables like corporate culture, employee empowerment, organizational learning, talent development protean career attitudes and cultural intelligence and information technology methods such as AI, machine learning, and predictive analytics. These also have impacts on the intention to remain by workers as it is affected by underlying EM and MM such as empowerment, socialization strategies or organisational size. The findings indicate that a mixture of traditional HR approaches and advanced analytics and specifically designed retention program enhances the quality of the predictions and, therefore, allows a proactive design of the staffing strategies. It offers applied views that are a blend of structure, human and technical aspects.

Author Contributions. All authors contributed to the conception and design of the study, literature review, methodology, data collection and analysis, manuscript preparation, revision, and approval of the final version of the manuscript.

Funding. The authors received no specific financial support from any funding agency, commercial organization, or not-for-profit institution for the research, authorship, and/or publication of this article.

Data Availability. The data supporting the findings of this study are available from the corresponding author upon reasonable request.

Declarations

Conflict of Interest. The authors declare that they have no competing interests or conflicts of interest related to this work.

Ethical Approval. This article does not involve studies with human participants or animals. Therefore, ethical approval was not required.

Informed Consent. Not applicable.

References

[1] Delen, D. (2010). A comparative analysis of machine learning techniques for student retention management. Decision Support Systems, 49(4), 498–506. https://doi.org/10.1016/j.dss.2010.06.003

[2] Delen, D., Zaim, H., Kuzey, C., & Zaim, S. (2013). A comparative analysis of machine learning systems for measuring the impact of knowledge management practices. Decision Support Systems, 54(2), 1150–1160. https://doi.org/10.1016/j.dss.2012.10.040

[3] Soller, A., Wiebe, J., & Lesgold, A. (2023). A machine learning approach to assessing knowledge sharing during collaborative learning activities. In Computer Support for Collaborative Learning (pp. 128–137). Routledge. https://doi.org/10.3115/1658616.1658635

[4] Lee-Gouet, V., Yamoun, L., Rodière, Z., Simon Chane, C., Jordan, M., Longhi, J., & Picard, D. (2025). A deep learning-based pipeline for the conservation assessment of bindings in archives and libraries. Multimedia Tools and Applications, 1–15. https://doi.org/10.1007/s11042-025-20615-6

[5] Salam, A., Abrar, M., Ullah, F., Khan, I. A., Amin, F., & Choi, G. S. (2023). Efficient data collaboration using multi-party privacy-preserving machine learning framework. IEEE Access, 11, 138151–138164. https://doi.org/10.1109/ACCESS.2023.3339750

[6] Yuan, J., Chen, C., Yang, W., Liu, M., Xia, J., & Liu, S. (2021). A survey of visual analytics techniques for machine learning. Computational Visual Media, 7(1), 3–36. https://doi.org/10.1007/s41095-020-0191-7

[7] Chang, J. M., Zhuang, D., & Samaraweera, G. D. (2023). Privacy-Preserving Machine Learning. Simon & Schuster.

[8] Zhong, J., Wei, S., Chen, Q., & Niu, B. (2025). Unlocking the power of artificial intelligence for pangolin protection: Revolutionizing wildlife conservation with enhanced deep learning models. Expert Systems with Applications, 267, 126206. https://doi.org/10.1016/j.eswa.2024.126206

[9] Lata, K., Singh, P., Saini, S., & Cenkeramaddi, L. R. (2024). Deep learning-based brain tumor detection in privacy-preserving smart health care systems. IEEE Access. https://doi.org/10.1109/ACCESS.2024.3456599

[10] Singh, K., Yadav, M., Barak, D., Bansal, S., & Moreira, F. (2025). Machine-learning-based frameworks for reliable and sustainable crop forecasting. Sustainability, 17(10), 4711. https://doi.org/10.3390/su17104711

[11] Singh, K., Yadav, M., & Yadav, R. K. (2024). IoT-based automated dust bins and improved waste optimization techniques for smart city. In Revolutionizing Automated Waste Treatment Systems: IoT and Bioelectronics (pp. 167–194). IGI Global Scientific Publishing. https://doi.org/10.4018/979-8-3693-6016-3.ch012

[12] Hajimahmud, V. A., Singh, Y., & Yadav, M. (2024). Using a smart trash can sensor for trash disposal. In Revolutionizing Automated Waste Treatment Systems: IoT and Bioelectronics (pp. 311–319). IGI Global Scientific Publishing. https://doi.org/10.4018/979-8-3693-6016-3.ch020
[13] Yadav, M., Hajimahmud, V. A., Singh, K., & Singh, Y. (2024). Convert waste into energy using a low-capacity igniter. In Revolutionizing Automated Waste Treatment Systems: IoT and Bioelectronics (pp. 301–310). IGI Global Scientific Publishing. https://doi.org/10.4018/979-8-3693-6016-3.ch019
[14] Singh, K., Yadav, M., Singh, Y., & Barak, D. (2024). Finding security gaps and vulnerabilities in IoT devices. In Revolutionizing Automated Waste Treatment Systems: IoT and Bioelectronics (pp. 379–395). IGI Global Scientific Publishing. https://doi.org/10.4018/979-8-3693-6016-3.ch023
[15] Njungle, N. B., Jahns, E., Wu, Z., Mastromauro, L., Stojkov, M., & Kinsy, M. (2025). GuardianML: Anatomy of privacy-preserving machine learning techniques and frameworks. IEEE Access.

https://doi.org/10.58225/sw.2026.1-101-115

FIRST-LEVEL SEISMIC RISK ASSESSMENT OF REINFORCED CONCRETE PUBLIC BUILDINGS CONSIDERING HILLTOP AND SLOPE EFFECTS IN SAMSUN, TÜRKIYE

Humberto Varum[1*], Azer Kasımzade[2], Aytaj Aliyeva[3]
[1*]*University of Porto, Porto Portugal*
[2]*Ondokuz Mayıs University, Samsun Türkiye*
[3]*Azerbaijan University of Architecture and Construction, Baku, Azerbaijan*
hvarum@fe.up.pt, azer@omu.edu.tr, aytaj.aliyeva@azmiu.edu.az

Abstract. Rapid seismic risk assessment methods are critical for mitigating disasters in seismically active regions. This study presents the first-level seismic assessment methodology applied to reinforced concrete buildings within Samsun Province, Türkiye. The evaluation relies on a multi-parameter scoring system that accounts for structural typology, building age, and various architectural irregularities. By analyzing key parameters—such as soft stories, heavy overhangs, short columns, and pounding effects—this method provides a rapid, efficient framework for identifying high-risk structures. The findings provide a basis for urban resilience planning and prioritization of buildings requiring detailed seismic evaluation.

Keywords: Rapid Seismic Assessment, Reinforced Concrete, Samsun, Building Performance Score, Structural Irregularities

Cite this article as: *H. Varum, A. Kasımzade, and A. Aliyeva, "FIRST-LEVEL SEISMIC RISK ASSESSMENT OF REINFORCED CONCRETE PUBLIC BUILDINGS CONSIDERING HILLTOP AND SLOPE EFFECTS IN SAMSUN, TÜRKIYE," SW AzUAC, vol. 1, 2026. https://doi.org/10.58225/sw.2026.1-101-115*
Article history: *Received: 18 May 2026 / Revised: 25 June 2026 / Accepted: 06 July 2026*

1. Introduction. Türkiye is situated in one of the most seismically active regions in the world, making proactive structural evaluations a matter of public safety. While detailed structural simulations offer the highest accuracy, they are time-consuming and economically unfeasible for regional or city-wide inventories. Consequently, "first-level" or rapid visual screening methods are widely adopted to quickly categorize the vulnerability of existing building stocks. [2,3].

This paper examines the specific parameters and scoring methodology utilized in the seismic risk screening of reinforced concrete buildings within Samsun Province, Türkiye. Located within a region influenced by several active tectonic structures, Samsun Province requires systematic monitoring of its building stock. [5]

2. Methods. Since the examined structures are public buildings, their address information is obtained directly from the relevant institution along with the official inspection request. The target zone for the street survey is delineated on the map. Architectural elevation photographs of the investigated building are captured and appended to the Data Collection Form for Reinforced Concrete Buildings.

The construction year of the building is of critical importance for the fieldwork, as it provides substantial insights into the seismic code in force at the time of construction, as well as the contemporary construction techniques employed, such as the utilization of deformed reinforcing bars, and the proper execution of confinement techniques.

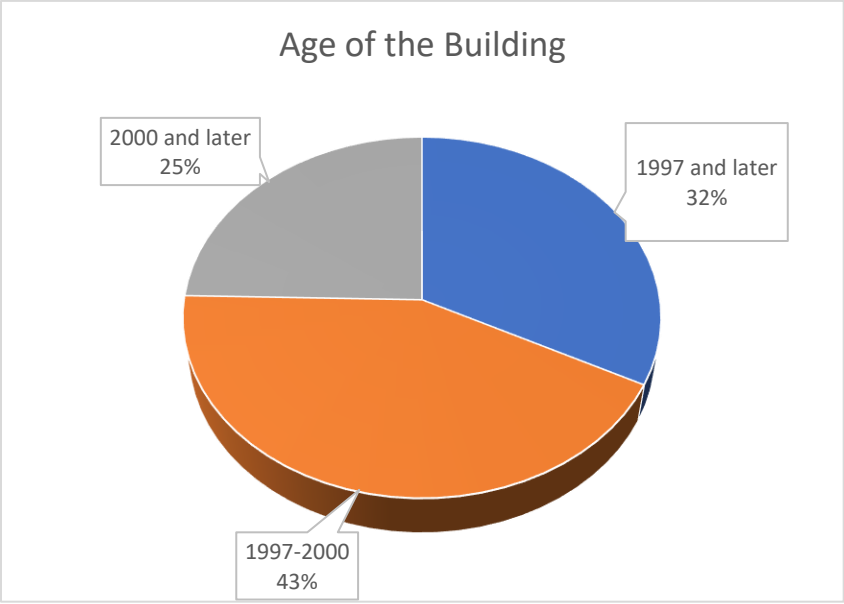

Fig.1. Distribution chart of building age

The structural systems of the investigated buildings were classified into two categories: Reinforced Concrete Frame (RCF) and Reinforced Concrete Frame-Wall (RCFW). [7]

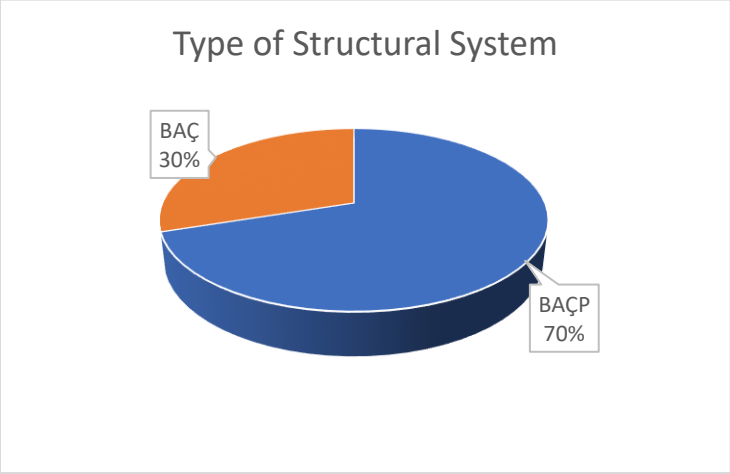

Fig.2. Distribution chart of structural system types of the buildings

Since the structures examined in this study are public buildings, a basement floor is present in the majority of them to accommodate the boiler room. For this reason, it has been observed that in buildings constructed prior to 1997, as well as those built in 1997 and thereafter, the basement floors feature reinforced concrete shear walls, or the basement frame is supported by vertical structural elements with an aspect ratio (long side to short side) of at least 7, as specified in the 2007 and 2018 Specifications for Buildings to be Built in Seismic Zones.

The total number of stories of a building is counted as the total number of floors situated above the foundation, including the basement and attic floors.

The assessment, conducted in compliance with the implementing regulation of the Law No. 6306 on the Transformation of Areas Under Disaster Risk, is applicable to buildings with 1 to 7 stories. Therefore, reinforced concrete public buildings with up to 7 stories were selected for this study.

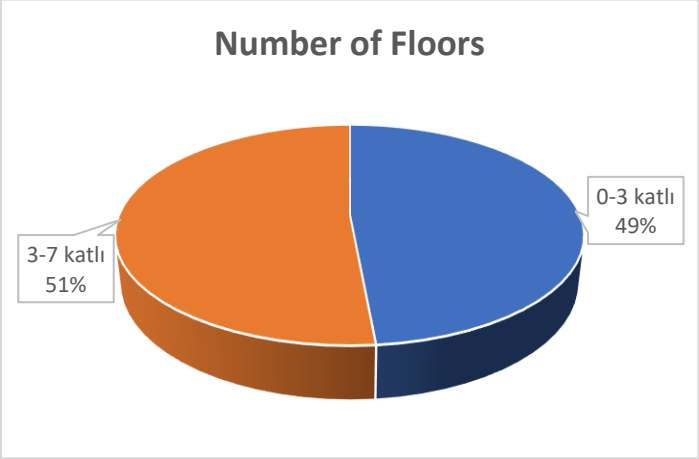

Fig.3. Distribution chart of the number of building stories

The quality of workmanship and materials utilized during the construction of a building, along with the diligence shown in its maintenance, directly influence the visual quality of the structure. In observational assessments, the visual quality of a building can be classified as good, moderate (fair), or poor. Structural quality and the risk of damage that may occur during a potential earthquake are closely interrelated. For a building with poor visual quality, the material strength under seismic loads is also expected to be lower than anticipated (Deprem Şurası, 2004) [4,5].

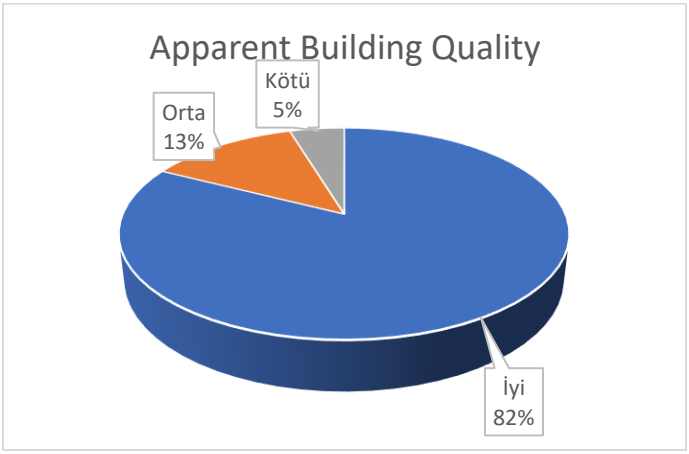

Fig.4. Distribution chart of the visual quality of the buildings

According to the form provided in the implementing regulation of the Law No. 6306 on the Transformation of Areas Under Disaster Risk, the selected buildings are classified into two categories observationally and categorized into three groups based on their visual quality: good, moderate, and poor.

Since this study focuses on public buildings across the province of Samsun, 82% of the structures were evaluated as "good" in terms of visual quality, attributed to the regular execution of their annual maintenance and repairs.

Fig.5. A school building with regularly maintained exterior facades

Based on investigations conducted around the structures, buildings that exhibited defects such as settlement in the surrounding parapets in heavily utilized areas like schoolyards, and whose observational evaluations were made regarding their construction year and workmanship, were classified as "moderate" at a rate of 13%. Furthermore, buildings that displayed cracks due to live loads at the expansion joint zones between structural junctions and reinforced concrete fire escapes or interior staircases, visible cracks at wall and column-beam joints, and deflections in structural floor slabs were evaluated as "poor" at a rate of 5%.

Considering the building age and the construction techniques employed (such as the non-utilization of ready-mixed concrete and ribbed rebars, or the usage of unwashed marine sand), public buildings constructed in 1997 and earlier are expected to be in a poorer condition than those built in 2000 and thereafter. However, since the supervision processes during the estimated cost estimation, tendering, and construction phases are executed by the technical personnel within public institutions, it has been observed that these buildings are in a better state in terms of visual quality and workmanship compared to the surrounding residential buildings of the same vintage.

Fig.6. Abandoned lodging buildings

Stories constructed without infill walls on the ground floors or with a height greater than that of other stories to generate revenue—such as for commercial spaces, parking lots, restaurants, showrooms, or banks—even when the upper stories remain structurally adequate. These modifications, made on ground floors to create larger spaces driven by economic considerations, lead to failure at the ground floor level despite the structural integrity of the upper stories. This is attributed to the fact that the vast majority of lateral displacement during an earthquake occurs within these specific stories, causing crushing at the column ends and resulting in heavy damage. The lateral stiffness of a soft storey is substantially lower than that of stories with infill walls. A weak storey irregularity also arises when the height of the ground floor is greater than that of the upper floors in the floor plans. This condition creates a vertical stiffness discontinuity, leading to a higher concentration of damage in these stories during seismic events.

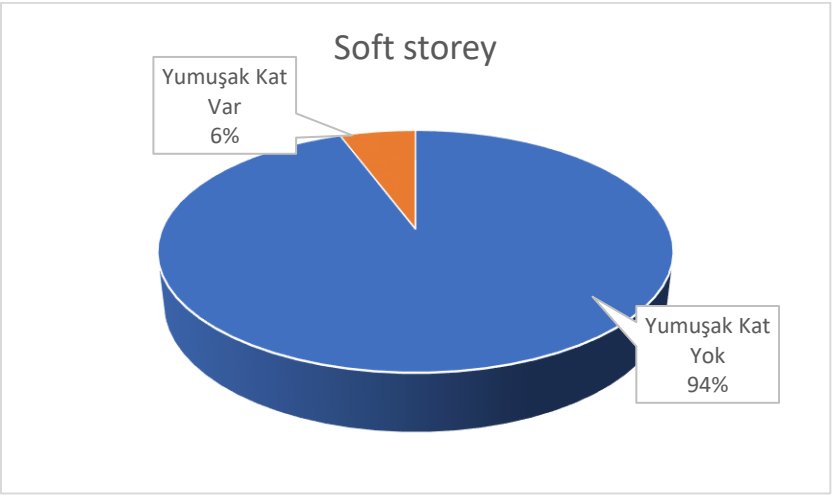

Fig.7. Distribution chart of soft storeys

Since the structures examined in this study are public buildings, their ground floors are not utilized for commercial purposes; consequently, it was observed that 94% of the buildings were constructed in compliance with standard floor plans and storey heights. In contrast, it was noted that in certain public buildings such as police stations and hospitals, which require the accommodation of specially equipped vehicles, the ground floors were constructed with greater heights to serve as vehicle parking or washing bays. This architectural configuration led to the formation of a soft storey irregularity in 6% of the investigated buildings.

Fig.8. A public building with a ground floor utilized as a garage

Overhangs are structural components that extend from floor slabs within the parcel boundaries, featuring at least one free or supported end, and whose dimensions are specified by implementation zoning plans or regulations. In other words, the ground footprint of the building differs from the floor plan areas of the upper stories. Overhangs are categorized into two types: open overhangs and enclosed overhangs.

Enclosed overhangs can be constructed on the street facades of parcels, provided they remain within the parcel boundaries, projecting a maximum of 1.50 meters beyond the building setback line. These overhangs must stay within the parcel limits for street facades and may similarly project up to 1.50 meters into yard setbacks.

Open overhangs, on the other hand, are projections constructed on the street facades of parcels, provided they remain within the parcel boundaries, extending a maximum of 1.50 meters from the building setback line. They may project 1.50 meters into rear and side yard setbacks, provided they do not approach closer than 3 meters to the parcel boundaries. However, in practice, cases are frequently encountered where open or enclosed overhangs are constructed facing adjacent neighbors without any street frontage, a condition that strictly violates zoning regulations.

Overhangs that do not comply with regulatory frameworks disrupt the structural frame system and induce mass irregularities in buildings. Consequently, the required load transfer mechanism between structural components cannot be properly established, and buildings with heavy overhangs sustain extensive damage during seismic events.

In this study, it was observed that public buildings constructed prior to 1997 were built in accordance with standardized type projects; as a result, they do not feature heavy overhangs that would disrupt the structural frame or prevent the load-bearing system from resisting seismic and other loads. Similarly, investigations conducted on public buildings built after the revised 1997 seismic code, and particularly those constructed after 2000, revealed no planning designs incorporating heavy overhangs.

The short column is a concept associated with the discrepancy between the designed column height and the actual effective column length. In buildings, particularly along exterior walls, when infill walls are not constructed continuously up to the upper floor slab, short column effects emerge during an earthquake within the clear portions of the columns where no partition wall is built. In structures with functional basement stories, openings are often left in the exterior walls to install strip windows and utilize natural light. If these walls do not extend through the full clear height of the column and are not structurally isolated from the frame to which they are connected, severe damage can occur in the columns during seismic events (Celep, Z. 2005).

In a structure, short columns exhibit a significantly more rigid behavior compared to other columns. Elements with high stiffness attract greater seismic forces because they absorb a larger portion of the seismic energy during an earthquake. Consequently, because short columns are subjected to exceptionally high shear and bending moment effects, shear failures develop along the clear length of the column.

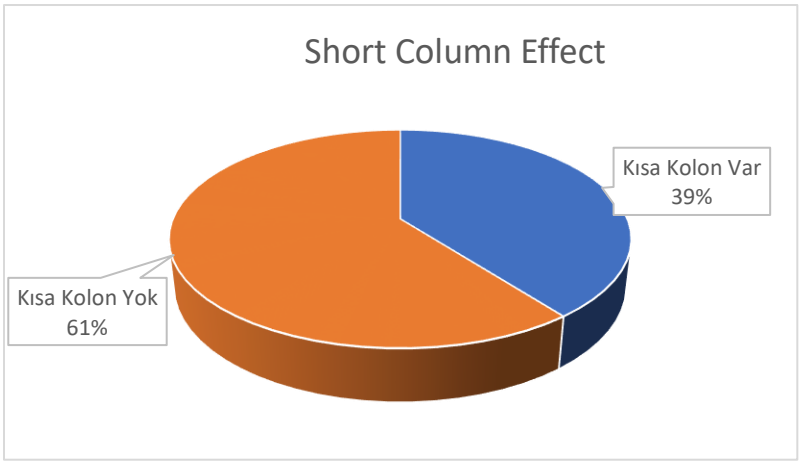

Fig.9. Distribution chart of the short column effect

Since the structures examined in this study are public buildings with high occupancy rates—such as hospitals, schools, and dormitories—facilities including boiler rooms, indoor parking lots, and storage rooms are constructed on the ground and basement floors. Due to the installation of strip windows for natural lighting in these areas, the short-column effect was observed in 71% of the investigated buildings.

Fig.10. A school building with strip windows in the basement floor

An urban settlement pattern in which adjacent buildings share one or more common side walls is referred to as an adjacent building layout (row housing system). In such configurations, neighboring reinforced concrete structures are susceptible to mutual damage resulting from seismic-induced vibrations and impact effects during earthquakes.Furthermore, another structural challenge in adjacent layouts arises when the floor slab elevations of the buildings differ, causing the floor slab level of one building to align with the clear column height of the neighboring structure. Especially during a potential earthquake, if the joint spacing is insufficient, the floor slab of the neighboring building can fracture the column of the adjacent structure as a result of seismic oscillation. Another phenomenon observed in adjacent layouts is the pounding (hammering) effect. The pounding effect can be defined as a phenomenon where, in cases where an adequate seismic joint spacing has not been provided between two adjacent structures based on structural calculations, the building with higher stiffness against overturning strikes the less rigid building as a result of its lateral displacement under seismic action, thereby inducing structural damage. The Specifications for Buildings to be Built in Seismic Zones (DBYBHY; 2007, 2018) emphasize specific precautions regarding this issue. Apart from the effects of temperature fluctuations and foundation translations and rotations induced by differential ground settlements, the code explicitly prescribes the criteria for seismic joint clearances to be maintained between existing old structures and newly planned buildings solely for seismic actions.

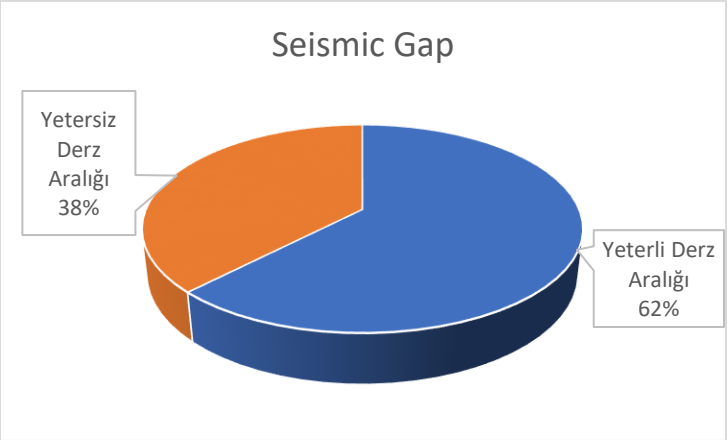

Fig.11. Distribution chart of joint spacings

Since the public buildings examined in this study—comprising schools, hospitals, nursing homes, dormitories, and police stations—are planned within their own parcels incorporating yards and parking spaces based on their occupancy types, an adjacent building layout is not applicable to these structures.

However, because the regional development characteristic is predominantly an adjacent layout, particularly in the downtown area of the İlkadım district in Samsun province, apartment-style lodging buildings belonging to various institutions in this zone were investigated regarding their joint spacings. Accordingly, it was observed that 62% of these buildings were constructed with adequate joint spacing; however, structures located in the relatively older settlements of the district in terms of urban zoning failed to satisfy the required joint clearance adequacy.

Fig.12. Adjacent building layout in Samsun city center

Buildings located on hilltops or on slopes exceeding 30° amplifies the seismic actions it will be or has been subjected to. This condition, which can be easily identified through observational assessment during the street survey method, must be taken into consideration when calculating the structural seismic score (Işık and Tozlu, 2015).

Public structures are planned not merely as standalone service buildings, but integrated with parking areas, yard spaces, additional service facilities, and outbuildings. Consequently, because multiple sections or buildings utilized for different purposes must be situated on single or multiple parcels, the land selection process for construction is executed by rigorously considering terrain conditions to determine the most optimal site. Therefore, it was observed that for the public buildings examined in this study, plots with a natural ground slope exceeding 30° were not selected.

Fig.13. A school building planned with its own yard

Vertical irregularity—namely, irregularity within the load-bearing system—emerges as a result of columns lacking continuity along the building height and varying floor areas across stories. Plan irregularity consists of structural axes that are not parallel to each other, forming broken-axis beams. In such cases, columns and shear walls are irregularly distributed in the plan configuration. Due to excessive opening ratios introduced in floor slabs for staircases or elevator shafts, the transfer of seismic loads to the structural system components becomes restricted. Since the structural statics do not comprise uniform frames, lateral loads cannot be regularly transferred from column to column; consequently, the forces change direction within the structure. Buildings featuring plan irregularities exhibit a high vulnerability to torsional effects.

The observations recorded under the "Heavy Overhangs" parameter are also valid for the "Vertical and Plan Irregularities" parameter. Public structures built prior to 1997 were constructed in accordance with standardized type projects, such as lodging facilities, dormitories, hospitals, and 8-classroom schools. In these low-rise type buildings, no plan or vertical irregularities were observed; furthermore, it was noted that bridging large spans for areas such as conference halls and gymnasiums without proper column and beam support was meticulously avoided. For public buildings constructed after 1997, the cross-sections of the structural system components were selected in strict compliance with the revised and updated seismic codes. Notably, investigations carried out on public structures built after 2000 revealed no evidence of plan irregularities.

Fig.14. A lodging building constructed in accordance with standardized public building type projects

3. Calculation of Building Performance Score. Following the completion of the outdoor visual inspections of the selected structures, and once the parameter values are determined and recorded into the Data Collection Form for Reinforced Concrete Buildings, the Building Performance Score is calculated. This score determines the prioritization of the investigated buildings for detailed seismic risk assessments. By following the methodology detailed in the appendix of the implementing regulation of the Law No. 6306 on the Transformation of Areas Under Disaster Risk, the calculation of vulnerability parameters—which serves as the preliminary stage of the performance score calculation—was executed for 406 public buildings.

According to the fundamental approach and methodology for calculating the building performance score outlined in the implementing regulation of the Law No. 6306 on the Transformation of Areas Under Disaster Risk, the risk zone is primarily determined based on the seismicity of the region where the structure is situated and the local soil type.

The conducted study encompasses the entire province of Samsun, and the districts of Samsun are located within I. II. and III degree seismic zones according to the earthquake risk map.
Accordingly:

Table 1. Selection of hazard zones for Samsun Province

District Name	Seismic Zone
19 Mayıs	III
Alaçam	III
Asarcık	I
Atakum	II
Ayvacık	I
Bafra	III
Canik	II
Çarşamba	II
Havza	I
İlkadım	II
Kavak	I

Ladik	I
Salıpazarı	II
Tekkeköy	II
Terme	III
Vezirköprü	I
Yakakent	III

Table 2. Selection of hazard zones based on soil class

Seismic Hazard Zone	Earthquake Zone According to DBYBHY	Soil Classification According to DBYBHY
I	1	Z3 / Z4
II	1	Z1 / Z2
II	2	Z3 / Z4
III	2	Z1 / Z2
III	3	Z3 / Z4
IV	3	Z1 / Z2
IV	4	All Soil Classes

After the hazard zones are determined for all districts, these data are utilized alongside Table 3 to obtain the Base Score and Structural System Score for each building. All structures investigated in this study are categorized as either RC-F (Reinforced Concrete Frame) or RC-FW (Reinforced Concrete Frame with Shear Walls). For buildings classified as RC-F, the additional structural system score is taken as 0 in the calculations, whereas for buildings classified as RC-FW, the additional system scores are determined based on their respective hazard zones [9].

Table 3. Base and Structural System Score Table

Total Number of Stories	Base Score by Hazard Zone				Structural System Score (SSS)	
	I	II	III	IV	RCF	RCFW
1–2	90	120	160	195	0	100
3	80	100	140	170	0	85
4	70	90	130	160	0	75
5	60	80	110	135	0	65
6–7	50	65	90	110	0	55

For the reinforced concrete buildings investigated in this study, the identified vulnerability parameters—such as Soft storey, Heavy Overhangs, Short Column, Hilltop/Slope Effect, and Plan Irregularity—are evaluated using Table 5. If no vulnerability parameters are detected, the parameter value is entered as "0" according to Condition 1 in Table 4. Conversely, if one or more vulnerability parameters are identified in the inspected building, the evaluation is conducted according to Condition 2, and the value for each parameter is taken as "1". Regarding the assessment based on the Apparent Quality values in Table 4., the vulnerability parameter value is taken as "0" for buildings whose apparent structural quality is considered "good"; similarly, for buildings evaluated as having "moderate" and "poor" apparent quality, the parameter values are adopted as "1" and "2", respectively.

Table 4. Vulnerability Parameter Values (O_i)

Deficiency Parameter No.	Deficiency Parameter	Condition 1		Condition 2	
		Presence	Parameter Value	Presence	Parameter Value
1	Soft storey	Absent	0	Present	1
2	Heavy Overhang	Absent	0	Present	1
3	Apparent Construction Quality	Good	0	Moderate (Poor)	1 (2)
4	Short Column	Absent	0	Present	1
5	Hill/Slope Effect	Absent	0	Present	1
6	Plan Irregularity	Absent	0	Present	1

The total vulnerability score of the building was determined by multiplying the identified vulnerability parameter values for the baseline structures—namely Soft storey, Heavy Overhangs, Short Column, Hilltop/Slope Effect, and Plan Irregularity—by the corresponding value matching the total number of stories in the Vulnerability Parameter Score OP_i table presented in Table 5. [2,7]

Table 5. Vulnerability Parameter Score (OP_i)

Total Number of Storeys	Structural Irregularity Penalty Scores (OP)										
	Soft Storey	Poor Visual Quality	Heavy Overhangs	Storey-Level Compatibility / Isolated Building Condition				Vertical Irregularity	Plan Irregularity / Torsional Effects	Short Column	Hilltop / Slope Effect
				Same Storey Level	Same Storey Level	Different Storey Level	Different Storey Level				
				Intermediate Position	Corner Position	Intermediate Position	Corner Position				
1–2	-10	-10	-10	0	-10	-5	-15	-5	-5	-5	-3
3	-20	-10	-20	0	-10	-5	-15	-10	-10	-5	-3
4	-30	-15	-30	0	-10	-5	-15	-15	-10	-5	-3
5	-30	-25	-30	0	-10	-5	-15	-15	-10	-5	-3
6–7	-30	-30	-30	0	-10	-5	-15	-15	-10	-5	-3

In accordance with Equation (1) provided in Annex-A of the implementing regulation of the Law No. 6306 on the Transformation of Areas Under Disaster Risk, the structural performance score was calculated by determining the corresponding regulatory values of the vulnerability parameters.

$$PP = TP + \sum_{i=1}^{n} O_i * OP_i + YSP \quad (1)$$

The terms in Equation (1), which is utilized to calculate the Building Performance Score, are defined below:
PP: Building performance score
TP: Base score
O_i: Vulnerability parameter value
OP_i: Vulnerability parameter score
YSP: Structural system score

In this study, the structural performance scores of the 406 investigated buildings were calculated, and a risk prioritization was established based on the final performance score values obtained through the First-Stage Evaluation Method. Due to the high number of buildings inspected and the occurrence of multiple structures sharing the identical Performance Score, a risk ranking grouping was implemented based on the Performance Scores. According to this approach:

Table 6. Risk Prioritization Evaluation Intervals

Performance Score Range	Risk Priority Value
0-30	1
31-50	2
51-70	3
71-100	4
101- ~	5

The structures are categorized into Risk Priority Values ranging from 1 to 5 based on their Performance Score intervals.

4. Conclusions. This study presented a first-level seismic risk assessment of reinforced concrete public buildings in Samsun Province, Türkiye, incorporating structural irregularities and hilltop/slope effects within a standardized scoring framework. The results indicate that the proposed rapid screening methodology is effective for identifying and prioritizing buildings requiring detailed seismic evaluation, thereby supporting efficient seismic risk management and decision-making at the urban scale [9].

Author Contributions. All authors contributed to the conception and design of the study, literature review, methodology, data collection and analysis, manuscript preparation, revision, and approval of the final version of the manuscript.
Funding. The authors received no specific financial support from any funding agency, commercial organization, or not-for-profit institution for the research, authorship, and/or publication of this article.
Data Availability. The data supporting the findings of this study are available from the corresponding author upon reasonable request.
Declarations
Conflict of Interest. The authors declare that they have no competing interests or conflicts of interest related to this work.
Ethical Approval. This article does not involve studies with human participants or animals. Therefore, ethical approval was not required.
Informed Consent. Not applicable.

References

[1] S. Özdemir, *Seismic Evaluation Methods and Applications of Public Buildings* [in Turkish], M.S. thesis, Samsun, Türkiye, 2019.
[2] A. Kasimzade, M. Erdik, T. Kundu, H. Sucuoğlu, and P. Clemente, Eds., *Earthquake Resistant Design, Protection, and Performance Assessment in Earthquake Engineering*, vol. 54. Cham, Switzerland: Springer Nature, 2024. DOI: https://doi.org/10.1007/978-3-031-65407-7
[3] A. A. Kasımzade, E. Şafak, E. C. Ventura, F. Naeim, and Y. Mukai, *Seismic Isolation, Structural Health Monitoring, and Performance Based Seismic Design in Earthquake Engineering: Recent Developments*. Cham, Switzerland: Springer, 2018. ISBN: 978-3-319-93156-2.
[4] A. A. Kasimzade *et al*., "Economic evaluation of 2000 Baku earthquake impact in view of building features," *Construction Economics and Management*, vol. 32, no. 3, pp. 191–206, 2025.
[5] A. A. Kasimzade *et al*., "System identification for non-destructive assessment of structures: Lessons learned," in *Communications in Computer and Information Science*, vol. 2225. Cham, Switzerland: Springer Nature, 2025, pp. 235–250. DOI: https://doi.org/10.1007/978-3-031-73417-5_18
[6] A. A. Kasimzade and E. Nematli, "New structural seismic isolation system for tower structures," in *Geotechnical, Geological and Earthquake Engineering*, vol. 54. Cham, Switzerland: Springer Nature, 2024. DOI: https://doi.org/10.1007/978-3-031-65407-7_1
[7] A. A. Kasimzade *et al*., "Novel approach on mathematical modelling and numerical evaluation of the seismic protection of structural dynamic systems," *Mathematical Methods in the Applied Sciences*, 2024.
[8] A. A. Kasımzade *et al*., "The contribution of natural seismic base isolation on the durability of traditional Japanese structures," in *Geotechnical, Geological and Earthquake Engineering*, vol. 54. Cham, Switzerland: Springer Nature, 2024. DOI: https://doi.org/10.1007/978-3-031-65407-7_3
[9] A. A. Kasimzade *et al*., "The new criterion on performance-based seismic design with application to high-rise building," in *Geotechnical, Geological and Earthquake Engineering*, vol. 54. Cham, Switzerland: Springer Nature, 2024. DOI: https://doi.org/10.1007/978-3-031-65407-7_11

https://doi.org/10.58225/sw.2026.1-116-124

NON-DESTRUCTIVE AND SEMI-DESTRUCTIVE TESTING FOR SEISMIC RISK ASSESSMENT OF PUBLIC BUILDINGS: FIELD FINDINGS FROM SAMSUN, TÜRKIYE

Sevda Özdemir[1*], Azer Kasımzade[2], Emin Nematli[3]
[1*]*Ministry of İnterior Disaster and Emergency Management Presidency, Türkiye*
[2]*Ondokuz Mayıs University, Samsun, Türkiye*
[3]*Azerbaijan University of Architecture and Construction, Baku, Azerbaijan*
sevdaozdemir@hotmail.com[*], azer@omu.edu.tr, emin.nematli@azmiu.edu.az

Abstract. This study evaluates the seismic risk of 406 reinforced concrete public buildings located across 17 districts in Samsun Province, Türkiye, within the framework of Law No. 6306. A multi-level assessment approach combining rapid visual screening and selected non-destructive and semi-destructive testing techniques was implemented. These included reinforcement detection using Ferroscan technology, localized concrete cover removal, and Schmidt rebound hammer testing. The buildings were classified into five risk categories based on structural performance scores, resulting in 14 buildings identified as first-degree high risk and 48 as second-degree risk requiring priority intervention. The remaining structures were distributed across lower risk categories, indicating varying levels of vulnerability. A regional database was developed to support continuous monitoring and risk prioritization of public infrastructure. The findings suggest that, under updated seismic code provisions introduced in 2019, several of the assessed buildings may exhibit higher vulnerability due to revised soil-structure interaction parameters and increased seismic demand definitions.
Keywords: Seismic Risk Assessment, Rapid Visual Screening, Law No. 6306, Non-Destructive Testing, Public Buildings

Cite this article as: *S. Özdemir, A. Kasımzade, and E. Nematli, "Non-Destructive and Semi-Destructive Testing for Seismic Risk Assessment of Public Buildings: Field Findings from Samsun, Türkiye," SW AzUAC, vol. 1, pp. 116–124, 2026. https://doi.org/10.58225/sw.2026.1-116-124*
Article history: *Received: 18 May 2026 / Revised: 25 June 2026 / Accepted: 06 July 2026*

1. Introduction. Ensuring the post-disaster operational continuity of critical public infrastructure (hospitals, schools, police stations) is vital for life safety and public order in earthquake-prone regions like Türkiye. Outdated building codes and rapid urbanization have left a large portion of the existing reinforced concrete (RC) inventory potentially vulnerable. To systematically address this challenge, the Turkish Government enacted Law No. 6306 for structural assessment and urban transformation.

Since detailed, code-based destructive testing for every structure is economically and temporally unfeasible, multi-level screening frameworks are essential. This study applies rapid visual screening combined with targeted non-destructive testing (NDT) across 406 public buildings in Samsun Province to establish a regional risk-priority matrix for emergency planning [1,3].

2. Methods. Since detailed destructive testing of all buildings was not feasible, a hierarchical assessment strategy was adopted. Initial evaluations were performed using rapid visual screening in accordance with Law No. 6306 guidelines. To improve accuracy, targeted non-destructive and semi-destructive tests were conducted, including reinforcement detection using a Hilti Ferroscan PS 200 device, localized concrete cover removal, and in-situ Schmidt rebound hammer testing. Reinforcement

detailing was investigated at selected structural elements per floor, while concrete quality was assessed at ground and basement levels to minimize variability effects [2].

Fig.1. A law enforcement building featuring exterior thermal insulation cladding

For the seismic assessment of the existing reinforced concrete structures, reinforcement detection was carried out on three randomly selected columns per floor in each building, using a rebar scanner (Hilti Ferroscan PS 200) as a non-destructive testing method. This procedure enabled the determination of reinforcement diameters along with the required confinement ratios within the critical zones of columns and beams [5].

Fig.2. Rebar detection in columns utilizing a Ferroscan

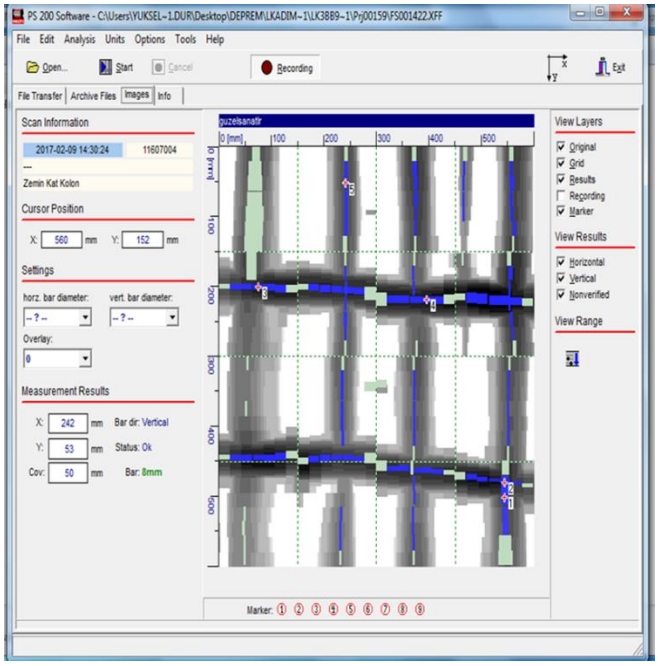

Fig.3. Software visualization of reinforcement detected with Ferroscan

In buildings with a basement, concrete chipping was performed on the basement columns, whereas in buildings without a basement, it was carried out on columns accessible from the exterior facades to evaluate the corrosion state of the reinforcement.

Fig.4. Concrete chipping process in columns

As a result of the concrete chipping process, it was concluded that the reinforcement diameters utilized in the columns were adequate, and the corrosion rates occurring in the reinforcement were within reasonable levels. The inspection revealed that stirrup confinement was not implemented at the column

ends only in the reinforced concrete buildings constructed in 1997 and earlier; the stirrup spacing varied between 20 and 30 cm along the column length, and consequently, the transverse reinforcement elements were found to be insufficient.

Fig.5. Concrete chipping process in columns

In the now-defunct residential buildings where concrete chipping was performed for reinforcement detection, results suggest that plain (smooth) rebar was used in some columns, and the reinforcement diameters selected during construction were incompatible with the column dimensions. Furthermore, within the critical confinement zones located at the end regions of columns and beams, observations indicate that the poorly cast concrete underwent segregation as a result of insufficient concrete curing and faulty workmanship, and the concrete quality was low.

Conversely, inspections of buildings constructed in 2000 and later revealed that transverse reinforcement in confinement zones generally consisted of ribbed Ø8 bars or larger, Additionally, the confinement spacings in the randomly selected columns were found to be no greater than 1/3 of the column cross-sectional dimension or 100 mm, and no less than 50 mm.

Fig.6. Corrosion in column reinforcement

When the seismic behavior of reinforced concrete structures is examined, it is known that an increase in concrete grade and quality leads to a decrease in the number of plastic hinges formed in columns, maximum plastic sectional rotation values, and relative story drift values (Uçar, 2007). For this reason, an in-situ concrete strength test was performed on all inspected buildings using an N-type Schmidt rebound hammer. The columns and shear walls to be tested were selected from the ground or basement floors. On the columns and shear walls designated for measurement, a 20*20cm area was cleared of paint, plaster, and mortar; the old reinforced concrete surfaces were scraped down by approximately 1 cm to reach the raw concrete, after which 10 rebound measurements were taken at 10 distinct points across 10 different structural elements. After determining the average rebound number, the corresponding concrete strength for that structural element was read from the calibration chart. These data were then entered into a Concrete Test Hammer Excel spreadsheet prepared by the technical personnel of the Samsun Provincial Directorate of Environment and Urbanization, enabling a comparative determination of concrete strengths based on cube and cylinder compressive strengths, factoring in concrete age and impact angle.

Particularly in buildings constructed prior to 1997, surface cleaning was meticulously performed before testing, taking into account that concrete surface carbonation—which is anticipated to reach depths of up to 15 mm—could cause misleading surface hardening. Furthermore, in addition to the carbonation effect, when considering the quality of construction techniques, inadequate workmanship, and the low rate of ready-mix concrete utilization in buildings constructed in 1997 and earlier, it was anticipated that concrete curing, aggregate granulometry, and segregation could cause varying strength results within the same structural element. Consequently, these test results were not utilized for a definitive seismic risk determination [6].

Table 1. Sample test report of the concrete rebound hammer

Schmidt Rebound Hammer Test Report										
Date of Testing	11 January 2019									
Building Name (Owner)	Chatalarmut Primary School									
Year of Construction	1997									
Test Location	Block B, Ground Floor									
Visual Inspection	Conducted									
Tested Element	Column	Column	Column	Column	Column	Column	Column	Column	Column	Column
Number of Blows (R-Q) 1	30	30	34	30	34	30	34	34	30	34
2	30	30	34	30	34	30	34	34	30	34
3	30	30	34	30	34	30	34	34	30	34
4	30	30	34	30	34	30	34	34	30	34
5	30	30	34	30	34	30	34	34	30	34
6	30	32	36	32	36	32	36	36	30	36
7	32	32	36	32	36	32	36	36	32	36
8	32	32	36	32	36	32	36	36	32	36

9	32	32	36	32	36	32	36	36	32	36
10	32	32	36	32	36	32	36	36	32	36
Total	308	310	350	310	350	310	350	350	308	350
Average	31.00	31.00	35.00	31.00	35.00	31.00	35.00	35.00	31.00	35.00
Correction for Impact Direction	0	0	0	0	0	0	0	0	0	0
Concrete Age Factor (Days)	8071	8071	8071	8071	8071	8071	8071	8071	8071	8071
Time Factor	0.6	0.6	0.6	0.6	0.6	0.6	0.6	0.6	0.6	0.6
Wmax(kg/cm²) Cube	154	154	194	154	194	154	194	194	154	194
Wmin(kg/cm²)Cube	116	116	154	116	154	116	154	154	116	154
Wmax+0.85 Cylinder	131	131	165	131	165	131	165	165	131	165
Findings	148,00 (kg/cm²)									

Summary of District Field Inspections. A ground condition assessment was conducted for the 406 public buildings, and findings were integrated into the first-stage evaluation methods to complete the Public Buildings Pre-Evaluation Form. The district-specific risk distributions revealed distinct regional trends:

- *19 Mayıs & Alaçam: Evaluated public buildings achieved consistently high performance scores (110–150), uniformly classifying them under Risk Priority Level 5 (low seismic risk requiring no urgent intervention).*
- *Asarcık, Atakum, & Ayvacık: Displayed highly heterogeneous risk profiles spanning Risk Priority Levels 1–5. Vulnerabilities were strongly correlated with construction quality variations and local soil conditions.*
- *Bafra: Performance scores ranged from 55 to 150 (Risk Priority Levels 1–5), driven by variations in structural system contributions and localized negative design parameters.*
- *Canik & Yakakent: Exhibited a concentrated, moderate risk profile restricted to Risk Priority Levels 3–4, indicating relatively uniform structural configurations with minor geometric irregularities.*
- *Çarşamba: Showed extensive variability across Risk Priority Levels 1–5. The structural vulnerabilities were primarily governed by localized geometric variations and configuration deficiencies.*
- *Havza, İlkadım, Ladik, & Vezirköprü: Displayed non-uniform distributions across Risk Priority Levels 1–5 (or 1–4). Vulnerabilities were heavily influenced by severe structural system deficiencies, vertical irregularities, soft-story defects, and hill/slope topographical effects.*
- *Kavak & Tekkeköy: Revealed moderate, spatially variable vulnerability profiles predominantly falling within Risk Priority Levels 2–5, governed by structural system contributions and slope irregularities.*
- *Terme: Exhibited a predominant concentration at Risk Priority Level 5, indicating a uniformly low and stable seismic vulnerability across its public building stock.*

3. Conclusions. In this study, as the initial phase of disaster mitigation efforts prior to the occurrence of a disaster with devastating impacts such as an earthquake, a total of 406 reinforced concrete public buildings within the provincial borders of Samsun were investigated. The structural evaluations were conducted between 2017 and 2018 based on rapid visual screening methods performed from the exterior facades of the buildings, in accordance with the implementing regulation of the Law No. 6306 on the Transformation of Areas Under Disaster Risk, which came into force in 2013. The spatial distribution of the examined buildings across the districts is as follows: 11 in 19 Mayıs, 3 in Alaçam, 8

in Asarcık, 30 in Atakum, 11 in Ayvacık, 3 in Bafra, 2 in Canik, 67 in Çarşamba, 45 in Havza, 45 in İlkadım, 24 in Kavak, 23 in Ladik, 13 in Salıpazarı, 11 in Tekkeköy, 44 in Terme, 56 in Vezirköprü, and 2 in Yakakent.

As a result of the study, the investigated structures were first ranked based on their building performance scores and subsequently categorized according to their risk levels. Through this classification, the number of risky buildings requiring high-priority intervention was determined.

Table 2. Distribution of the number of buildings based on risk levels by district

District Name	*Number of Buildings*	*Risk Levels (Number of Buildings)*				
		1st Degree	*2nd Degree*	*3rd Degree*	*4th Degree*	*5th Degree*
19.May	2					2
Alaçam	3					3
Asarcık	8	2	1	1	3	1
Atakum	30	2	3	3	12	10
Ayvacık	11	1	1	4	4	1
Bafra	21			2	3	16
Canik	2			1	1	
Çarşamba	67	3	3	7	20	34
Havza	45	2	10	14	19	
İlkadım	45	1	3	9	16	16
Ladik	23		6	8	9	
Vezirköprü	56	2	13	17	24	
Kavak	24		6	8	10	
Salıpazarı	13	1	1	2	5	4
Tekkeköy	11		1	3	3	4
Terme	44			4	7	33
Yakakent	2			1	1	
Total	**406**	**14**	**48**	**84**	**137**	**124**

As a result of the evaluation, 14 buildings were identified as first-degree high-risk structures and 48 buildings identified as 2nd-degree high risk in the districts of Asarcık, Atakum, Ayvacık, Çarşamba, Havza, Ladik, Kavak, and Vezirköprü were reported as " High seismic risk requiring immediate intervention." For these structures, the Existing Public Buildings Pre-Evaluation Form was prepared, and the relevant institutions were informed accordingly. Furthermore, 84 buildings were classified as 3rd-degree risk and 137 buildings as 4th-degree risk. The deficiencies observed in these structures were detailed, reported as "Resolvable with mitigation measures," and the Existing Public Buildings Pre-Evaluation Form was issued to notify the respective administrations regarding the seismic retrofitting of the buildings.

Within the scope of the investigation, no visible defects were found in 124 buildings, and these structures were categorized as 5th-degree risk based on their building performance scores.

The Existing Public Buildings Pre-Evaluation Form was also issued for these assets, and the relevant authorities were informed that periodic annual maintenance and repair operations would be sufficient for these buildings.

Since the study spans a two-year period encompassing 2017 and 2018, the investigated structures were evaluated under the implementing regulations in force as of 2017. However, significant amendments introduced as of 2019—both in the Seismic Code and the implementing regulation of Law No. 6306—have enabled more realistic soil effect calculations through a more detailed handling of the soil class-seismic hazard relationship and the introduction of the seismic hazard map concept [4]. This clearly demonstrates that the existing reinforced concrete buildings, which were identified as risky even under the more conservative and limited approaches prior to 2019, could be evaluated as substantially weaker in terms of resisting seismic ground motions and surviving a potential earthquake compared to calculations based on the previous codes. Therefore, to mitigate potential casualties and economic losses, the risky public buildings particularly located in districts within the 1st-degree seismic zone—such as Asarcık, Ayvacık, Havza, Ladik, Kavak, and Vezirköprü- must be evacuated, followed by the execution of necessary demolition and redesign processes [7].

Furthermore, considering the post-disaster chaos experienced after past devastating earthquakes in Türkiye, ensuring that critical public facilities such as police stations, hospitals, dormitories, and public housing units remain operational immediately after an earthquake is of paramount importance for both the continuity of public order and the safety of citizens. Consequently, priority must be given to public infrastructure in seismic risk assessments conducted within the current building stock, and indispensable measures must be implemented promptly. In this direction, within the scope of this study, the rapid visual screening methodology was utilized to rank the performance scores of the public building stock across Samsun Province prior to the generation of regional seismic risk maps. Ultimately, a comprehensive database was established to enable the annual monitoring of the examined public structures and to provide information regarding these buildings to the relevant institutions and organizations whenever necessary [8,9].

Author Contributions. All authors contributed to the conception and design of the study, literature review, methodology, data collection and analysis, manuscript preparation, revision, and approval of the final version of the manuscript.

Funding. The authors received no specific financial support from any funding agency, commercial organization, or not-for-profit institution for the research, authorship, and/or publication of this article.

Data Availability. The data supporting the findings of this study are available from the corresponding author upon reasonable request.

Declarations

Conflict of Interest. The authors declare that they have no competing interests or conflicts of interest related to this work.

Ethical Approval. This article does not involve studies with human participants or animals. Therefore, ethical approval was not required.

Informed Consent. Not applicable.

References

[1] S. Özdemir, *Seismic Evaluation Methods and Applications of Public Buildings* [in Turkish], M.S. thesis, Samsun, Türkiye, 2019.

[2] A. Kasimzade, M. Erdik, T. Kundu, H. Sucuoğlu, and P. Clemente, Eds., *Earthquake Resistant Design, Protection, and Performance Assessment in Earthquake Engineering*, vol. 54. Cham, Switzerland: Springer Nature, 2024. Available: https://doi.org/10.1007/978-3-031-65407-7

[3] A. A. Kasımzade, E. Şafak, E. C. Ventura, F. Naeim, and Y. Mukai, *Seismic Isolation, Structural Health Monitoring, and Performance Based Seismic Design in Earthquake Engineering: Recent Developments*. Cham, Switzerland: Springer, 2018. ISBN: 978-3-319-93156-2.
[4] A. A. Kasimzade *et al*., "Economic evaluation of 2000 Baku earthquake impact in view of building features," *Construction Economics and Management*, no. 3, vol. 32, pp. 191–206, 2025.
[5] A. A. Kasimzade *et al*., "System identification for non-destructive assessment of structures: Lessons learned," in *Communications in Computer and Information Science*, vol. 2225, Cham, Switzerland: Springer Nature, 2025, pp. 235–250. Available: https://doi.org/10.1007/978-3-031-73417-5_18
[6] A. A. Kasimzade and E. Nematli, "New structural seismic isolation system for tower structures," in *Geotechnical, Geological and Earthquake Engineering*, vol. 54, Cham, Switzerland: Springer Nature, 2024. Available: https://doi.org/10.1007/978-3-031-65407-7_1
[7] A. A. Kasimzade *et al*., "Novel approach on mathematical modelling and numerical evaluation of the seismic protection of structural dynamic systems," *Mathematical Methods in the Applied Sciences*, 2024. Available: https://doi.org/10.1002/mma.10790
[8] A. A. Kasımzade *et al*., "The contribution of natural seismic base isolation on the durability of traditional Japanese structures," in *Geotechnical, Geological and Earthquake Engineering*, vol. 54, Cham, Switzerland: Springer Nature, 2024. Available: https://doi.org/10.1007/978-3-031-65407-7_3
[9] A. A. Kasimzade *et al*., "The new criterion on performance-based seismic design with application to high-rise building," in *Geotechnical, Geological and Earthquake Engineering*, vol. 54, Cham, Switzerland: Springer Nature, 2024. Available: https://doi.org/10.1007/978-3-031-65407-7_11

https://doi.org/10.58225/sw.2026.1-125-131

CORRELATION BETWEEN STRUCTURAL STABILITY, OXIDATION BEHAVIOR AND LATTICE DYNAMICS IN GAMMA-IRRADIATED TiN NANOPARTICLES

Alena V. Shershneva[1*], Mahmoud Ibrahim[1,2]
[1]*Tomsk Polytechnic University, Tomsk 634050, Russia.*
[2]*Joint Institute for Nuclear Research, Dubna 141980, Russia*
**avs322@tpu.ru*

Abstract. This study presents an integrated assessment of the crystal structure, post-irradiation oxidation behavior and vibrational response of titanium nitride (TiN) nanoparticles exposed to gamma radiation. Nanopowders with an average particle size below 20 nm were irradiated using a ^{60}Co source at absorbed doses of 50, 200, 900 and 3500 kGy. Structural changes after annealing at 1173 K were examined by X-ray diffraction and Rietveld refinement, while dose-dependent lattice dynamics were evaluated by Raman spectroscopy in the 100–600 cm^{-1} range. The cubic Fm-3m structure remained stable throughout irradiation, and no radiation-induced phase transformation was detected. After annealing, rutile TiO_2 was identified as a minor phase; its fraction decreased from 6.40 % in the unirradiated specimen to 3.88% after irradiation at 3500 kGy. High-dose irradiation followed by annealing reduced microstrain and dislocation density and increased the average crystallite size to approximately 50 nm. Four Raman modes near 152, 246, 359 and 500 cm^{-1} persisted at every dose, although their positions, widths and areas changed. The combined results show that gamma irradiation does not destabilize the TiN framework but modifies defects, interatomic distances and surface-bound species, thereby suppressing subsequent oxidation and altering the vibrational response.

Keywords: TiN nanoparticles, gamma irradiation, Rietveld refinement, oxidation, Raman spectroscopy, lattice dynamics

Cite this article as: *A. V. Shershneva and M. Ibrahim, "CORRELATION BETWEEN STRUCTURAL STABILITY, OXIDATION BEHAVIOR AND LATTICE DYNAMICS IN GAMMA-IRRADIATED TiN NANOPARTICLES",* SW AzUAC, *vol. 1, 2026, https://doi.org/10.58225/sw.2026.1-125-131*
Article history: *Received: 25 May 2026 / Revised: 3 June 2026 / Accepted: 04 July 2026*

1. Introduction. Titanium nitride is a refractory ceramic combining a high melting point, high hardness, electrical conductivity and resistance to chemical degradation. These properties support its use in nuclear systems, protective coatings, diffusion barriers, plasmonic devices and components exposed to aggressive thermal environments [1–3]. Its mechanical, corrosion-resistant and electronic characteristics further broaden the range of potential applications. TiN nanoparticles have also attracted interest as near-infrared photothermal and plasmonic agents [4]. At the nanoscale, however, the large surface-to-volume ratio increases the contribution of adsorbed oxygen, water and structural defects; consequently, irradiation and heating may affect nanopowders differently from bulk TiN.

Energetic particles can produce vacancies, interstitials, residual stress and symmetry-lowering distortions in TiN. Ar-ion irradiation has been associated with lattice expansion and dislocation formation, whereas Xe implantation caused peak splitting, lattice contraction and rhombohedral distortion in thin films [5]. Electron irradiation likewise modifies the structural and functional response of TiN films [6]. These observations show that the response depends on particle type, energy, fluence and specimen morphology. Gamma photons mainly interact through electronic excitation and secondary electrons, so their crystallographic consequences can be subtler than those caused by direct ion displacement [7].

Temperature introduces an additional mechanism because TiN surfaces oxidize when oxygen becomes sufficiently mobile. Rutile TiO_2 develops during heating, and oxidation progresses from the surface toward the interior with nitrogen release [8]. The thermal behavior is also affected by particle size, surface chemistry and irradiation history [9]. Gamma irradiation may modify oxidation by removing weakly bound surface species, generating defects and changing diffusion paths. Earlier diffraction work demonstrated that nanocrystalline TiN retains its cubic phase up to 3500 kGy, although small contractions of the unit cell occur. Post-irradiation annealing further changes phase fractions, crystallite size and microstrain [10].

Diffraction provides information on long-range order and phase composition, whereas Raman spectroscopy probes local bonding, phonon behavior and disorder. Raman measurements are therefore valuable for identifying irradiation-induced changes that do not produce a new crystallographic phase [10-17]. Vibrational spectroscopy has been successfully used to connect local structural rearrangement with macroscopic stability in a wide range of crystalline systems [18].

The present work correlates XRD/Rietveld observations after irradiation and annealing with the dose-dependent Raman response of TiN nanoparticles. The objective is to determine whether the preserved average crystal symmetry is accompanied by local vibrational and defect evolution, and to clarify how prior gamma exposure influences subsequent oxidation.

2. Materials and Methods. Commercial TiN nanopowder supplied by US Research Nanomaterials, Inc. was used. The purity was 99.2%, the particle size was below 20 nm, the specific surface area was 50–80 m^2 g^{-1}, the bulk density was 0.08 g cm−3 and the true density was approximately 5.24 g cm^{-3}. TiN has a face-centered cubic structure described by space group Fm-3m [11,12].

Irradiation was conducted in air at room temperature using a 60Co gamma source at the Institute of Radiation Problems. Absorbed doses were 50, 200, 900 and 3500 kGy. The irradiation conditions and facility characteristics are described in [10]. For the thermal series, each irradiated powder and an unirradiated reference were annealed at 1173 K for 9 h under a vacuum of about 10^{-6} Torr; heating and cooling rates were 5 °C min^{-1}.

XRD patterns were recorded at room temperature with a PANalytical EMPYREAN diffractometer using Cu Kα radiation (λ = 1.5405 Å) in θ/2θ geometry. The angular interval was 20–100°, with a 0.02° step. Rietveld refinement was carried out with the FullProf suite. Phase fractions, lattice parameters and fit indices were refined. Crystallite size and microstrain were estimated from line broadening by the Williamson–Hall approach.

Raman spectra were collected at room temperature with a Horiba LabRAM HR spectrometer using a 633 nm He–Ne laser, an 1800 groove mm−1 grating, a 100 μm confocal aperture and a 50× objective. Laser power was 0.5 mW. Spectra were acquired for 30 s over ten accumulations, and five measurements were averaged per specimen. The 100–600 cm−1 spectra were fitted with mixed Lorentzian–Gaussian components.

3. Results and Discussion

3.1. Crystal structure after gamma irradiation and annealing. Figure 1 presents the Rietveld-refined diffraction patterns of the initial TiN powder and the specimens annealed at 1173 K after irradiation at different doses. The annealed diffraction patterns are dominated by reflections of cubic TiN. Rietveld analysis confirms space group Fm-3m for all specimens. Weak reflections at approximately 54.33° and 56.63°, assigned to the (211) and (220) planes of tetragonal rutile TiO_2 (P42/mnm), reveal limited oxidation during annealing. No other crystalline products were detected.

The oxide fraction decreases systematically as the preceding gamma dose rises: 6.40% for the unirradiated sample, 5.16% at 50 kGy, 5.10% at 200 kGy, 4.00% at 900 kGy and 3.88% at 3500 kGy. Thus, irradiation does not itself generate a detectable bulk oxide phase; instead, it weakens the subsequent oxidation response. A plausible explanation is the radiation-induced decomposition and desorption of surface-bound water and oxygen-bearing species, accompanied by defect rearrangement and partial structural compaction [19].

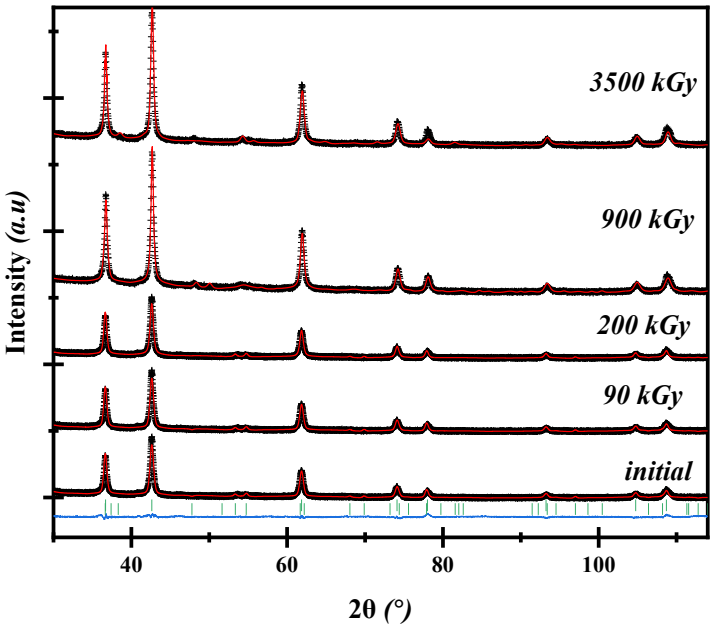

Fig.1. Rietveld-refined XRD patterns of TiN nanoparticles irradiated at different gamma doses and annealed at 1173 K

The principal (111) and (200) reflections retain their positions and overall profiles, confirming the stability of the cubic TiN phase. Their intensities and breadths nevertheless change with irradiation dose. After irradiation at 900 and 3500 kGy followed by annealing, the reflections become more intense, indicating improved crystalline ordering. The residual line broadening shows that irradiation-induced stress and defects are not completely removed. The refined lattice parameter varies only slightly around 4.24 Å, while the unit-cell volume remains within 76.1–76.3 $Å^3$.

The structural parameters summarized in Table 1 show that annealing increases the average crystallite size from the nominal 20 nm powder value to 43.5 nm in the unirradiated reference. Values of 42.1, 42.6, 50.0 and 49.9 nm were obtained after 50, 200, 900 and 3500 kGy, respectively. Microstrain decreases from 26.65×10^{-4} to 25.78×10^{-4}, while the calculated dislocation-density indicator falls from 2.04×10^{-6} to 1.72×10^{-6} at the maximum dose. These changes indicate thermally assisted defect recombination and crystallite coarsening, most pronounced after high-dose exposure.

Table 1. Principal structural parameters of annealed TiN specimens

Dose	a (Å)	V ($Å^3$)	Crystallite size (nm)	Microstrain ($\times10^{-4}$)
Initial	4.2400	76.230	43.5	26.65
50 kGy	4.2369	76.060	42.1	25.50
200 kGy	4.2360	76.060	42.6	25.30
900 kGy	4.2404	76.246	50.0	25.97
3500 kGy	4.2410	76.287	49.9	25.78

The diffraction-line broadening was further evaluated by the Williamson–Hall (W–H) method [20]. The measured FWHM values were corrected for instrumental broadening using the LaB_6 standard and analyzed with the uniform-deformation relation:

$$\beta\cos\theta = \frac{k\lambda}{D} + 4\varepsilon\sin\theta \qquad (1)$$

Here, β is the instrument-corrected peak broadening expressed in radians, θ is the Bragg angle, k is the shape factor (0.9), λ is the Cu Kα wavelength (1.5405 Å), D is the volume-weighted average crystallite size, and ε is the microstrain. In the conventional W–H representation, β cos θ is plotted against 4 sin θ; the intercept equals kλ/D and the slope gives ε. Figure 2 displays the FWHM input points as a function of 2θ, while the values of D and ε were obtained after applying the W–H transformation in Eq. (1).

The W–H results are consistent with the values summarized in Table 1. The average crystallite sizes are 43.5 nm for the annealed initial sample and 42.1, 42.6, 50.0, and 49.9 nm for the samples irradiated at 50, 200, 900, and 3500 kGy, respectively, before annealing. Thus, the low-dose specimens remain close to 42 nm, whereas irradiation at 900 and 3500 kGy followed by annealing produces crystallites of about 50 nm. The corresponding microstrain values are 26.65, 25.50, 25.30, 25.97, and 25.78 × 10^{-4}. The lowest microstrain is obtained at 200 kGy; all irradiated and annealed samples nevertheless show lower microstrain than the annealed unirradiated reference. These results indicate partial relaxation of irradiation-induced lattice defects during annealing, accompanied by enhanced crystallite coarsening at high doses.

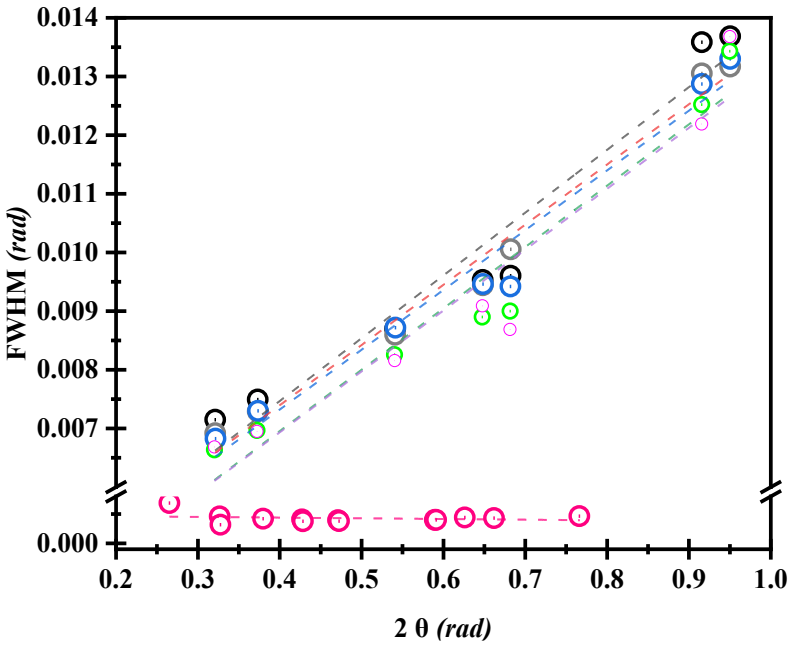

Fig. 2. Williamson–Hall analysis of TiN nanoparticles after annealing

The FWHM data points are plotted against 2θ and were transformed according to Eq. (1) for determination of the crystallite size and microstrain. The black open circles and black dashed line represent the annealed initial sample; the gray open circles and red dashed line correspond to 50 kGy; the blue, green, and magenta open circles with their respective dashed fits correspond to 200, 900, and 3500 kGy, respectively. The bright-pink points and dashed line at the bottom represent the instrumental LaB_6 standard used to evaluate instrumental broadening.

3.2. Raman spectra and local lattice dynamics. The Raman spectrum of the initial powder contains four broad bands centered near 152, 246, 359 and 500 cm^{-1}. Their broad shape is consistent with disorder-activated scattering in non-stoichiometric or nanoscale TiN. Studies of TiN films reported acoustic modes in the 216–440 cm^{-1} region and an optical contribution near 570 cm^{-1} [13–15]. The lower frequencies measured here are compatible with weaker effective bonding, nanoscale disorder and the different stress state of free nanoparticles.

Figure 3 compares the Raman spectra of the initial specimen with those irradiated at 50, 200, 900 and 3500 kGy. All four principal bands remain present at every dose, providing no evidence of a radiation-induced vibrational phase transition. Their widths and intensities nevertheless vary with dose. The ν_3 band near 359 cm^{-1} exhibits the clearest positional shift, whereas the modes near 152, 246 and 500 cm^{-1} change more weakly.

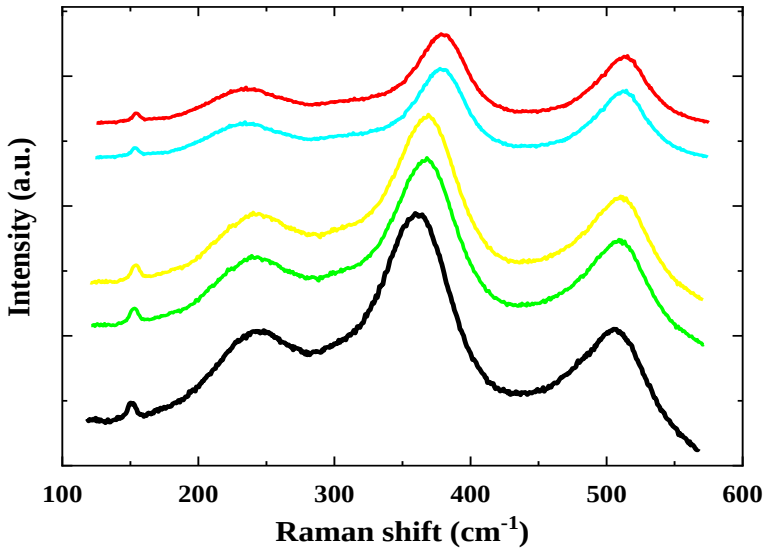

Fig.3. Raman spectra of titanium nitride nanoparticles before and after gamma irradiation

For clarity, the spectra are vertically offset and arranged from bottom to top in order of increasing irradiation dose: initial, 50, 200, 900, and 3500 kGy. Analysis of the Raman line-shape parameters shows that the full width at half maximum (FWHM) of ν_1 rises from 5.93 to 7.30 cm^{-1} while its integrated area decreases from 13,375 to 5,045. For ν_3, the FWHM increases from 35.0 to 46.35 cm^{-1} and the area falls from 804,432 to 488,674, consistent with reduced vibrational coherence and increased local disorder. The ν_2 area decreases overall but partially recovers at 3500 kGy relative to 900 kGy. In contrast, the ν_4 area is non-monotonic and increases at the highest dose. The dose response is therefore mode-specific rather than governed by one identical mechanism.

The XRD and Raman findings are therefore complementary. XRD establishes preservation of the long-range cubic framework and reveals reduced post-irradiation oxide formation. Raman data show that gamma exposure still alters the local lattice through defect redistribution, fragmentation of weak bonds and changes in Ti–N interatomic distances. The removal of adsorbed species can densify the near-surface structure, whereas defect creation and recombination modify the distribution of vibrational states [21-25].

4. Conclusion. Gamma irradiation at doses up to 3500 kGy preserves the cubic *Fm-3m* framework of TiN nanoparticles. Subsequent annealing at 1173 K produces only a minor rutile TiO_2 fraction, and the amount of this oxide decreases from 6.40% to 3.88% as the prior irradiation dose increases. High-dose irradiation followed by annealing promotes crystallite growth to about 50 nm and reduces microstrain and dislocation density. Raman spectra retain four characteristic modes throughout the dose range, while their positions and line-shape parameters change. Therefore, the average crystal structure remains stable even though local bonds, defect populations and surface species evolve. The combined diffraction and vibrational evidence identifies TiN as radiation resistant while showing that gamma exposure can regulate its later oxidation and nanoscale defect state.

Author Contributions. A.V.S. (Alena V. Shershneva) conceived and designed the study, performed the formal analysis, conducted the investigation, prepared the original draft of the manuscript, and reviewed and edited the manuscript. M.I. (Mahmoud Ibrahim) contributed to the methodology, validation of the results, data analysis and interpretation, reviewed and edited the manuscript, supervised the research, and approved the final version of the manuscript. All authors have read and agreed to the published version of the manuscript.
Funding. Not applicable.
Data Availability. The data supporting the findings of this study are available from the corresponding author upon reasonable request.
Declarations
Conflict of Interest. The authors declare no conflict of interest.
Competing Interests. The authors declare that they have no competing interests.
Ethical Approval. This article does not involve studies with human participants or animals. Therefore, ethical approval was not required.
Informed Consent. Not applicable.
Acknowledgment. The authors gratefully acknowledge the support and research facilities provided by Tomsk Polytechnic University, Tomsk, Russian Federation.

References

[1] Akhtanova, G., Yerlanuly, Y., Parkhomenko, H. P., Solovan, M. V., Mostovyi, A. I., Nurmukhanbetova, A. K., Kireyev, A. V., Danko, I. V., Oreshkin, P. A., Zholdybayev, T. K., Janseitov, D. M., Ramazanov, T. S., & Brus, V. V. (2024). Electron irradiation-induced degradation of TiN thin films on quartz and sapphire substrates. *ACS Omega, 9*(1), 925–933. https://doi.org/10.1021/acsomega.3c07053

[2] Gao, L., Gstöttner, J., Emling, R., et al. (2004). Thermal stability of titanium nitride diffusion barrier films for advanced silver interconnects. *Microelectronic Engineering, 76*(1–4), 76–81. https://doi.org/10.1016/j.mee.2004.07.020

[3] Patsalas, P., Kalfagiannis, N., Kassavetis, S., et al. (2018). Conductive nitrides: Growth principles, optical and electronic properties, and their perspectives in photonics and plasmonics. *Materials Science and Engineering R: Reports, 123*, 1–55. https://doi.org/10.1016/j.mser.2017.11.001

[4] Xue, J. X., Zhang, G. J., Xu, F. F., et al. (2013). Lattice expansion and microstructure evaluation of Ar ion-irradiated titanium nitride. *Nuclear Instruments and Methods in Physics Research Section B: Beam Interactions with Materials and Atoms, 308*, 62–67. https://doi.org/10.1016/j.nimb.2013.05.011

[5] Popović, M., Novaković, M., Mitrić, M., et al. (2017). Xenon implantation effects on the structural and optical properties of reactively sputtered titanium nitride thin films. *Materials Research Bulletin, 91*, 36–41. https://doi.org/10.1016/j.materresbull.2017.03.031

[6] Chen, H. Y., & Lu, F. H. (2005). Oxidation behavior of titanium nitride films. *Journal of Vacuum Science & Technology A, 23*(4), 1006–1009. https://doi.org/10.1116/1.1914815

[7] Arai, Y., & Nakajima, K. (2000). Preparation and characterization of PuN pellets containing ZrN and TiN. *Journal of Nuclear Materials, 281*(2–3), 244–247. https://doi.org/10.1016/S0022-3115(00)00393-7

[8] Fahrenholtz, W. G., Hilmas, G. E., Talmy, I. G., & Zaykoski, J. A. (2007). Refractory diborides of zirconium and hafnium. *Journal of the American Ceramic Society, 90*(5), 1347–1364. https://doi.org/10.1111/j.1551-2916.2007.01583.x

[9] Sutthiruangwong, S., & Mori, G. (2003). Corrosion properties of Co-based cemented carbides in acidic solutions. *International Journal of Refractory Metals and Hard Materials, 21*(3–4), 135–145. https://doi.org/10.1016/S0263-4368(03)00027-1

[10] Mahvash, F., Eissa, S., Bordjiba, T., Tavares, A. C., Szkopek, T., & Siaj, M. (2017). Corrosion resistance of monolayer hexagonal boron nitride on copper. *Scientific Reports, 7*, 42139. https://doi.org/10.1038/srep42139

[11] Morales, H. M., Vieyra, H., Sanchez, D. A., et al. (2024). Synthesis and characterization of titanium nitride–carbon composites and their use in lithium-ion batteries. *Nanomaterials, 14*(7), 624. https://doi.org/10.3390/nano14070624

[12] Christensen, A. N., Romano, V., & Hesse, R. (1975). A neutron diffraction investigation on single crystals of titanium carbide, titanium nitride, and zirconium nitride. *Acta Chemica Scandinavica A, 29A*, 563–568. https://doi.org/10.3891/acta.chem.scand.29a-0563

[13] Saoula, N., Djerourou, S., Yahiaoui, K., et al. (2010). Study of the deposition of Ti/TiN multilayers by magnetron sputtering. *Surface and Interface Analysis, 42*(6–7), 1176–1179. https://doi.org/10.1002/sia.3299

[14] Cheng, Y. H., Tay, B. K., Lau, S. P., et al. (2002). Substrate bias dependence of Raman spectra for TiN films deposited by filtered cathodic vacuum arc. *Journal of Applied Physics, 92*(4), 1845–1849. https://doi.org/10.1063/1.1491588

[15] Ding, Z. H., Yao, B., Qiu, L. X., & Lv, T. Q. (2006). Raman scattering investigation of nanocrystalline δ-TiN_x synthesized by solid-state reaction. *Journal of Alloys and Compounds, 421*(1–2), 247–251. https://doi.org/10.1016/j.jallcom.2005.11.017

[16] Deluca, M., Hu, H., Popov, M. N., et al. (2023). Advantages and developments of Raman spectroscopy for electroceramics. *Communications Materials, 4*, 78. https://doi.org/10.1038/s43246-023-00400-4

[17] Gupta, H., Joshi, K., Gautam, S. K., et al. (2020). Raman scattering from irradiated nanocrystalline zinc oxide thin films: Perspective view on effects of energy loss, ion fluence, and ion flux. *Vacuum, 181*, 109598. https://doi.org/10.1016/j.vacuum.2020.109598

[18] Biradar, S., Chandrashekara, M. N., Manjunatha, Dinkar, A., Devidas, G. B., Bennal, A. S., Rajaramakrishna, R., & Sayyed, M. I. (2024). Synergistic optimization of physical, thermal, structural, mechanical, optical and radiation shielding characteristics in borate glasses doped with Bi_2O_3. *Optical Materials, 155*, 115815. https://doi.org/10.1016/j.optmat.2024.115815

[19] Jiang, W., Fu, Q., Wei, H., & Yao, A. (2019). TiN nanoparticles: Synthesis and application as near-infrared photothermal agents for cancer therapy. *Journal of Materials Science, 54*, 5743–5756. https://doi.org/10.1007/s10853-018-03272-z

[20] Cao, L., Zhang, Q., Du, L., et al. (2024). Synthesis and characterization of high-entropy $(TiVNbTaM)_2AlC$ (M = Zr, Hf) ceramics. *Journal of Advanced Ceramics, 13*(2), 237–246. https://doi.org/10.26599/JAC.2024.9220847

[21] Hazem, R., Izerrouken, M., Cheraitia, A., & Djehlane, A. (2019). Raman study of ion beam irradiation damage on nanostructured TiO_2 thin film. *Nuclear Instruments and Methods in Physics Research Section B: Beam Interactions with Materials and Atoms, 444*, 62–67. https://doi.org/10.1016/j.nimb.2019.02.011

[22] Rana, A., Sharma, N. K., Bera, S., et al. (2024). Tuning the plasmonic resonance in TiN refractory metal. *Scientific Reports, 14*, 7905. https://doi.org/10.1038/s41598-024-55000-0

[23] Trang, V. T. T., Hang, H. T., Nhi, P. Q., et al. (2024). Enhancement of photothermal conversion by TiN nanoparticles-embedded black paint and applications in solar drying of red chilli. *Materials, 17*(17), 4393. https://doi.org/10.3390/ma17174393

[24] Okrusch, M., Hock, R., Schüssler, U., Brummer, A., Baier, M., & Theisinger, H. (2003). Intergrown niobian rutile phases with Sc- and W-rich ferrocolumbite: An electron-microprobe and Rietveld study. *American Mineralogist, 88*(7), 986–995. https://doi.org/10.2138/am-2003-0706

[25] Dutta, S., Chattopadhyay, S., Sarkar, A., Chakrabarti, M., Sanyal, D., & Jana, D. (2009). Role of defects in tailoring structural, electrical and optical properties of ZnO. *Progress in Materials Science, 54*(1), 89–136. https://doi.org/10.1016/j.pmatsci.2008.07.002